2017

Exact Numerical Study of Disordered Systems

Conrad Wilson Moore
Louisiana State University and Agricultural and Mechanical College, cmoor54@lsu.edu

EXACT NUMERICAL STUDY OF DISORDERED SYSTEMS

A Dissertation

Submitted to the Graduate Faculty of the
Louisiana State University and
Agricultural and Mechanical College
in partial fulfillment of the
requirements for the degree of
Doctor of Philosophy

in

The Department of Physics and Astronomy

by
Conrad Wilson Moore
B.S., Bucknell University
August 2017

To a memory from 2011.

Acknowledgments

First and foremost, I would like to acknowledge my advisor Mark Jarrell and his instruction and for especially his patience with me throughout this work, as I am sure at times my progress was unduly frustrating for him. I would also like to acknowledge the guidance of Juana Moreno and the postdocs that we have had in our research group. Especially in this regard, I would like to thank Ka Ming Tam for his invaluable discussions and insight: I have talked more physics with him than anyone else listed here by a long shot. Also, I thank the postodcs Hanna Terletska and Yi Zhang for their collaboration on much of this work. Also Shuxiang Yang for his help on my initial project at LSU and throughout his time at LSU. Next I would like to thank the former students and colleagues I have gotten to work with at LSU. Sameer Abu Asal who I worked with closely in the Center for Computation and Technology over the years. And Sean Hall, Peter Reis, Herbert Fotso, Chinedu Ekuma, Sheng Fang, Enzhi Li and Samuel Keller who I have known from the group and got to interact with both inside and outside the lab. Finally, I would like to acknowledge my committee members: David Koppelman, Phil Adams, Christopher Arges, and Zhiqiang Mao.

There are of course more people beyond those I had contact with professionally that are not listed. They know who they are and my gratitude.

Table of Contents

Acknowledgments . . . . . **iii**

Abstract . . . . . **vi**

Chapter 1 Introduction **1**
1.1 Ordered Systems: Metals and Insulators 1
1.2 Experiments on Localization and Disorder in Materials 7
1.3 Theory of Disordered Systems 12
1.4 Thesis Structure 22

Chapter 2 Numerical Methods for Disordered Systems **24**
2.1 Transfer Matrix Method 24
2.2 Quantum Cluster Methods 26
2.3 Multifractal Analysis 28

Chapter 3 TMDCA Study of Off-diagonal Disorder **31**
3.1 Introduction 32
3.2 Formalism 35
3.3 Results and Discussion 43
3.4 Conclusion 55

Chapter 4 TMDCA Study of Multi-band Systems **57**
4.1 Introduction 59
4.2 Formalism 61
4.3 Results 67
4.4 Conclusion 76

Chapter 5 Multifractal Study of Quasiparticle Localization in Disordered Superconductors **79**
5.1 Introduction 80
5.2 Model and Methods 81
5.3 Results 87
5.4 Conclusion 92

References **93**

Appendix A: Permissions **103**

Vita **105**

Abstract

This thesis presents work on the development of new techniques to study the problem of localization in various models of disordered systems with the goal of being able to extend these model calculations to real materials where these various mechanisms of disorder can all be present. I consider the Anderson Model with diagonal, off-diagonal disorder, multiple bands and superconductivity is included at the level of a Bogoliubov - De Gennes mean field (superconductivity is considered by adding the symmetries of the Bogoliubov - De Gennes Hamiltonian on top of the disordered lattice Hamiltonian). The localization of electrons is studied with the transfer matrix method (TMM) in order to compare mobility edge predictions with that of the newly developed Typical Medium Dynamical Cluster Approximation (TMDCA) for systems with both off diagonal disorder and multiple bands. It is verified this method can accurately predict the localization transition in model systems. A model of a disordered superconductor is considered with extended s-wave pairing, but in this case the excitations are no longer electrons but Bogoliubov quasiparticles or bogolons. I study the multifractal properties of the bogolon wavefunction and apply a multifractal analysis similar to what has been applied to the Anderson model and verify the ability to capture the localization of the bogolon quasiparticle excitations with comparison to the TMM.

Chapter 1

Introduction

1.1 Ordered Systems: Metals and Insulators

This thesis is work related to the problem of localization which results in the inhibition of transport in materials. A system is said to undergo a localization transition when the carriers of of some physical quantity (charge, energy etc.) have become "stuck" somewhere in the material and are unable to conduct over large distances in the material. This thesis will be focused on the question of localization induced by disorder or localization in the *Anderson* sense. I will be focusing on *disordered* systems, but before addressing the problem of disorder, I will review some aspects of the theory of *ordered* systems.

The first aspect of ordered systems that will be necessary to understand is the so called tight binding model in order to understand the model Hamiltonians that will be introduced. This is reviewed below in Sec.1.1.1. Next, a mechanism of localization not related to disorder and known as the Mott transition or *Mott* localization (emphasis to explicitly differentiate it from Anderson localization) will be reviewed in Sec.1.1.2. As I will be later discussing disordered superconductors, I will review ordered superconductors in Sec.1.1.3

1.1.1 Independent Electrons and the Tight Binding model

We first make the independent electron approximation which means we will be neglecting any effects of electron-electron interaction and only consider a single electron. As a single electron travels through a material, it will experience a potential $V(\mathbf{x})$ that varies as a function of position which is produced by the positive ions that make up the lattice. We consider an ordered system and so this potential must have the same translational symmetry of the lattice. Let $\mathbf{l}$ be a vector such

that displacing every point in the lattice by it leaves the lattice invariant. The potential the electron experiences must then obey $V(\mathbf{x}+\mathbf{l}) = V(\mathbf{x})$. This has profound effect on the time independent Schrödinger equation for the electron

$$H(x)\,|\psi(x)\rangle = E\,|\psi(x)\rangle \tag{1.1}$$

where $H(x)$ is the Hamiltonian that includes the potential ($V(x)$) and is an operator that acts on the state vector $|\psi(x)\rangle$ of the electron and returns its energy E. The result of the translational symmetry has the effect on the wavefunction solutions, causing them to take the form

$$\psi_k(x) = e^{ik\cdot x}u_k(x) \tag{1.2}$$

i.e. the electrons form extended plane wave states multiplied by a function $u_k(x)$ that has the periodicity of the lattice and this is known as Bloch's theorem. Any metallic or delocalized state can thus be expressed as a sum of Bloch waves.

We now consider the form of the Hamiltonian and assume the basis vectors to be states that are localized to some atomic site i and so $|\psi(x)\rangle = |i\rangle$ which is short hand for a vector

$$|i\rangle = \begin{pmatrix} 0 \\ \vdots \\ 1 \\ \vdots \\ 0 \end{pmatrix}. \tag{1.3}$$

This is known as the tight binding model and can be written in second quantized notation as

$$H = -t \sum_{<i,j>} (c_i^\dagger c_j + \text{h.c.}) \tag{1.4}$$

where c_i destroys an electron on site i and $c_i^\dagger$ creates an electron on site i, and so it describes a single electron hopping on a lattice with kinetic energy t. The restriction on the sum denoted by

$< i, j >$ is to nearest neighbors which will always be followed in this thesis. This is summarized in Fig.1.1

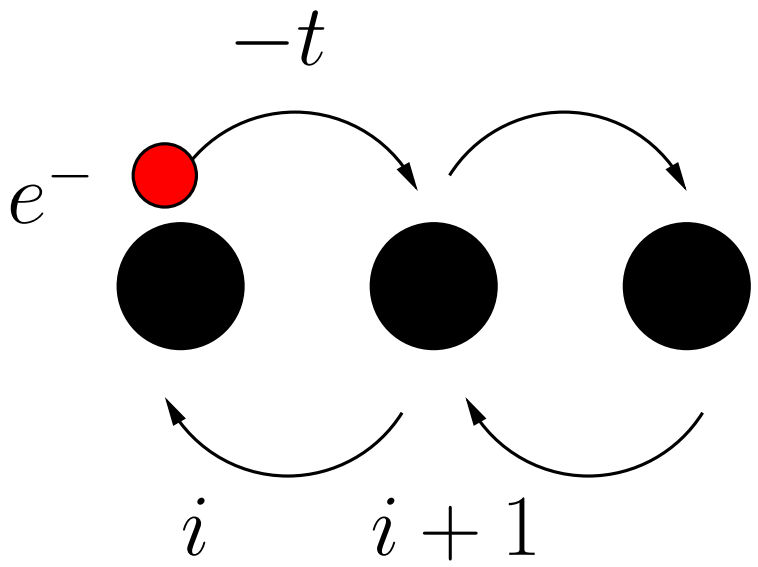

Figure 1.1: Example of Eq. 1.4 on a one dimensional chain. The hopping from site i to $i+1$ is described by the term $c^\dagger_{i+1}c_i$ as .

This can be diagonalized by Fourier transform to

$$H_0 = \sum_{\mathbf{k}} \epsilon_{\mathbf{k}} c^\dagger_{\mathbf{k}} c_{\mathbf{k}} \tag{1.5}$$

where $\epsilon_{\mathbf{k}}$ is known as the dispersion and gives the allowed electronic energies. For the case of a linear chain, $\epsilon_{\mathbf{k}} = cos(k)$. The range of allowed energies is referred to as a band. The above discussion was considering only a single band, and for systems with multiple bands we introduce the band index n to the dispersion $\epsilon_{n\mathbf{k}}$. If the Fermi energy (the largest available electronic energy and is the energy of the electrons that participate in transport) falls within a gap between the allowed energies of the bands n and n' the material is said to be a band insulator. This is different from an insulator due to disorder and due to electron-electron interaction which is described below in Sec.1.1.2.

1.1.2 Mott Transition

As already stated, this thesis will be focused on localization from disorder, but it is important to note that localization can appear without disorder and the original argument was made by Mott[1]. We imagine bringing together an array of Hydrogen atoms to form a lattice with some lattice spacing a. From the above discussion of the tight binding model, we know that if the lattice spacing becomes large enough then the wave functions will no longer overlap, no bands will form and the electrons will be localized to their respective Hydrogen atomic orbitals. This makes it seem as if, from the perspective of the tight binding model, that the transition from metal to insulator is continuous as a function of lattice spacing a (or alternatively the density of ionized electrons n), but it is well known that this is not the case (having been observed in transition metal oxides[3]) and so there must be some mechanism of localization that is not related to disorder.

The resolution is that it is a failure of the independent electron approximation which neglects the electron-electron interaction[2]. As an electron leaves an ionic site, leaving a positive charge which will attract the electron and possibly form a bound state. However, this potential is not just the coulomb potential $-e^2/r$, but the screened potential

$$-\frac{e^2}{r}e^{-\lambda r} \tag{1.6}$$

due to the presence of the other electrons. For a given density of free electrons n, the screening length takes the form

$$\lambda^2 \approx \frac{4me^2n^{1/3}}{\hbar^2} \tag{1.7}$$

The ground state of Hydrogen has the well known radius

$$a_H = \frac{\hbar^2}{me^2} \tag{1.8}$$

and so if this length is longer than the screening length $1/\lambda$ then the electron can not be bound and

can be free to wander. And so the condition for localization is

$$\frac{1}{\lambda} < a_H \tag{1.9}$$

or

$$n^{-\frac{1}{3}} < 4a_H. \tag{1.10}$$

Thus, there is a sudden transition from a metallic state to an insulating state for some density of free charge carriers n which is not due to disorder and purely from taking the interaction of electrons into account. This is referred to as Mott localization and is a distinctly different mechanism than Anderson localization which will be the focus of this thesis. Therefore, any mention of localization in this thesis should be implied to be in the Anderson sense unless stated otherwise.

1.1.3 Superconductivity

The body of literature on the theory and experiments related to superconductivity is incredibly expansive, and so I will focus on the ascpects necessary to understand the application to disordered systems that I will address in Sec.1.3.3.

According to Drude theory of electrons in metals, the resistivity of a metal at low temperature should behave as [2]

$$\rho = \rho_0 + aT^2 + \cdots \tag{1.11}$$

and so it is expected to continuously decrease to some constant ρ_0 which is given by the density of impurities (which is independent of T, being related to the intrinsic properties of the material). However, it was then discovered in 1911 from experiments on Mercury that around a temperature of $4°K$ that the resistivity suddenly vanishes[9]. Therefore, in some materials there is some critical temperature T_c below which the electrons in a material can transport without loss of energy. It was not until 1959 that a microscopic explanation for superconductivity was provided[10] and the essential parts of the theory are realizing there can be an attractive interaction between electrons which leads to the formation of so called cooper pairs.

Although the coulomb interaction is much weaker in a solid due to screening as mentioned in

Sec.1.1.2, it still remains repulsive. The attractive interaction comes from an electron in a Bloch state $\psi_{n\mathbf{k}}(\mathbf{r})$ can excite a phonon mode with some momentum $\hbar\mathbf{q}$ and losing $\hbar\mathbf{q}$ in turn. Additionally, a second electron can then later gain that momentum and this leads to an effective retarded interaction between electrons. To see that the interaction is attractive we imagine an electron moving through a metal and the resulting deformation of the lattice as seen in Fig.1.2. From these arguments, we can write down the term in the Hamiltonian that will capture this attractive interaction between two electrons with wave vectors $\mathbf{k}_1$ and $\mathbf{k}_2$ that then interact and electron $\mathbf{k}_2$ gives up momentum $\hbar q$ which is later absorbed by electron $\mathbf{k}_1$ as

$$H_1 = -U \sum c^\dagger_{\mathbf{k}_1+\mathbf{q},\sigma_1} c^\dagger_{\mathbf{k}_2-\mathbf{q},\sigma_2} c_{\mathbf{k}_1,\sigma_1} c_{\mathbf{k}_2,\sigma_2} \tag{1.12}$$

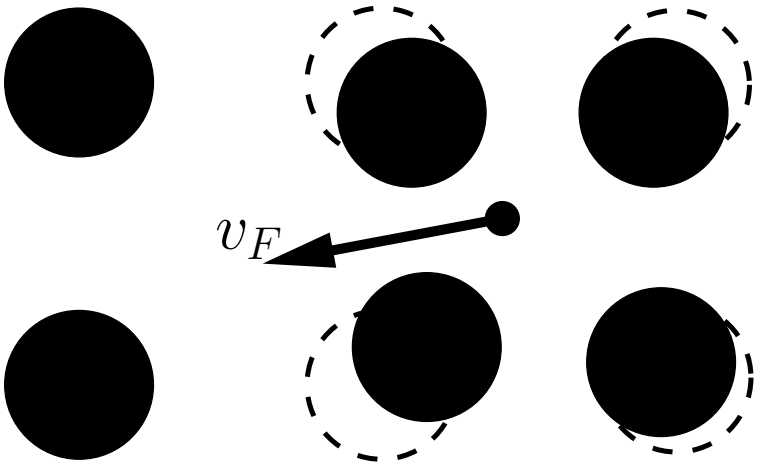

Figure 1.2: As an electron moves through a lattice with Fermi velocity v_F, it attracts the positive large ions and this in turn leads to a build up of positive charge with respect to the rest of the lattice and will attract a second electron.

It was then Cooper[11] that showed this attractive interaction (no matter how weak) leads to any two electrons above the Fermi surface to form a bound state of zero total momentum: they form a *pair* of $(\mathbf{k},\sigma)$ and $(-\mathbf{k},\sigma)$ where σ denotes the spin. The bound state is assumed to be a singlet and so the two electrons have opposite spin, but it is worth noting that they can have the same spin if the spin state formed is a triplet state.

And so within BCS theory, we can write the Hamiltonian for an ordered superconductor as

$$H = H_0 + H_1 \tag{1.13}$$

where H_0 is given by Eq. 1.5 and H_1 from above Eq. 1.12. From the above discussion of Cooper pairs and spin, we drop all terms except terms that pair electrons such that $\mathbf{k}_1 = -\mathbf{k}_2$ and $\sigma_1 = -\sigma_2$ which leads to the Hamiltonian

$$H = \sum_{\mathbf{k}\sigma} \epsilon_{\mathbf{k}} c^\dagger_{\mathbf{k}\sigma} c_{\mathbf{k}\sigma} - U \sum_{\mathbf{k}\mathbf{k}'} c^\dagger_{\mathbf{k}\uparrow} c^\dagger_{-\mathbf{k}\downarrow} c_{-\mathbf{k}'\downarrow} c_{\mathbf{k}'\uparrow} \tag{1.14}$$

1.2 Experiments on Localization and Disorder in Materials

In this section, I review experiments on disordered systems to motivate the theoretical study of the disorder induced metal-insulator transition. An appreciation of the importance of understanding metal-insulator transitions came very soon after the theory of band insulators (discussed in Sec.1.1.1) established a basic distinction between metals and insulators: whether the Fermi level falls in a gap or not. It was then realized that insulators with a small band gap would lead to semiconducting behavior, and 16 years later the transistor was invented which had obvious practical technological impact. However, there was still much that complicates this simple picture: already mentioned in Sec.1.1.2 was the effect of electron-electron interaction and the Mott transition. Experiments determined that many transition-metal oxides with partially filled d-electron band could still be insulators[13] despite band theory predicting otherwise. In Sec.1.2.1-1.2.2, experiments on non-superconducting systems will be reviewed and Sec.1.2.3 will review disordered superconductors.

1.2.1 Weak Localization

The scaling theory of localization predicts that in two dimensions all metals should become insulating in the limit $T \to 0$. This behavior was verified in experiments of this Cu films at low temperatures[18] (see Fig.1.3 for experiment and details) where the mean free path is of the order of the film thickness. This effect is attributed to the quantum mechanical interference of electron wave-

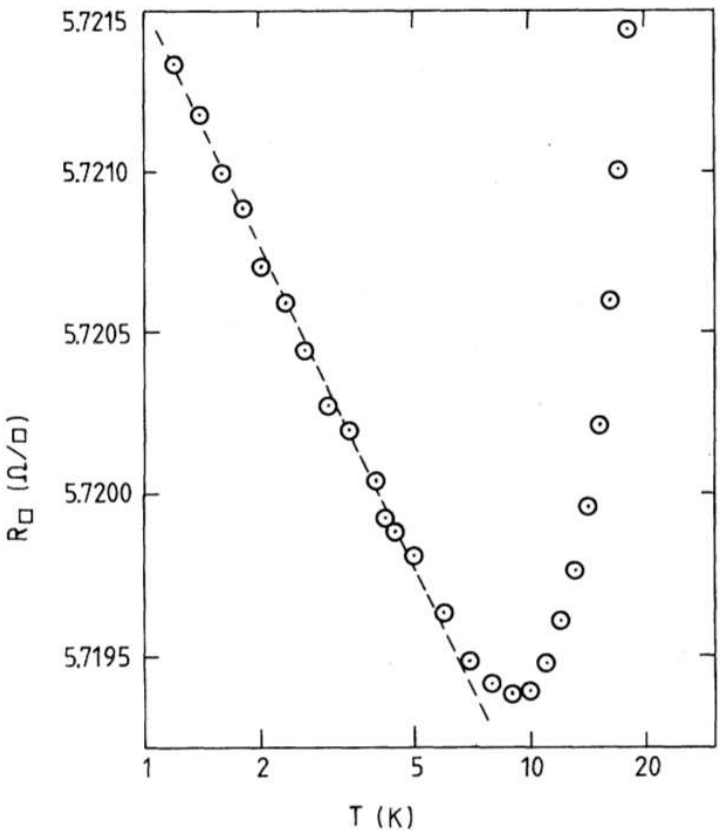

Figure 1.3: Resistivity (reported as resistance per square $R_\square$) as a function of Temperature in a thin Cu film with thickness 119Åand resistivity $6.8 \times 10^{-6} \Omega cm$. Film thickness was measured with a quartz-crystal thickness monitor. Film resistance was measured via four-terminal measurements with a conducting channel 0.235mm wide and probe separation of 4mm. The samples were prepared at a pressure of 10^{-6}Torr. The films were prepared with 99.999% Cu.

functions or coherent backscattering, and this is referred to as the *weak localization* effect. Coherent back scattering will be discussed in detail in Sec.1.3.1, but it is a phase coherence that the electron acquires in the backscattering direction and this constructive interference increases the probability of the electron returning to any site: it is a localizing effect that enhances resistivity. Although experiments showed the predicted T dependence, it was found that electron-electron interactions will result in the same behavior. To resolve this dilemma, further experiments were performed involving magnetic fields [19] demonstrating negative magnetoresistance such as Fig.1.4. The fact that a negative magnetoresistance is demonstrated shows it is an effect of coherent backscattering as an external field disrupts the phase coherence and increases the localization length. In contrast,

the effect of electron-electron interactions would show a positive magnetoresistance. As the effects

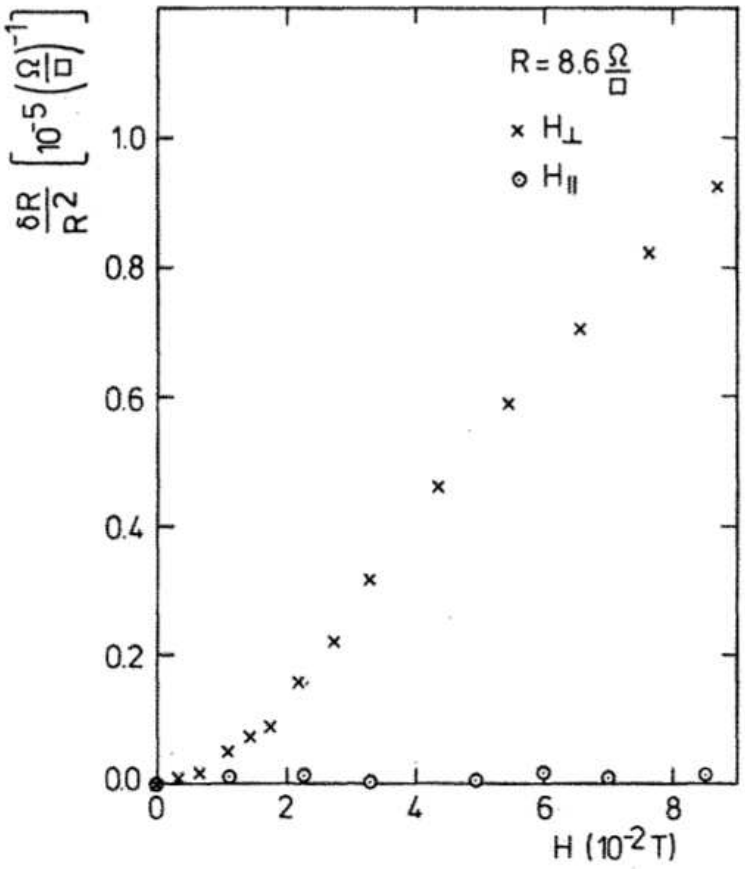

Figure 1.4: Negative magnetoresistance as a function of applied field for a thin Cu film with a sheet resistance of $R = 8.6\Omega/\Box$. Shown are for both transverse ($H_\perp$) and parallel ($H_\parallel$) fields. The increase in a transverse field has the expected effect of increasing the localization length, lowering the resistance. The effect is not pronounced for a parallel field, demonstrating it is not due to any spin effects and is due to localization. Figure is from [19].

of spin-orbit interactions would also disrupt the phase coherence, it was also experimentally confirmed that this behavior was indeed due to some phase coherence in the sample by later studies involving introducing spin-orbit coupling[20] which has the effects of disrupting the phase coherence and "turning off" the localization[148].

1.2.2 Anderson Transition in Doped Semiconductors

The weak localization effect described above in Sec.1.2.1 is often refered to as the precursor to Anderson localization: as disorder increases the electrons are more strongly back scattered and it was hypothesized that for sufficiently strong disorder the conductivity of a material can vanish, inducing a metal-insulator transition. The most famous case is phosphorous doped silicon (Si:P) were it was observed for uncompensated samples[152] and is described as an Anderson transition.

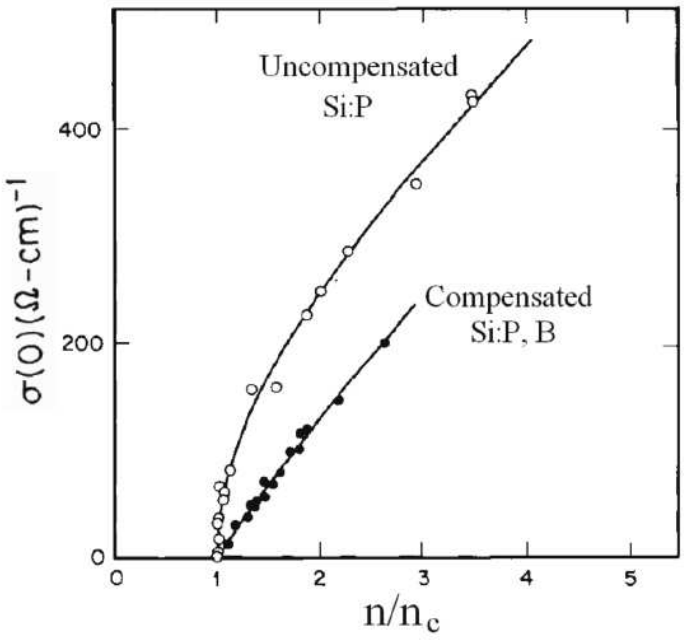

Figure 1.5: Conductivity of uncompensated and compensated Si:P as a function of carrier concentration. Figure is from [152]. Demonstrating the existence of a critical concentration of impurities n_c at which the conductivity vanishes.

1.2.3 Superconductor to Insulator Transition

In Sec.1.1.3, I reviewed the basic theory of clean superconductors and disorder can have profound impact on these properties such the critical temperature T_c which will be a particular focus. Based on the BCS theory described in Sec.1.1.3, at least in the weak disorder limit, T_c is presumed to be unaffected by disorder and this is famously known as Anderson's Theorem[22].

The question of how superconductivity is destroyed, just as how metallic behavior is destroyed,

is an active area of research. The complication from the systems discussed above is that now there can be three phases that can interact in complicated and surprising ways: metal, insulator and superconductor. For example, in Fig.1.6 is an example of two possible scenarios.

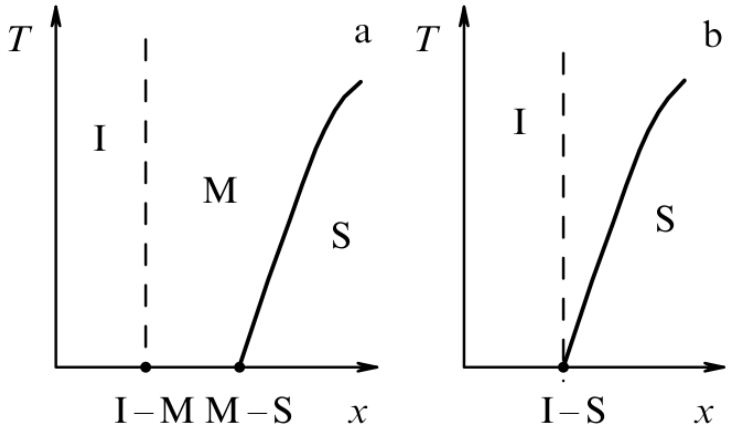

Figure 1.6: Two examples of a phase diagram of a superconducting system where x is some tuning parameter (film thickness, disorder or magnetic field). The phases are metal (M), Insulator (I) and Superconductor (S). The Insulator transition is denoted with a dashed line to indicate that the insulating phase is only strictly defined for $T = 0$. Figure from [7].

An example of the first scenario is provided in Fig.1.7 and also demonstrates the predicted suppression of T_c from theory

An experiment on FeSe is provided in Fig.1.9. This is an example of a direct superconductor to insulator transition without an intermediate metallic phase. In addition, it also demonstrates this SIT can be invoked with a perpendicular magnetic field: when the superconductivity is destroyed in a film, scaling theory predicts that it should be an insulator and that is what is observed.

It has been argued that the enhancement of superconductivity could be due to the presence of disorder[192] such as in experiments related to Al films such as shown in Fig.1.10. This demonstrates that the exact mechanism behind the influence of disorder and weak localization and T_c in superconductors is still not well understood: some materials can behave drastically different in the presence of disorder. In addition, disordered thin Al films can also realize novel phases, such as a disordered Fulde-Ferrell-Larkin-Ovchinnikov (FFLO) phase[15] (see Fig.1.11).

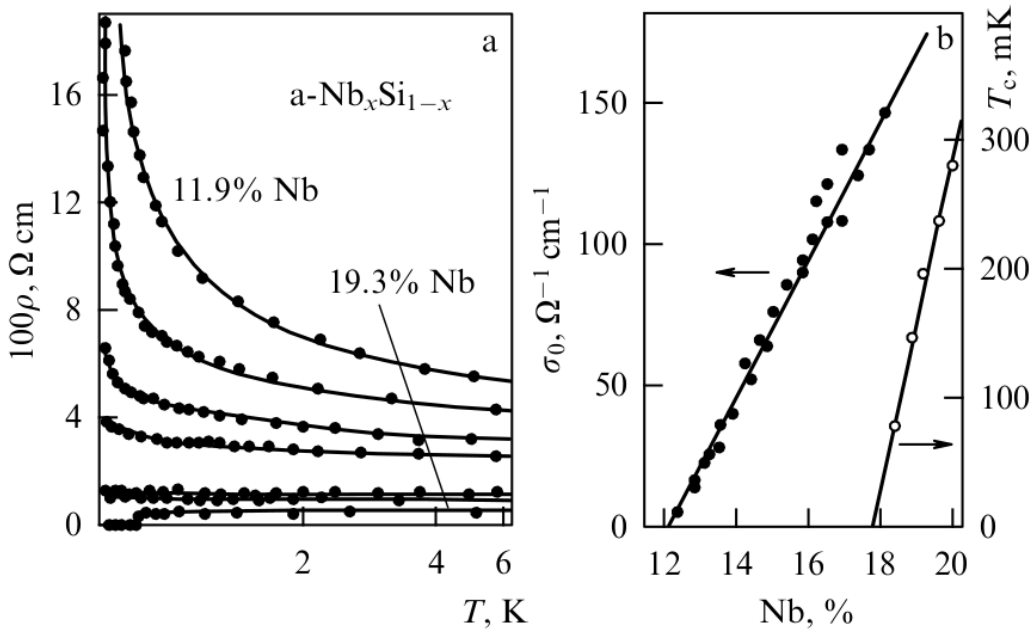

Figure 1.7: Superconducting-Insulating transition in Nb_xSi_{1-x} demonstrating an intermediate metallic phase between insulating and superconducting phase (a). At low temperature and 19.3% Nb doping, the material is superconducting (vanishing resistivity) and goes from finite values (metallic) to exponentially increasing (insulating). Also notable is the suppression of T_c in accordance with theory [8](b). Figure from [7]

1.3 Theory of Disordered Systems

There are multiple ways that disorder can be present in materials. In Fig.1.12, an example of substitutional disorder and off-diagonal disorder is given. There exist other forms of disorder such as structural disorder which deviates from the lattice structure (found in amorphous semiconductors), but that is not a focus of this work. For a perfectly ordered lattice, the Schrödinger equation admits plane wave solutions with the periodicity of the lattice and the electron energies form bands of allowed and forbidden energies, as discussed above. The details of the band structure are given by the symmetries of the lattice (for example, the lattice in Fig.1.12 would have the symmetries of a square 2d lattice). A material can be classified as a metal or insulator as to whether or not there are available states for electrons that can participate in transport: the impact on conductivity (whether or not the material is a metal or insulator) is determined solely by translational symmetry

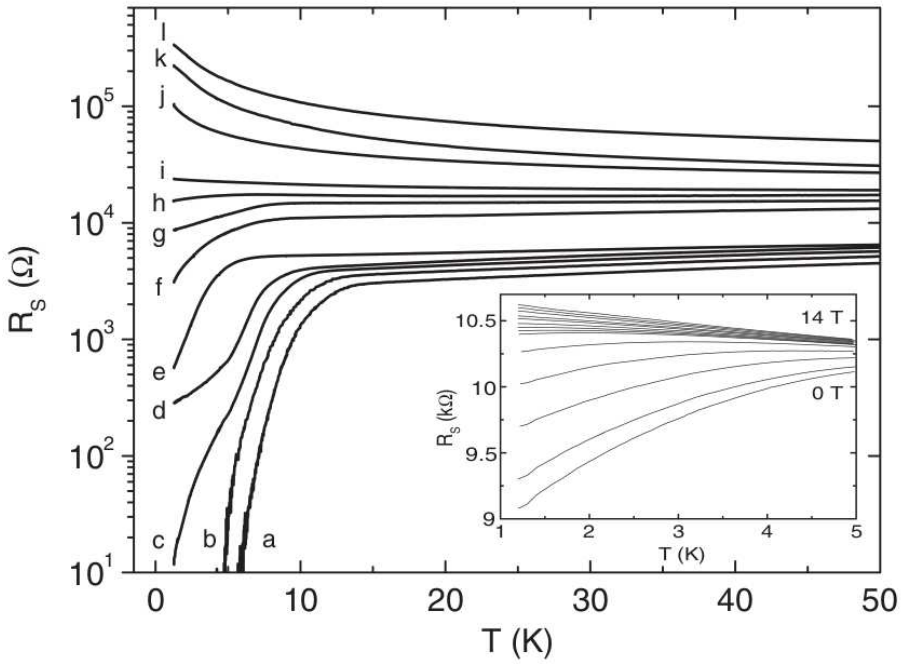

Figure 1.8: SIT in a thin film of FeSe. Shown is the sheet resistance as a function of T for various film thickness: $a \to l$ is decreasing in film thickness from 1300nm to 1nm. The inset shows the sheet resistance a film of thickness 30nm (which is close to film f with 29nm) and each curve shows increasing perpendicular magnetic field from $0T \to 14T$. Data from [4].

and any other symmetries of the lattice.

There is another way the transport properties of a material can be impacted and that is by spatial localization of electrons. Rather than from band theory as described above, a material can be an insulator if the electrons able to carry current become physically confined to a region of the lattice and one way this may happen is by disorder. For example, the red impurity sites in Fig.1.12 may be very large potential wells and so electrons will be more likely to be bound to them, and so the strength of disorder could be considered the concentration of impurities which is something that can be tuned in the lab. Naturally, being able to control the conductivity of a material has significant technological applications and effect of disorder on materials has been well studied experimentally.

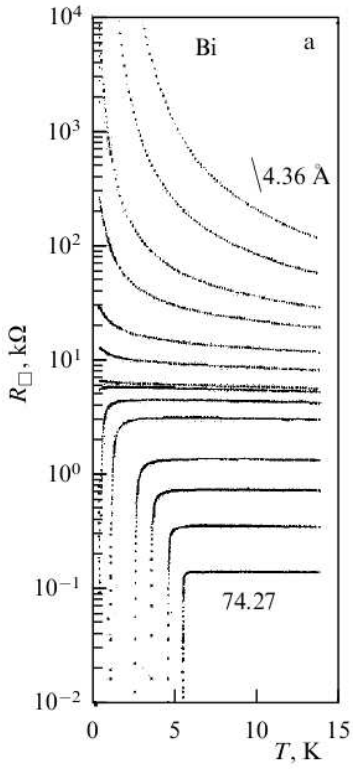

Figure 1.9: SIT in thin Bi films that also demonstrates the suppression of T_c from increasing disorder. [5]

1.3.1 Anderson Localization Theory

To be explicit, we will be considering the Anderson model which is given by the Hamiltonian

$$H = -t \sum_{<i,j>} (c_i^\dagger c_j + \text{h.c.}) + \sum_i V_i c_i^\dagger c_i \tag{1.15}$$

which is just the tight binding Hamiltonian given in Eq. 1.4 with the addition of an onsite potential V_i that pulled from some probability distribution $P(V_i)$ which models the addition of disorder.

The Anderson Transition is a metal-insulator transition in a non-interacting disordered electron gas at T=0. It was first hypothesized by Anderson[147] and is due to the coherent back scattering of time reversed electronic states for strong disorder. The coherent backscattering effect leads to a decrease in the classical diffusion constant and is most effective in systems with time reversal invariance. To see this we consider the forward scattered path (solid black) and the back scattered

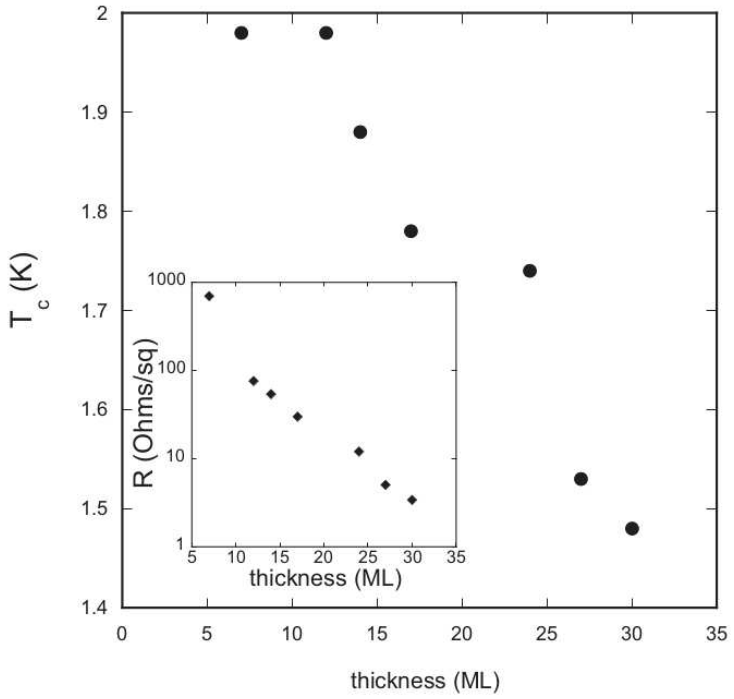

Figure 1.10: Superconducting transition temperature T_c as a function of mono layer film thickness in an epitaxial Al film. In this experiment, the thickest film of 30ML corresponds to a film thickness of 72Å which is much less than the superconducting coherence length of $\xi \sim 300$Å, making them effectively 2D superconductors. Inset shows that indeed as the film thickness is decreased the material is becoming two dimensional and the effects of weak localization are increasing. However, as the T_c saturates but the sheet resistance continues to increase one can not purely attribute this behavior to weak localization. Figure from [193].

path (dotted path) in Fig.1.13). We consider the return probability for an electron starting from position 0 to return in some time t

$$P_0(t) = \left| \sum_{i \in S} A_i(t) \right|^2 \tag{1.16}$$

where $A_i(t)$ is the probability amplitude that an electron following an i'th scattering path to return in time t. The reason for the sum is the fact we must sum over all possible paths. We now split all these paths into two subsets: on set will denote the forward scattered paths (S^f) and the

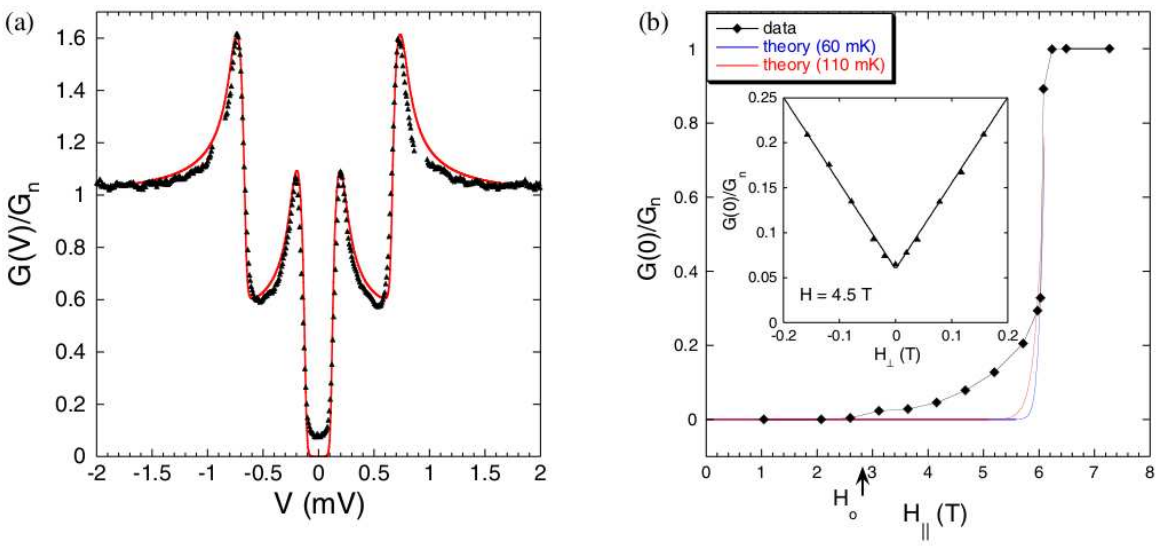

Figure 1.11: Tunneling conductance G for a superconducting Al film at $100mK$ in a parallel magnetic field. The discrepancy with theory is attributed to a disordered FFLO phase which is contributing states in the predicted gap from BCS theory (a). Also shown is the application of a parallel magnetic field also deviates from predicted theory (b). Figure from [15].

corresponding time reversed back scattered paths (S^b). we now have

$$P_0(t) = \left| \sum_{i \in S^f} A_i(t) + \sum_{i \in S^b} A_i(t) \right|^2 \tag{1.17}$$

$$= \left| \sum_{i \in S^f} A_i^f(t) + A_i^b(t) \right|^2 \tag{1.18}$$

where $A_i^f(t)$ ($A_i^b(t)$) denotes probability amplitude for forward (back) scattering. The modulus is expanded and the cross (interference) terms can be separated out

$$P_0(t) = \sum_{i \in S^f} \left| A_i^f(t) + A_i^b(t) \right|^2 + \left(\text{Interference terms for } \sum_{i \neq j \in S^f} \right). \tag{1.19}$$

From cancellation of constructive and destructive interference, the interference terms vanish and we

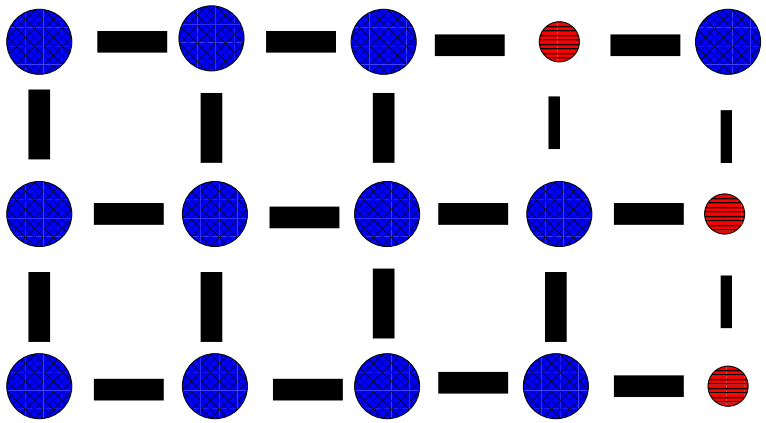

Figure 1.12: A cartoon of disorder realized on a lattice. The left region of the lattice is perfectly ordered. One type of disorder is adding red "impurities" with different onsite potentials in random places of the lattice, so called *diagonal* disorder. Another is changing the coupling strength between atoms denoted by the size of the rectangles that describes the ability of the electrons to hop around the lattice, so called *off-diagonal* disorder.

now invoke time reversal invariance so $A_i^f(t) = A_i^b(t) = A_i(t)$ and arrive at

$$P_0(t) = 4 \sum_{i \in S^f} |A_i(t)|^2 \tag{1.20}$$

which is twice the classical return probability which is obtained from Eq.1.16 by ignoring any cross terms and so $P_0(t) = \sum_{i \in S} |A_i(t)|^2 = 2 \sum_{i \in S^f} |A_i(t)|^2$. This reduction of the classical diffusion constant is refered to as the weak localization effect and is from the phase coherence of the paths f and b as mentioned in Sec.1.2.1. For sufficiently strong disorder (which increases the back scattering), this weak localization can lead to states that would be extended classically (as is energy E_2 in Fig.1.14) to be localized in space with a characteristic length scale λ called the localization length (Fig.1.15).

To appreciate the effect of the time reversal invariance, we now consider the addition of a magnetic field. A magnetic field introduces a magnetic flux Φ_i to the probability amplitude

$$A_i^f(t) = A_i(t) e^{\frac{2\pi\Phi_i}{\Phi_0}} \tag{1.21}$$

where Φ_0 is a flux quantum $\Phi_0 = hc/e$ and the effect of time reversal is

$$A_i^b(t) = A_i(t)e^{-\frac{2\pi\Phi_i}{\Phi_0}}. \tag{1.22}$$

Therefore, the return probability in the presence of a magnetic field (analog of Eq.1.20) is

$$P_0(t) = 4\sum_{i\in S^f} |A_i(t)|^2 \cos^2\left(\frac{2\pi\Phi_i}{\Phi_0}\right) \tag{1.23}$$

which is less than Eq.1.20 and demonstrates the negative magnetoresistance effect.

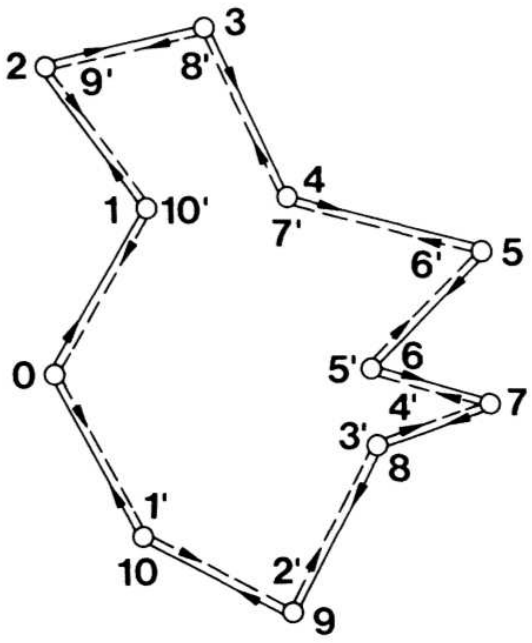

Figure 1.13: Coherence between a forward scattered path and its time reversed path. Figure from [20].

1.3.2 Scaling Theory

The basic concept of scaling is that the results are independent of any local details of the physical model. The transition only depends on symmetries of the lattice and dimensionality it will not depend on the form of the distribution $P(V_i)$, strength of couplings t_{ij} etc. that appear in

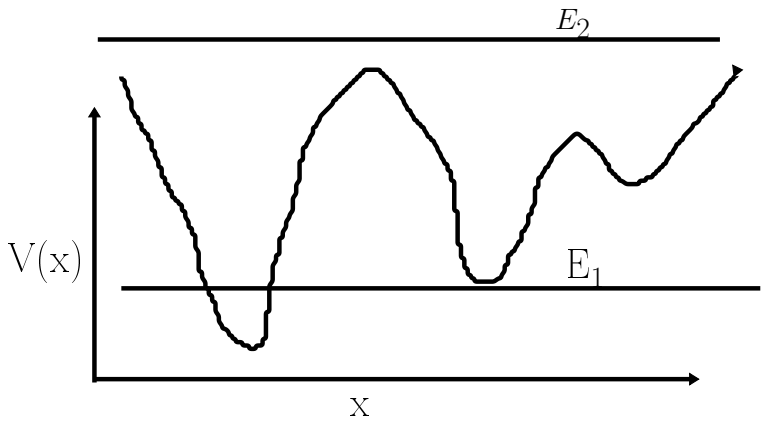

Figure 1.14: A potential in space created by some realization of disordered potentials. A state with E_1 would be localized in the region of the lowest potential well (but could possibly tunnel as well). A state with E_2 would always be extended classically, but quantum interference effects can allow this state to be localized.

the Hamiltonian Eq. 1.15. This behavior is encapsulated by the so called renormalization group originally proposed by Kenneth Wilson. Any theory is parametrized by some set $\{g_i\}$ of coupling constants and the basic idea of the renormalization group is to consider how these coupling constants will change as a function of coarse graining or equivalently changes in length scale (system size) of the problem. For the case of only a single (for simplicity) coupling constant g we write the β function as

$$\beta(g) = \frac{dg}{d\log b} \tag{1.24}$$

where b corresponds to some length scale of the problem: either the system size or some coarse graining that rescales the system by a length scale b. The β-function is defined in this way as we are interested in how the system behaves in relation to a change in length scale and its effect on the relevant coupling constants. Any point where $\beta(g) = 0$ we call a fixed point and it corresponds to a point where the system is scale invariant (any coarse graining of the system has no effect) and thus experiences a transition. This can also be interpreted from the perspective of fractals which have a self similar structure, meaning the fractal will have the same structure under any dilation of the structure.

We now apply the above to the Anderson model. We consider a d dimensional metal with linear

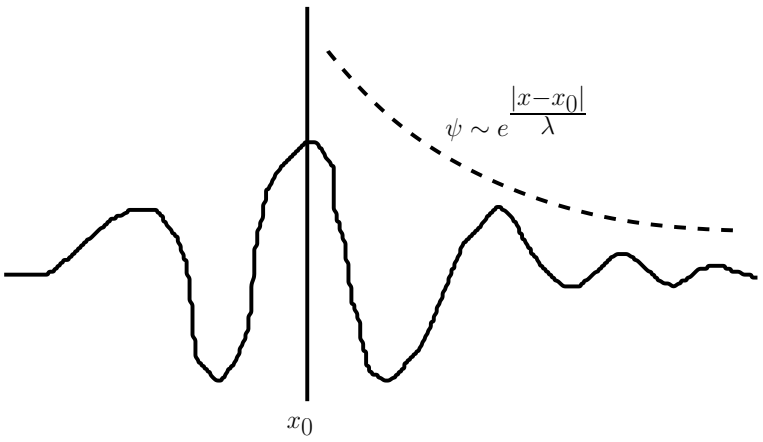

Figure 1.15: A localized state of position x_0 that decays exponentially with a characteristic localization length λ.

size L that has conductance $G(L)$ and then with the β-function considered by[47]

$$\beta(g) = \frac{d \log g}{s \log L} = \frac{L}{g}\frac{dg}{dL} \tag{1.25}$$

where g is the dimensionless conductance defined as $g = \hbar G(L)/e^2$. This function is used as it was discovered that the only single relevant coupling constant for the Anderson transition is the conductivity[79]. From Ohm's law, we know for a metal that $G(L) \propto L^{d-2}$ and an insulator with have a small conductance $G(L) \propto e^{-L/\xi}$. This leads to the following asymptotic behavior

$$\beta(g) \sim \begin{cases} d-2 & \text{metallic (large g)} \\ \log g & \text{insulating (small g)} \end{cases} \tag{1.26}$$

and thus the renormalization flows in Fig.1.16. It is worth noting that although the above expression might imply a fixed point in the limit $g \to \infty$ for the case $d = 2$, but a more careful treatment of the perturbation series leads to the higher order correction

$$\beta(g) = d - 2 - \frac{a}{g} + \cdots \tag{1.27}$$

and so the next term beyond order $d-2$ is negative and so, although this leads to rather special be-

havior that is referred to as *marginal* for $d = 2$, there is no localization transition in two dimensions. The above scaling arguments are incredibly powerful, implying that even the smallest amount of disorder will always lead to localization in dimensions less than three.

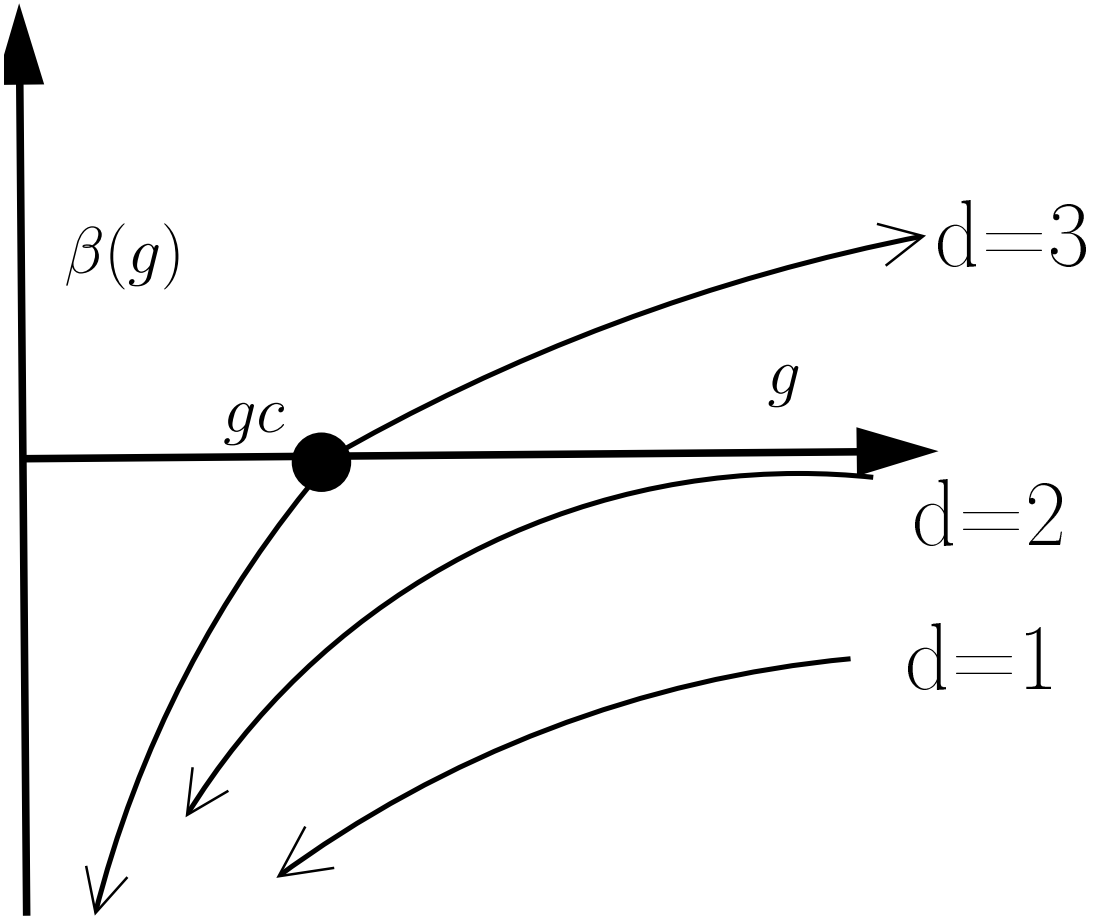

Figure 1.16: Renormalization flows for Anderson transition. The existence of the fixed point gc in only $d = 3$ shows that the metal insulator transition exists only in three dimensions and all states are exponentially localized in $d = 1$ and $d = 2$.

1.3.3 Model for Dirty Superconductors

As overviewed in Sec.1.2.3, disordered superconductors have received much experimental attention and display a wide range of interesting behaviors. Specifically mentioned was the enhancement of the the critical temperature of superconductivity with disorder and one proposal is that this is due to multifractility of the wavefunction[171] and other theoretical studies[43] have proposed it. This

motivates the simulation of models of disordered superconductors and the multifractal study that will appear in Chapter 4.

The analog of the BCS Hamiltonian for disordered systems (without translational invariance and so k is no longer a good quantum number) is

$$H = \sum_{<ij>\sigma} (c^\dagger_{j\sigma} c_{i\sigma} + \text{h.c.}) - U \sum_i n_{i\uparrow} n_{i\downarrow} + \sum_i \mu_i n_{i\sigma} \tag{1.28}$$

where $n_{i\sigma} = c^\dagger_i c_i$ and U is the strength of the attractive Hubbard interaction and $\mu_i = \mu + v_i$ is an on-site chemical potential where v_i is the disorder potential. We consider only box disorder. We introduce a MF pairing field for each site to decouple the interaction in the paring channel as

$$-U c^\dagger_{i\uparrow} c^\dagger_{i\downarrow} c_{i\downarrow} c_{i\uparrow} \rightarrow \Delta_i c^\dagger_{i\uparrow} c^\dagger_{i\downarrow} + \text{h.c.} \tag{1.29}$$

The Hamiltonian in Eq. 1.28 can then be put into $2N \times 2N$ matrix form and can be solved by diagonalization and determining the fields Δ_i self consistently. This leads to the Bogoliubov - De Gennes (bdg) Hamiltonian

$$H_{bdg} = \begin{pmatrix} \hat{t}_{ij} - \mu + V_i & \hat{\Delta}_i \\ \hat{\Delta}_i & -\hat{t}_{ij} + \mu - V_i \end{pmatrix}$$

where $\hat{\Delta}_i$ is a diagonal sub-matrix. Diagonalization of the bdg Hamiltonian leads to the bogolon wavefunction with amplitudes $|\psi_i|^2 = |u_i|^2 + |v_i|^2$ for a site i. Alternatively, the pairing matrix $\hat{\Delta}_i$ need not be determined self-consistently or be diagonal in which case it may take a more exotic form which will be considered in Chapter 4.

1.4 Thesis Structure

Chapter 2 will review the numerical methods that are implemented to study disordered systems. Chapter 3 will describe the work I did on off-diagonal disordered systems which validated mobility edge predictions of Typical Medium Dynamical Cluster Approximation (TMDCA) against TMM

calculations. Similiarly, Chapter 4 will present the work I did on the validation the multiband disordered systems, demonstrating the ability to extend TMDCA to real materials (that exibit both off-diagonal disorder and multiple bands in practice). Finally, Chapter 5 will show how established methods of multifractal analysis can be applied to study localization in a model of a disordered gapless superconductor.

Chapter 2

Numerical Methods for Disordered Systems

In this chapter, I give an overview of the various numerical methods of studying disordered systems.

2.1 Transfer Matrix Method

The Schrödinger equation $H\psi = E\psi$ for the Hamiltonian in Eq.1.15 is written in an iterative fashion[150]

$$\mathbf{t}_{n,n+1}\psi_{n+1} = (E - \mathbf{H}_n)\psi_n - \mathbf{t}_{n,n-1}\psi_{n-1} \tag{2.1}$$

where ψ_n denotes the wavefunction for slice n of the quasi-1D system of width M and length L (see Fig.2.1) and $\mathbf{t}_{n,m}$ is a matrix that describes the coupling between layers n and m. This can be written in terms of the transfer matrix

$$T_n = \begin{pmatrix} t_{n,n+1}^{-1}(E - H_n) & -\mathbf{t}_{n,n+1}^{-1}\mathbf{t}_{n,n-1} \\ 1 & 0 \end{pmatrix} \tag{2.2}$$

as

$$\begin{pmatrix} \psi_{n+1} \\ \psi_n \end{pmatrix} = T_n \begin{pmatrix} \psi_n \\ \psi_{n-1} \end{pmatrix}. \tag{2.3}$$

It is well known[98] how the matrix product

$$\tau_N = \prod_i^N T_i. \tag{2.4}$$

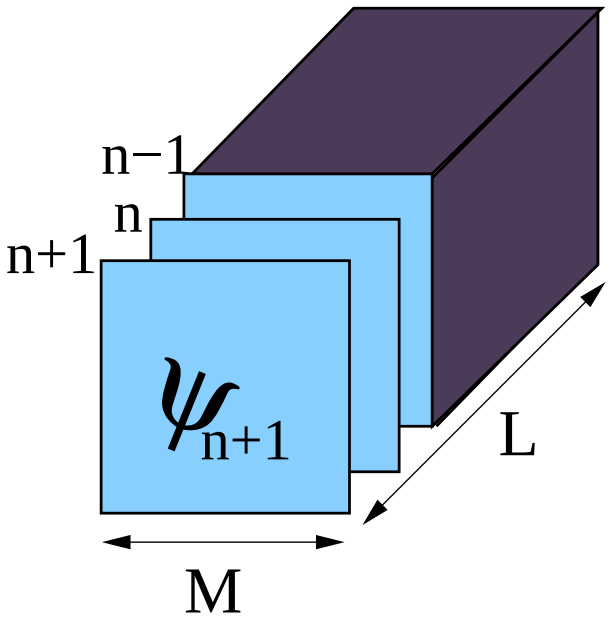

Figure 2.1: The wavefunction ψ_n for slice n a quasi-1D system with width M and length L.

is related to the decay of the wavefunction for a localized state

$$\psi \sim \exp(-\gamma|x - x_0|). \tag{2.5}$$

And so the algorithm proceeds as follows:

1) Generate Transfer Matrix

2) Multiply

3) Orthogonalize every 2-5 steps with a QR decomposition

4) Accumulate the Matrix norms b_n which are the diagonal elements of the R matrix

5) Update the localization length $\gamma_n = \gamma_{n-1} + \log b_n$

The slowest decaying γ_n is then the γ in Eq.2.5 or the inverse of the localization length λ. The Kramer-MacKinnon scaling parameter[149] can then be calculated as $\Lambda = \lambda/M$. A localized state has a well defined λ for a particular disorder strength, therefore as M is increased Λ will decrease for localized states. For an extended state, the localization length will be larger than M and so Λ

must increase as a function of M. At the critical disorder strength W_c, Λ will be scale invariant and this is how the transition can be found. In addition, the correlation length ξ exponent ν defined by the assumption the the correlation length decays as

$$\xi \sim \frac{1}{|W - W_c|^\nu} \tag{2.6}$$

can be determined from the scaling ansatz

$$\Lambda = f(M/\xi) \tag{2.7}$$

i.e. all the data points should fall on the curve f. This is accomplished by Taylor expanding f and least squares fitting is used to fit W_c, ν and the Taylor coefficients.

2.2 Quantum Cluster Methods

2.2.1 Dynamical Cluster Approximation (DCA)

All mean field treatments of disordered systems fail to capture Anderson localization. For instance, while the Coherent Potential Approximation (CPA)[32] can provide accurate results for densities of states, it does not capture any mobility edge behavior. Even systematic corrections to the CPA by the Dynamical Cluster Approximation (DCA)[72][73] fail to capture localization[74]. This can be understood from Fig.2.2

2.2.2 Typical Medium Dynamical Cluster Approximation (TMDCA)

We saw above that a theory relying on defining the effective medium via linear averages will fail to describe localization. Therefore, one must consider the *typical* value of the hybridization as this *can* become zero (and hence localize the electron) even if there are some sites with large hybridization. As the typical hybridization is determined by the typical density of states, it is reasonable to assume the typical density of states will function as the order parameter for the localization transition. This is the argument for typical medium theory[100] where the bath is not determined by average

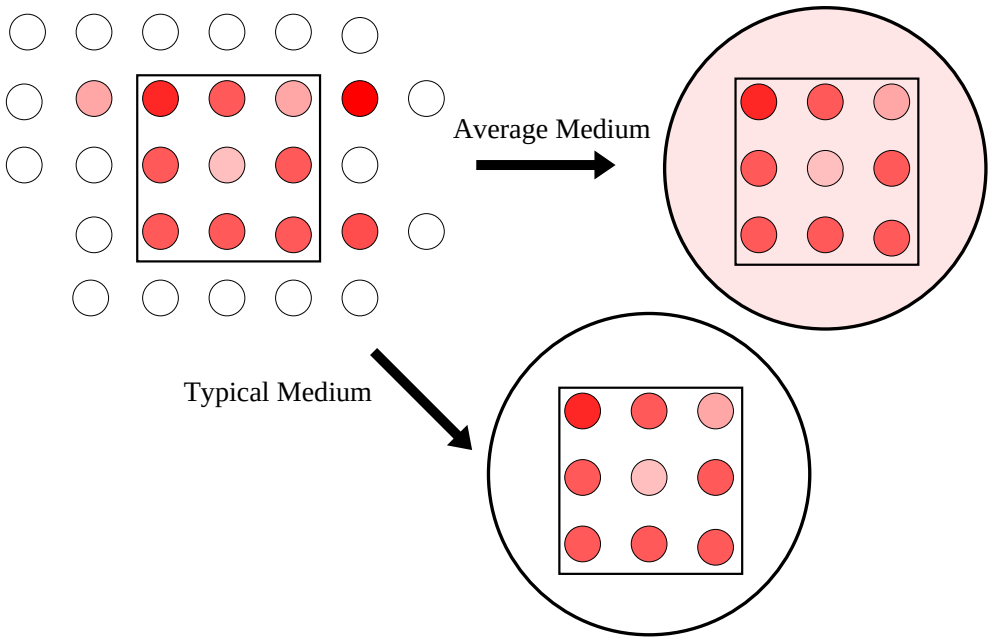

Figure 2.2: Considering the average hybridization of an electron on a site with the neighboring sites, a linear average will always result in a finite hybridization and so the electron can always escape to other lattice sites which will produce a metallic solution.

quantities, but rather typical quantities which are approximated by geometric averages. This is also motivated by considering the distribution of the local density of states as in Fig.2.4. Unfortunately, using the true typical value could only be used if the distribution were known *a priori* which a simulation would not have access to. However, because the distribution is log-normal the geometric average of the density of states provides a good approximation to the typical value or

$$\rho_g(\omega) = e^{\langle \log \rho \rangle} \approx \rho_{typ}(\omega). \tag{2.8}$$

The next step would then to develop, just like with the extension of the CPA, a Typical Medium Dynamical Cluster Approximation (TMDCA) where the usual Dynamical Cluster Approximation (DCA) embedding is replaced by a typical one (approximated by the geometric mean) as seen in Fig.2.3.

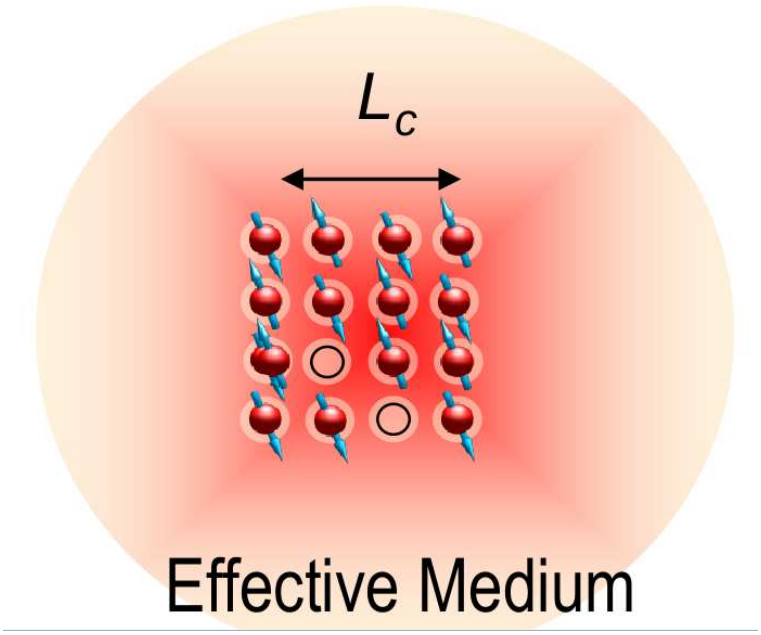

Figure 2.3: Picture of DCA embedding for a cluster of 16 sites with linear cluster length L_c. Electrons on cluster hybridize with the effective medium. For TMDCA the typical hybridization is used instead for reasons described in the text. Figure is taken from [12].

2.3 Multifractal Analysis

We want to analyze the multifractal properties of some local variable x_i. In the case of the Anderson Model, it is the wave function amplitude $x_i = |\psi_i|^2$. To do so, we coarse grain this variable by a box length scale $\ell < L$ and define the coarse grained quantity

$$\mu_{b(\ell)} = \sum_{i \in b(\ell)} x_i \tag{2.9}$$

and the associated singularity strength

$$\tilde{\alpha} = \frac{\log \mu}{\log \lambda} \tag{2.10}$$

were λ represents the coarse graining $\lambda = \ell/L$ and the tilde denotes that it is defined for a fixed value of λ (in the limit of infinite system size or $\lambda \to 0$, $\tilde{\alpha}$ becomes the "true" multifractal exponent α). This comes from the assumption that the "mass" in different boxes grows with different exponents i.e. $\mu_{b(\ell)} \sim (\ell/L)^{\alpha}$ where each α corresponds to a fractal dimension $f(\alpha)$ that gives how the number

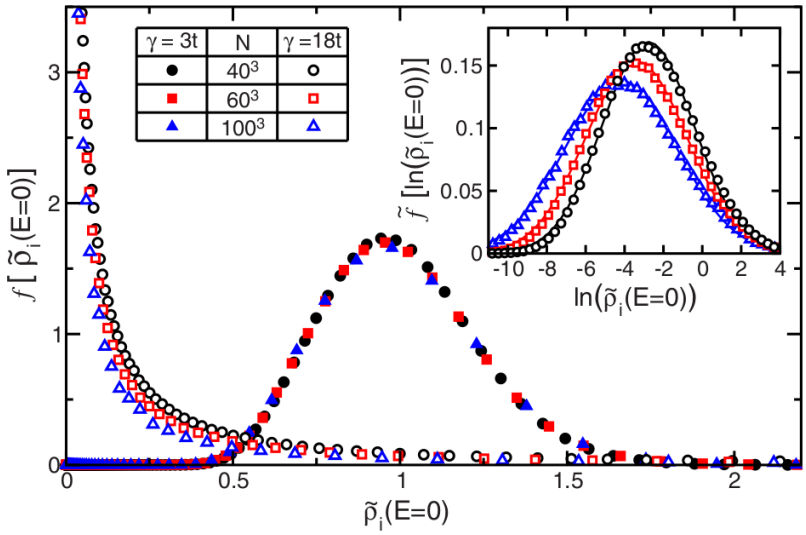

Figure 2.4: Distribution of the density of states for small $\gamma = 3t$ disorder and large $\gamma = 18t$ disorder. In the small disorder regime, the distribution is gaussian and largely independent of system size. Past the transition, in the localized regime the distribution is log-normal and it can be seen that as the system size is increased that the typical value is approaching zero. This motivates the usage of the typical value as an order parameter for the transition. Figure is taken from [31].

of boxes for that α scales, $N(\alpha) \sim (\ell/L)^{-f(\alpha)}$. See Fig. 2.5.

In general, the q-th moments of α are

$$\tilde{\alpha}_q = \frac{\langle \sum_k \mu_k^q \log \mu_k \rangle}{\langle \sum_k \mu_k^q \rangle \log \lambda} \tag{2.11}$$

and the procedure to perform the finite size scaling of these moments and fit the critical parameters will be described in Sec.5.2.3 .

α_1	α_2	α_3
α_4	α_4	α_2
α_1	α_1	α_1

α_1	$f(\alpha_1) = A$
α_2	$f(\alpha_2) = B$
α_3	$f(\alpha_3) = C$
α_4	$f(\alpha_4) = D$

Figure 2.5: Schematic picture of $\alpha - f(\alpha)$ pairs. A system of characteristic length L is divided into boxes of length ℓ. The largest fractal dimension would correspond to A as it covers the most boxes. Figure taken form [41]

It has been established that at the critical point the eigenstates of the 3D Anderson model exhibit multifractality [158]. Although interesting, the multifractal analysis depends on knowing the critical point a-priori as the multifractal exponents are defined only at the critical point. However, it has been shown that a very similar analysis can be made on the distributions of these multifractal exponents for finite λ(see Fig.2.6) which allows for a finite size analysis[167] similar to that described in Sec.5.2.2 for Λ. This provides another way of determining the critical disorder strength, but with additional information of the spatial variation of the wavefunction.

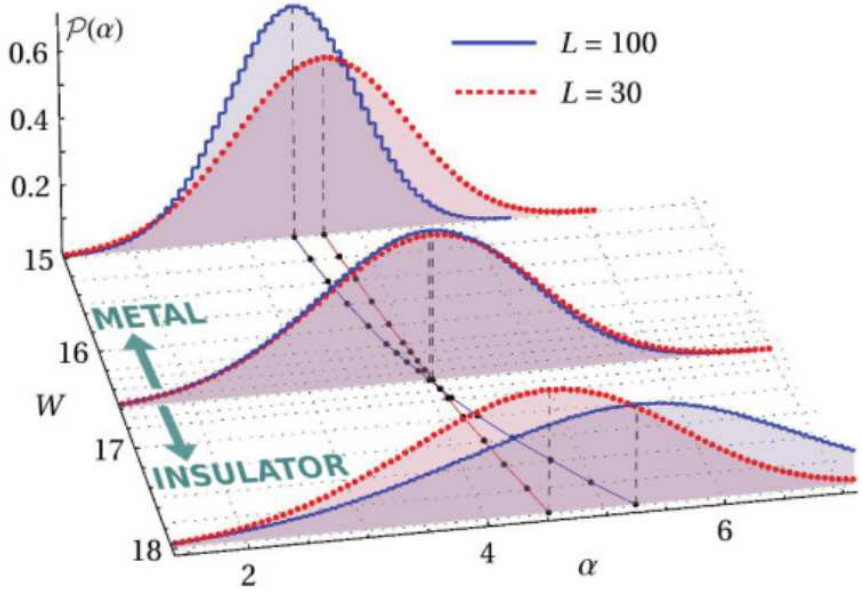

Figure 2.6: Evolution of the distribution of wave function intensities for Anderson Model for $\lambda = \ell/L = 0.1$. Here $\alpha = \log \mu_k / \log \lambda$ where $\mu_k = \sum_{i \in k} |\psi_i|^2$ where the sum denotes a sum over points i in box k. The crossing of the typical value in the $W - \alpha$ plane that indicates the critical disorder strength and shows this quantity can be used to determine the critical parameters. Figure taken from [167]

Chapter 3

TMDCA Study of Off-diagonal Disorder

Previous work on TMDCA had been restricted to purely diagonal or local disorder[105]. The work in this chapter [1] will show how even non-local disorder correlations can be correctly accounted for within the TMDCA by comparisons with the Kernel Polynomial Method for the density of states and the TMM for the trajectory of the mobility edge. My contribution to this result was primarily the TMM data in Fig. 3.7 and Fig. 3.8 which shows the evolution of the mobility edge. I developed a large scale perfectly parallel code over energy and disorder strength and calculated the Kramer-MacKinnon scaling parameter for the system lengths and widths described in the captions (see Sec.5.2.2 for description of TMM). I found the critical point by finite size scaling analysis of the Kramer-MacKinnon scaling parameter as described in Sec5.2.2.

[1] This chapter includes previously published work published by American Physical Society and appears in [37] and is reproduced here under term 3 of Author's rights of the APS Transfer of Copyright Agreement to "The right to use all or part of the Article, including the APS-prepared version without revision or modification ... for educational or research purposes."

3.1 Introduction

Disorder which is inevitably present in most materials can dramatically affect their properties [101, 102]. It can lead to changes in their electronic structure and transport. One of the most interesting effects of disorder is the spatial confinement of charge carriers due to coherent backscattering off random impurities which is known as Anderson localization [103, 47]. Despite progress over the last decades, the subject of Anderson localization remains an active area of research. The lack of quantitative analytical results has meant that numerical investigations [104, 49, 50, 51, 52, 53, 54] have provided a significant role in understanding the Anderson transition [55, 98, 57].

The simplest model used to study the effects of disorder in materials is a single band tight binding model with a random on-site disorder potential [58]. Such a model is justified when the disorder is introduced by substitutional impurities, as in a binary alloy. The substitution of host atoms by impurities only leads to changes of the local potential on the substitutional site and, on average, does not affect the neighbors [58, 59]. In this situation, the disorder appears only in the diagonal terms of the Hamiltonian and hence is referred to as diagonal disorder. However, when the bandwidth of the dopant is very different from the one of the pure host, such substitution results not only in the change of the local potential but may also affect the neighboring sites [58]. Consequently, a simple model to capture such effects should include both random local potentials and random hopping amplitudes which depend on the occupancy of the sites. The dependence of the hopping amplitude on the disorder configuration is usually referred to as off-diagonal disorder. It is apparent that a proper theoretical description of realistic disordered materials [58, 60, 62, 61, 63] (for e.g. many substitutionally disordered alloys and disordered ferromagnets) requires the inclusion of both diagonal and off-diagonal randomness. While the role of the diagonal disorder has been extensively studied over the last several decades [64], the effect of off-diagonal disorder is not well studied, although the effect is expected to be different. It has been shown [65, 61] that off-diagonal randomness can lead to the delocalization of the states near the band-center. Also recently, there has been a growing interest in the effect of the off-diagonal randomness in graphene systems, where studies show that different types of disorder can induce different localization behavior. [67, 68, 66]

The coherent potential approximation (CPA) is a widely used single site mean field theory for

systems with strictly diagonal disorder [59]. Blackman, Esterling and Berk (BEB) [69] have extended the CPA to systems with off-diagonal disorder. However, being single-site approximations, the CPA and the BEB theories neglect all disorder induced non-local correlations.

There have been a number of attempts to develop systematic nonlocal extensions to the CPA. These include cluster extensions such as the molecular coherent potential approximation (MCPA) [70, 71], the dynamical cluster approximation (DCA) [72, 73, 74], etc. Self-consistent mean field studies of off-diagonal disorder have been conducted by a number of authors [75, 76, 77, 71]. However, all these studies have been performed at the local single-site BEB level. To include the effects of off-diagonal disorder, Gonis [70] extended the Molecular CPA, which uses a self-consistently embedded finite size cluster to capture non-local corrections to the CPA. However, he criticized the MCPA for violating translational invariance and other critical properties of a valid quantum cluster theory [58, 105]. In order to take into account such non-local effects on off-diagonal disorder models while maintaining translational invariance, we extend the BEB formalism using the DCA scheme [72, 73, 74].

While the CPA, DCA, and BEB have shown to be successful self-consistent mean-field theories for the quantitative description of the density of states and electronic structure of disordered systems, they can not properly address the physics of Anderson localization. These mean field approaches describe the effective medium using the average density of states which is not critical at the transition [79, 105, 55, 80]. Thus, theories which rely on such averaged quantities will fail to properly characterize Anderson localization. As noted by Anderson, the probability distribution of the local density of states must be considered, focusing on the most probable or the *typical* value [103, 81]. Close to the Anderson transition, the distribution is found to have very long tails characteristic of a log-normal distribution[53, 82, 106]. In fact, the distribution is log-normal up to ten orders of magnitude [84] and so the typical value [85, 107, 106, 87] is the geometrical mean. Based on this idea, Dobrosavljević *et. al.* [100] formulated a single site typical medium theory (TMT) for the Anderson localization. This approximation gives a qualitative description of the Anderson localization in three dimensions. However, it fails to properly describe the trajectory of the mobility edge (which separates the extended and localized states) as it neglects non-local corrections and

so does not include the effects of coherent backscattering [89]. It also underestimates considerably the critical strength of the disorder at which the localization happens. In addition, TMT is only formulated for diagonal disorder.

Recently, by employing the DCA within the typical medium analysis, we developed a systematic Typical Medium Dynamical Cluster Approximation (TMDCA) formalism. [105] The TMDCA provides an accurate description of the Anderson localization transition for modest cluster sizes in three-dimensional models with diagonal disorder while recovering the TMT for a one-site cluster. In this work, we generalize our recently proposed TMDCA scheme to address the question of electron localization in systems with both diagonal and off-diagonal disorder.

In this paper, to go beyond the local single-site CPA-like level of the BEB formalism, we employ the DCA [72, 73, 74] scheme which systematically incorporates non-local spatial correlation effects. We first present an extension of the DCA for systems with both diagonal and off-diagonal disorder. Comparing our single site and finite cluster results, we demonstrate the effect of non-local correlations on the density of states and the self-energy.

Up to now, there exist no typical medium formalism for systems with off-diagonal disorder. So far, the typical medium analysis has been applied to systems with only diagonal disorder [100, 105]. In this paper, we develop a typical medium dynamical cluster approximation formalism capable of characterizing the localization transition in systems with both diagonal and off-diagonal disorder. We perform a systematic study of the effects of non-local correlations and off-diagonal randomness on the density of states and electron localization. By comparing single site and finite cluster results for the typical density of states and the extracted mobility edges, we demonstrate the necessity of including the non-local multi-sites effects for proper and quantitative characterization of the localization transition. The results of our calculations are compared with the ones obtained with other numerical methods for finite size lattices, including exact diagonalization, kernel polynomial, and transfer matrix methods.

The paper is organized as follows: following the Introduction in Sec. 5.1 we present the model and describe the details of the formalism we used in Sec. 4.2. In Sec. 3.3.1 we present our results of the average density of states for both diagonal and off-diagonal disorder cases. In Sec. 3.3.1

we consider the effects of diagonal and off-diagonal disorder on the typical density of states, from which we extract the mobility edges and construct a complete phase diagram in the disorder-energy parameter space. We summarize and discuss future directions in Sec. 5.4.

3.2 Formalism

3.2.1 Dynamical cluster approximation for off-diagonal disorder

The simplest model widely used to study disordered systems is the single band tight binding Hamiltonian

$$H = -\sum_{<i,j>} t_{ij}(c_i^\dagger c_j + h.c.) + \sum_i v_i n_i, \tag{3.1}$$

where disorder is modeled by a local potential v_i which is a random variable with probability distribution function $P(v_i)$. We will focus on the binary disorder case, where some host A atoms are substituted with B impurities with a probability distribution function of the form

$$P(v_i) = c_A \delta(v_i - V_A) + c_B \delta(v_i - V_B), \tag{3.2}$$

where $c_B = 1 - c_A$. For the diagonal disorder case when the bandwidth of the pure host A is about the same that the bandwidth of the B system, such substitution results only in a change of the local potential v_i at the replaced site i. This corresponds to changes in the diagonal elements of the Hamiltonian. In this case it is assumed that substitution of impurity atoms on average has no effect on hopping amplitudes to the neighboring atoms.

For systems with off-diagonal disorder, the randomness is introduced not only locally in the random diagonal potential v_i, but also through the hopping amplitudes. To model this, BEB [69]

introduced the disorder configuration dependent hopping amplitude of electrons t_{ij} as

$$\begin{aligned} t_{ij} &= t_{ij}^{AA}, \text{ if } \quad i \in A, \quad j \in A \\ & \quad t_{ij}^{BB}, \text{ if } \quad i \in B, \quad j \in B \\ & \quad t_{ij}^{AB}, \text{ if } \quad i \in A, \quad j \in B \\ & \quad t_{ij}^{BA}, \text{ if } \quad i \in B, \quad j \in A, \end{aligned} \tag{3.3}$$

where t_{ij} depends on the type of ion occupying sites i and j. For off-diagonal disorder BEB [69] showed the scalar CPA equation becomes a 2×2 matrix equation, with corresponding AA, AB, BA, and BB matrix elements. In momentum space, if there is only near-neighbor hopping between all ions, the bare dispersion can be written as (the under-bar denotes matrices)

$$\underline{\varepsilon_k} = \begin{pmatrix} t^{AA} & t^{AB} \\ t^{BA} & t^{BB} \end{pmatrix} \varepsilon_k \tag{3.4}$$

where in three dimensions $\varepsilon_k = -2t(\cos(k_x) + \cos(k_y) + \cos(k_z))$ with $4t = 1$ which sets our unit of energy, and t^{AA}, t^{BB}, t^{AB}, and t^{BA} are unitless prefactors.

The BEB approach is local by construction, hence all non-local disorder induced correlations are neglected. [69] In order to take into account non-local physics, we extend the BEB formalism to a finite cluster using the DCA scheme. Here in the following, we present the algorithm and details of our non-local DCA extension of the BEB formalism for off-diagonal disorder. Just as in the DCA scheme, [74] the first Brillouin zone is divided into $N_c = L^D$ (D is the dimension and L is the linear cluster size) coarse-grained cells with centers K surrounded by points $\tilde{k}$ within the cell so that an arbitrary $k = K + \tilde{k}$.

For a given DCA K-dependent effective medium hybridization $\underline{\Delta(K,\omega)}$ matrix we use an underline to denote a 2×2 matrix in momentum space)

$$\underline{\Delta(K,\omega)} = \begin{pmatrix} \Delta^{AA}(K,\omega) & \Delta^{AB}(K,\omega) \\ \Delta^{BA}(K,\omega) & \Delta^{BB}(K,\omega) \end{pmatrix} \tag{3.5}$$

we solve the cluster problem, usually in real space. For this we stochastically sample random configurations of the disorder potential V and calculate the corresponding cluster Green's function by inverting $N_c \times N_c$ matrix, i.e.,

$$G_{ij} = \left(\omega\mathbb{I} - \overline{t}' - \Delta' - V\right)^{-1}_{ij} \tag{3.6}$$

where V is a diagonal matrix for the disorder site potential. The primes stand for the configuration dependent Fourier transform (FT) components of the hybridization and hopping, respectively. I.e.,

$$\Delta'_{ij} = \begin{cases} FT(\Delta^{AA}(K,\omega)), \text{ if } \quad i \in A, \quad j \in A \\ FT(\Delta^{BB}(K,\omega)), \text{ if } \quad i \in B, \quad j \in B \\ FT(\Delta^{AB}(K,\omega)), \text{ if } \quad i \in A, \quad j \in B \\ FT(\Delta^{BA}(K,\omega)), \text{ if } \quad i \in B, \quad j \in A \end{cases} \tag{3.7a}$$

and

$$\overline{t}'_{ij} = \begin{cases} FT(\overline{\epsilon}^{AA}(K)), \text{ if } \quad i \in A, \quad j \in A \\ FT(\overline{\epsilon}^{BB}(K)), \text{ if } \quad i \in B, \quad j \in B \\ FT(\overline{\epsilon}^{AB}(K)), \text{ if } \quad i \in A, \quad j \in B \\ FT(\overline{\epsilon}^{BA}(K)), \text{ if } \quad i \in B, \quad j \in A \end{cases} \tag{3.7b}$$

with

$$\underline{\overline{\epsilon}(K)} \quad = \begin{pmatrix} t^{AA} & t^{AB} \\ t^{BA} & t^{BB} \end{pmatrix} \frac{N_c}{N} \sum_{\tilde{k}} \varepsilon_k, \tag{3.7c}$$

where Δ'_{ij} and $\overline{t}'_{ij}$ are $N_c \times N_c$ real-space matrices (where N_c is the cluster size), and e.g., $FT(\Delta^{AA}(K,\omega)) = \sum_K \Delta^{AA}(K,\omega)e^{iK(r_i - r_j)}$. The hopping can be long ranged, but since they are coarse-grained quantities are effectively limited to the cluster. Physically, Δ'_{ij} represents the hybridization between sites i and j which is configuration dependent. For example, the AA component of the hybridization corresponds to both A species occupying site i and j, while the AB component means that site i is occupied by an A atom and site j by a B atom. The interpretation of the hopping matrix is the same as for the hybridization function.

In the next step, we perform averaging over the disorder $\langle(...)\rangle$ and in doing so we re-expand the Green function (Eq. 3.6) into a $2N_c \times 2N_c$ matrix

$$G_c(\omega)_{ij} = \begin{pmatrix} \left\langle G_c^{AA}(\omega)\right\rangle_{ij} & \left\langle G_c^{AB}(\omega)\right\rangle_{ij} \\ \\ \left\langle G_c^{BA}(\omega)\right\rangle_{ij} & \left\langle G_c^{BB}(\omega)\right\rangle_{ij} \end{pmatrix}. \tag{3.8}$$

This may be done by assigning the components according to the occupancy of the sites i and j

$$\begin{aligned} (G_c^{AA})_{ij} &= (G_c)_{ij} \text{ if } \quad i \in A, \quad j \in A \\ (G_c^{BB})_{ij} &= (G_c)_{ij} \text{ if } \quad i \in B, \quad j \in B \\ (G_c^{AB})_{ij} &= (G_c)_{ij} \text{ if } \quad i \in A, \quad j \in B \\ (G_c^{BA})_{ij} &= (G_c)_{ij} \text{ if } \quad i \in B, \quad j \in A \end{aligned} \tag{3.9}$$

with the other components being zero. Because only one of the four matrix elements is finite for each disorder configuration (each site can be occupied by either A or B atom), only the sum of the elements in Eq. 3.8 is normalized as a conventional Green function.

Having formed the disorder average cluster Green function matrix, we then Fourier transform each component to K-space (which also imposes translational symmetry) and construct the K-dependent disorder averaged cluster Green function matrix in momentum space

$$\underline{G_c(K,\omega)} = \begin{pmatrix} G_c^{AA}(K,\omega) & G_c^{AB}(K,\omega) \\ \\ G_c^{BA}(K,\omega) & G_c^{BB}(K,\omega) \end{pmatrix}. \tag{3.10}$$

Once the cluster problem is solved, we calculate the coarse-grained lattice Green function matrix as

$$\begin{aligned} \underline{\overline{G}(K,\omega)} &= \begin{pmatrix} \overline{G}^{AA}(K,\omega) & \overline{G}^{AB}(K,\omega) \\ \overline{G}^{BA}(K,\omega) & \overline{G}^{BB}(K,\omega) \end{pmatrix} \\ &= \frac{N_c}{N} \sum_{\tilde{k}} \Big(\underline{G_c(K,\omega)}^{-1} + \underline{\Delta(K,\omega)} \\ &- \underline{\varepsilon_k} + \underline{\overline{\epsilon}(K)} \Big)^{-1}, \end{aligned} \tag{3.11}$$

here we use an overbar to denote the cluster coarse-grained quantities. It is important to note that each component of the Green function matrix above does not have the normalization of a conventional, i.e., scalar, Green function. Only the sum of the matrix components has the conventional normalization, so that $\overline{G}(K,\omega) \sim 1/\omega$, with the total coarse grained lattice Green function being obtained as

$$\begin{aligned} \overline{G}(K,\omega) &= \overline{G}^{AA}(K,\omega) + \overline{G}^{BB}(K,\omega) \\ &+ \overline{G}^{AB}(K,\omega) + \overline{G}^{BA}(K,\omega). \end{aligned} \tag{3.12}$$

Next, to construct the new DCA effective medium $\underline{\Delta(K,\omega)}$, we impose the BEB DCA (2×2) matrix self-consistency condition, requiring the disorder averaged cluster and the coarse-grained lattice Green functions to be equal

$$\underline{G_c(K,\omega)} = \underline{\overline{G}(K,\omega)}. \tag{3.13}$$

This is equivalent to a system of three coupled scalar equations

$$\overline{G}^{AA}(K,\omega) = G_c^{AA}(K,\omega), \tag{3.14a}$$

$$\overline{G}^{BB}(K,\omega) = G_c^{BB}(K,\omega), \quad \text{and} \tag{3.14b}$$

$$\overline{G}^{AB}(K,\omega) = G_c^{AB}(K,\omega). \tag{3.14c}$$

Note $\overline{G}^{BA}(K,\omega) = \overline{G}^{AB}(K,\omega)$ automatically if $t^{AB} = t^{BA}$.

We then close our self-consistency loop by updating the corresponding hybridization functions for each components as

$$\begin{aligned}
\Delta_n^{AA}(K,\omega) &= \Delta_o^{AA}(K,\omega) \\
&+ \xi\left(G_c^{-1}(K,\omega)^{AA} - \overline{G}^{-1}(K,\omega)^{AA}\right) \\
\Delta_n^{BB}(K,\omega) &= \Delta_o^{BB}(K,\omega) \\
&+ \xi\left(G_c^{-1}(K,\omega)^{BB} - \overline{G}^{-1}(K,\omega)^{BB}\right) \\
\Delta_n^{AB}(K,\omega) &= \Delta_o^{AB}(K,\omega) \\
&+ \xi\left(G_c^{-1}(K,\omega)^{AB} - \overline{G}^{-1}(K,\omega)^{AB}\right) \\
\Delta_n^{BA}(K,\omega) &= \Delta_n^{AB}(K,\omega)
\end{aligned} \tag{3.15}$$

where 'o' and 'n' denote old and new respectively, and ξ is a linear mixing parameter $0 < \xi < 1$. We then iterate the above steps until convergence is reached.

There are two limiting cases of the above formalism which we carefully checked numerically. In the limit of $N_c = 1$, we should recover the original BEB result. Here the cluster Green function loses its K dependence, so that

$$\begin{pmatrix} G_c^{AA}(\omega) & 0 \\ 0 & G_c^{BB}(\omega) \end{pmatrix} = \frac{1}{N}\sum_k \left(\underline{G_c(\omega)}^{-1} + \underline{\Delta(\omega)} - \underline{\varepsilon(k)}\right)^{-1} \tag{3.16}$$

which is the BEB self-consistency condition. Here we used that $\overline{\epsilon}(K) = 0$ for $\mathrm{N}_c = 1$. The second limiting case is when there is only diagonal disorder so that $t^{AA} = t^{BB} = t^{AB} = 1$. In this case the above formalism reduces to the original DCA scheme. We have verified numerically both limits.

3.2.2 Typical medium theory with off-diagonal disorder

To address the issue of electron localization, we recently developed the typical medium dynamical cluster approximation (TMDCA) and applied it to the three-dimensional Anderson model. [105] In Ref. [105] we confirmed that the typical density of states vanishes for states which are localized and it is finite for extended states. In the following we generalize our TMDCA analysis to systems with off-diagonal disorder to address the question of localization and the mobility edge in such models.

First, we would like to emphasize that the crucial difference between TMDCA [105] and the standard DCA [74] procedure is the way the disorder averaged cluster Green function is calculated. In the TMDCA analysis instead of using the algebraically averaged cluster Green function in the self-consistency loop, we calculate the typical (geometrically) averaged cluster density of states

$$\rho^c_{typ}(K,\omega) = e^{\frac{1}{N_c}\sum_i \langle \ln \rho_{ii}(\omega)\rangle} \left\langle \frac{-\frac{1}{\pi}\operatorname{Im} G_c(K,\omega)}{\frac{1}{N_c}\sum_i(-\frac{1}{\pi}\operatorname{Im} G_{ii}(\omega))} \right\rangle, \tag{3.17}$$

with the geometric averaging being performed over the local density of states $\rho_{ii}(\omega) = -\frac{1}{\pi}\operatorname{Im} G_{ii}(w)$ only. Using this $\rho^c_{typ}(K,\omega)$ the cluster averaged typical Green function is constructed via a Hilbert transform

$$G_c(K,\omega) = \int d\omega' \frac{\rho^c_{typ}(K,\omega')}{\omega - \omega'}. \tag{3.18}$$

In the presence of off-diagonal disorder, following BEB, the typical density of states becomes a 2×2 matrix, which we define as

$$\underline{\rho^c_{typ}(K,\omega)} = \exp\left(\frac{1}{N_c}\sum_{i=1}^{N_c}\langle \ln \rho_{ii}(\omega)\rangle\right) \times \begin{pmatrix} \left\langle \frac{-\frac{1}{\pi}\operatorname{Im} G^{AA}_c(K,\omega)}{\frac{1}{N_c}\sum_{i=1}^{N_c}(-\frac{1}{\pi}\operatorname{Im} G_{ii}(\omega))} \right\rangle & \left\langle \frac{-\frac{1}{\pi}\operatorname{Im} G^{AB}_c(K,\omega)}{\frac{1}{N_c}\sum_{i=1}^{N_c}(-\frac{1}{\pi}\operatorname{Im} G_{ii}(\omega))} \right\rangle \\ \left\langle \frac{-\frac{1}{\pi}\operatorname{Im} G^{BA}_c(K,w)}{\frac{1}{N_c}\sum_{i=1}^{N_c}(-\frac{1}{\pi}\operatorname{Im} G_{ii}(\omega))} \right\rangle & \left\langle \frac{-\frac{1}{\pi}\operatorname{Im} G^{BB}_c(K,\omega)}{\frac{1}{N_c}\sum_{i=1}^{N_c}(-\frac{1}{\pi}\operatorname{Im} G_{ii}(\omega))} \right\rangle \end{pmatrix} \tag{3.19}$$

Here the scalar prefactor depicts the local typical (geometrically averaged) density of states, while the matrix elements are linearly averaged over the disorder. Also notice that the cluster Green function $(\underline{G_c})_{ij}$ and its components G_c^{AA}, G_c^{BB} and G_c^{AB} are defined in the same way as in Eqs. (3.6-3.9).

In the next step, we construct the cluster average Green function $G_c(K,\omega)$ by performing Hilbert transform for each component

$$\underline{G_c(K,\omega)} \;=\; \begin{pmatrix} \int d\omega' \frac{\rho_{typ}^{AA}(K,\omega')}{\omega-\omega'} & \int d\omega' \frac{\rho_{typ}^{AB}(K,\omega')}{\omega-\omega'} \\ \\ \int d\omega' \frac{\rho_{typ}^{BA}(K,\omega')}{\omega-\omega'} & \int d\omega' \frac{\rho_{typ}^{BB}(K,\omega')}{\omega-\omega'} \end{pmatrix}. \tag{3.20}$$

Once the disorder averaged cluster Green function $G_c(K,\omega)$ is obtained from Eq. 3.20, the self-consistency steps are the same as in the procedure for the off-diagonal disorder DCA described in the previous section: we calculate the coarse-grained lattice Green function using Eq. 3.11 which is then used to update the hybridization function with the effective medium via Eq. 3.15.

The above set of equations provide us with the generalization of the TMDCA scheme for both diagonal and off-diagonal disorder which we test numerically in the following sections. Also notice that for $N_c = 1$ with only diagonal disorder ($t^{AA} = t^{BB} = t^{AB} = t^{BA}$) the above procedure reduces to the local TMT scheme. In this case, the diagonal elements of the matrix in Eq. 3.19 will contribute c_A and c_B, respectively, with the off-diagonal elements being zero (for $\mathrm{N}_c = 1$ the off-diagonal terms vanish because a given site can only be either A or B). Hence, the typical density reduces to the local scalar prefactor only, which has exactly the same form as in the local TMT scheme.

Another limit of the proposed ansatz for the typical density of states of Eq. 3.19 is obtained at small disorder. In this case, the TMDCA reduces to the DCA for off-diagonal disorder, as the geometrically averaged local prefactor term numerically cancels with the contribution from the linearly averaged local term in the denominator of Eq. 3.19.

Finally, we also want to mention that the developed cluster TMDCA fulfills all the essential requirements expected of a "successful" cluster theory [58] including causality and translational invariance.

We note that in our formalism, instead of doing the very expensive enumeration of the disorder configurations which scales as 2^{Nc}, we instead do a stochastic sampling of the disorder configurations which greatly reduces the computational cost enabling us to study larger systems. Larger system sizes need fewer realizations. Since the convergence criterion is achieved when the TDOS($\omega = 0$) does not fluctuate anymore with iteration number, within the error bars, our computational cost does not even scale as N_c. For a typical $N_c = 64$ size cluster, about 500 disorder realizations are needed to get reliable data and this number decreases with increasing cluster size.

3.3 Results and Discussion

To illustrate the generalized DCA and TMDCA algorithms described above, we present our results for the effects of diagonal and off-diagonal disorder in a generalized Anderson Hamiltonian (Eq. 3.1) for a three dimensional system with binary disorder distribution ($V_A = -V_B$) and random hopping ($t^{AA} \neq t^{BB}, t^{AB} = t^{BA}$) with other parameters as specified. The results are presented and discussed in Subsections 3.3.1 and 3.3.1.

3.3.1 DCA results for diagonal and off-diagonal disorder

The effect of off-diagonal disorder on the average density of states (DOS) calculated within the DCA for cubic cluster ($N_c = 4^3$) is presented in Fig. 3.1. The DOS we present in our results is a local density of states calculated as

$$\begin{aligned} DOS(\omega) &= -\frac{1}{\pi N_c} \sum_{K=1}^{N_c} \Big(\mathrm{Im}\, \overline{G}^{AA}(K,\omega) + \mathrm{Im}\, \overline{G}^{AB}(K,\omega) \\ &+ \mathrm{Im}\, \overline{G}^{BA}(K,\omega) + \mathrm{Im}\, \overline{G}^{BB}(K,\omega) \Big). \end{aligned} \tag{3.21}$$

Notice that our DCA procedure for $N_c = 1$ reduce to the original CPA-like BEB. For a fixed concentration $c_A = 0.5$, we examine the effects of off-diagonal disorder at two fixed values of the diagonal disorder potential $V_A = 0.4$ (below the split-band limit) and $V_A = 0.9$ (above the split-band limit). The off-diagonal randomness is modeled by changes in the hopping amplitudes t^{AA}, t^{BB} with $t^{AB} = 0.5(t^{AA} + t^{BB})$. For a diagonal disorder case (top panel of Fig. 3.1) with

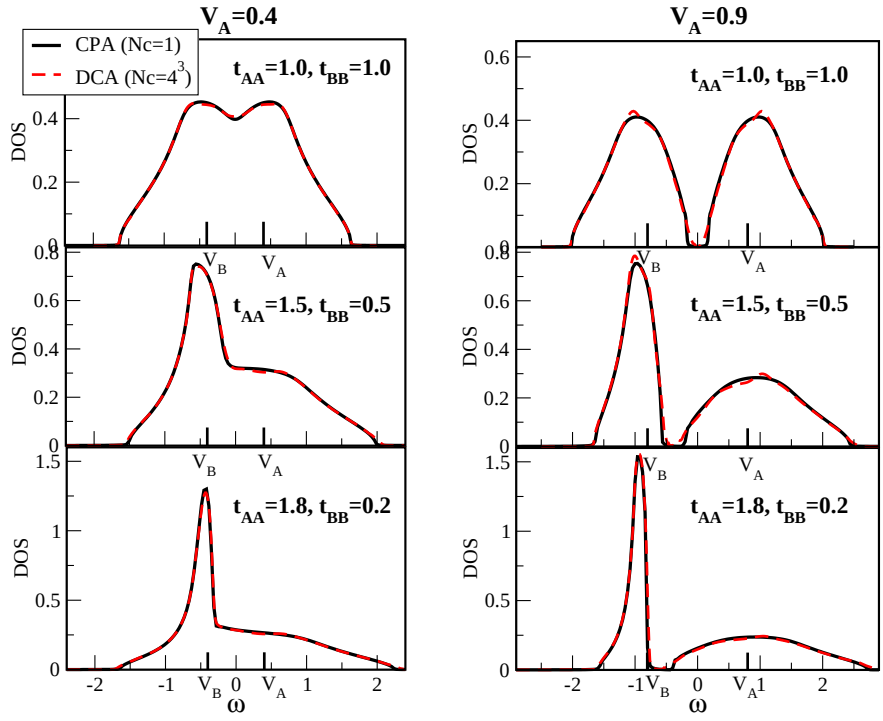

Figure 3.1: (Color online). The effect of off-diagonal disorder on the average density of states calculated in the DCA scheme with $N_c = 4^3$. Our DCA results for $N_c = 1$ corresponds to a single site CPA BEB scheme. We consider two values of local disorder potential below ($V_A = 0.4$) and above ($V_A = 0.9$) the band-split limit, and examine the effect of changing the off-diagonal hopping strength (which amounts to a change in the non-local potential). We start with the diagonal disorder case $t^{AA} = t^{BB} = t^{AB} = 1.0$ and then consider two off-diagonal disorder cases: $t^{AA} = 1.5, t^{BB} = 0.5$ and $t^{AA} = 1.8, t^{BB} = 0.2$, respectively. We fix $t^{AB} = t^{BA} = 0.5(t^{AA} + t^{BB})$ and $c_A = 0.5$. For this parameter range of off-diagonal disorder, we do not observe a significant difference between the CPA ($N_c = 1$) and the DCA ($N_c = 4^3$) results indicating that non-local inter-site correlations are weak.

$t^{AA} = t^{BB} = t^{AB} = t^{BA}$ we have two subbands contributing equally to the total DOS. While as shown in the middle and bottom panels, the change in the strength of the off-diagonal disorder leads to dramatic changes in the DOS. An increase of the AA hoping results in the broadening of the AA subband with the development of a resonance peak at the BB subband. For this parameter range both the DCA ($N_c = 64$) and CPA ($N_c = 1$) provide about the same results indicating that disorder-induced non-local correlations are negligible.

In Fig. 3.2 we show the average density of states calculated for fixed off-diagonal-disorder parameters and different diagonal disorder potentials V_A. We again compare the local CPA ($N_c = 1$) and

the DCA ($N_c = 4^3$) results. To benchmark our off-diagonal extension of the DCA, we also compare

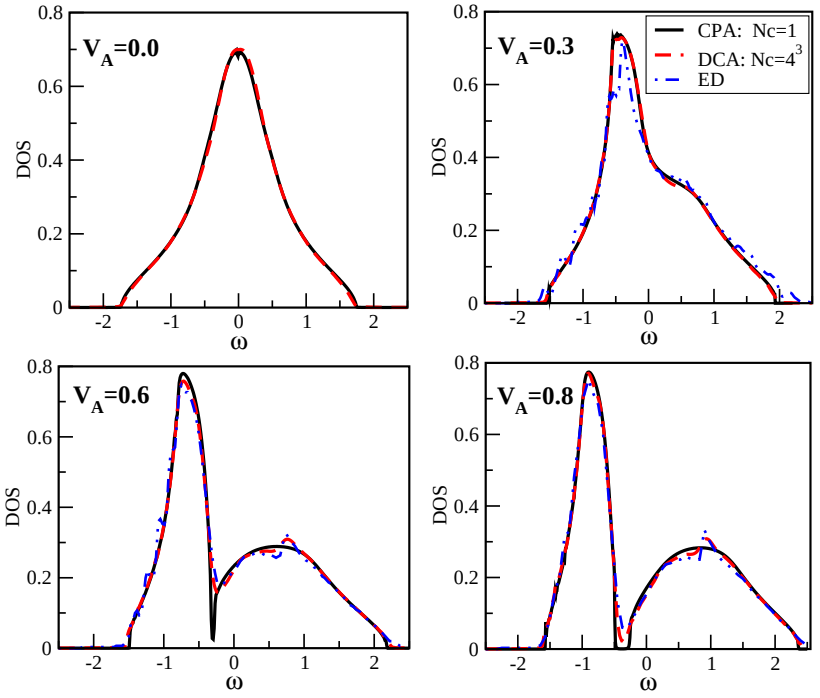

Figure 3.2: (Color online). The effect on the average density of states of an increasing diagonal disorder potential V_A for a fixed off-diagonal disorder calculated with our modified DCA scheme with $t^{AA} = 1.5$, $t^{BB} = 0.5$, $t^{AB} = 0.5(t^{AA} + t^{BB})$, and $c_A = 0.5$. Results are obtained for $N_c = 1$ (corresponding to the CPA) and $N_c = 4^3$ cluster sizes. We also compare our DCA average DOS with the DOS obtained using exact diagonalization (ED) for a 12^3 cubic lattice cluster with 48 disorder realizations. For ED results, we used a $\eta = 0.01$ broadening in frequency.

our results with those obtained from exact diagonalization. For small V_A, there is no difference between the CPA ($N_c = 1$) and the DCA ($N_c = 4^3$) results. As local potential V_A is increased, noticeable differences start to develop. We can see that for larger V_A a gap starts to open and is more dramatic in the CPA scheme. While in the DCA ($N_c = 4^3$) this gap is partially filled due to the incorporation of non-local inter-site correlations which are missing in the CPA. Furthermore, the DOS obtained from the DCA procedure provides finer structures which are in basic agreement with the DOS calculated with exact diagonalization for a cluster of size $12 \times 12 \times 12$. The agreement we get with ED results is a good indication of the the accuracy of our extension of the DCA to off-diagonal disorder. The additional structures observed in the DOS for $N_c > 1$, which are absent in the CPA, are believed to be related to the local order in the environment of each site. [58, 74]

Notice that while the DCA accounts for non-local backscattering effects which lead to the Anderson localization, the average local DOS does not capture the transition, as it is not an order parameter for the Anderson localization.

To further illustrate the important effect of the non-local contributions from the cluster, we also show in Fig. 3.3 the imaginary part of the self-energy $Im\Sigma(K,w)$ for $\mathrm{N}_c = 1$ (dash line) and for ($\mathrm{N}_c = 4^3$) (solid lines) at different values of cluster momenta $K = (0,0,0)$, $(\pi,0,0)$, $(\pi,\pi,0)$ and $(\pi/2,\pi/2,\pi/2)$ for small $V_A = 0.1$ (top) and larger $V_A = 0.6$ (bottom) disorder potentials. At

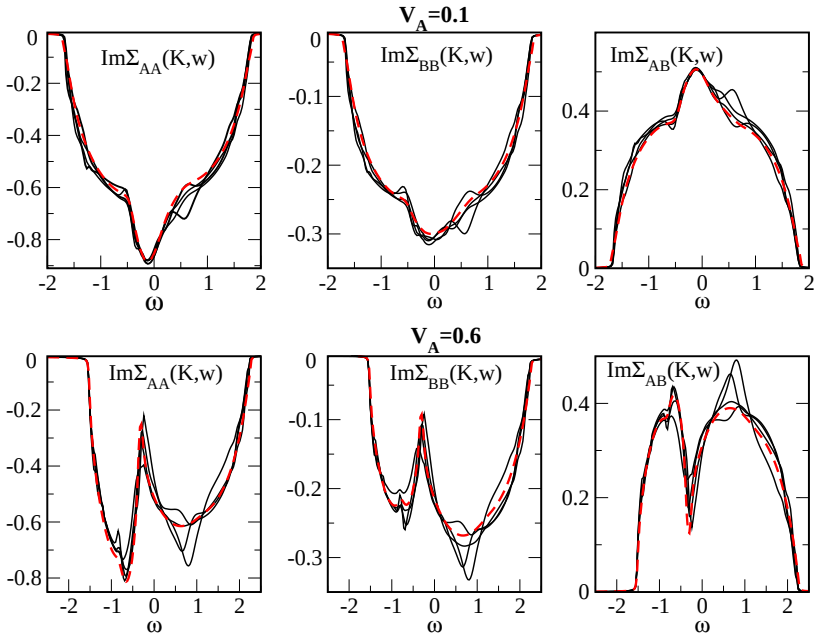

Figure 3.3: (Color online). The imaginary part of the self-energy vs frequency ω for $\mathrm{N}_c = 1$ (red dash-line) and $\mathrm{N}_c = 4^3$ (solid lines) at various K momenta points: $(0,0,0)$, $(\pi,0,0)$, $(\pi,\pi,0)$, and $(\pi/2,\pi/2,\pi/2)$, for $V_A = 0.1$ (top) and $V_A = 0.6$ (bottom) diagonal disorder potential with $t^{AA} = 1.5$, $t^{BB} = 0.5$, $t^{AB} = 0.5(t^{AA} + t^{BB})$, and $c_A = 0.5$. For small disorder $V_A = 0.1$, the self-energy for $\mathrm{N}_c = 1$ is essentially the same as that of the various K points of the $\mathrm{N}_c = 4^3$ cluster, indicating that non-local effects are negligible for such small disorder. For a larger value of the disorder $V_A = 0.6$, the single site and the finite cluster data differ significantly, which illustrates that at larger disorder, the momentum dependence of the self-energy increases and becomes important.

small disorder $V_A = 0.1$, there is a little momentum dependence for the $\mathrm{N}_c = 4^3$ self-energy and different K momenta curves practically fall on top of each other. The results for the $\mathrm{N}_c = 1$ and $\mathrm{N}_c = 4^3$ are essentially the same, which indicates that for small disorder the CPA still presents a good approximation for the self-energy. On the hand, for larger disorder $V_A = 0.6$ the $\mathrm{N}_c = 1$ and

$N_c = 4^3$ results differ significantly, with the $N_c = 4^3$ self-energy having a noticeable momentum dependence, indicating that non-local correlations become more pronounced for larger disorder values.

3.3.2 Typical medium finite cluster analysis of diagonal and off-diagonal disorder

Typical medium analysis of diagonal disorder

To characterize the Anderson localization transition, we now explore the typical density of states (TDOS) calculated within our extension of the TMDCA presented in Sec. 3.2.2. In the typical medium analysis, the TDOS serves as the order parameter for the Anderson localization transition. In particular, the TDOS is finite for extended states and zero for states which are localized.

First we consider the behavior of the TDOS and compare it with the average DOS for diagonal disorder. In Fig. 3.4 we show our results for $N_c = 1$ (left panel) and $N_c > 1$ (right panel). To demonstrate a systematic convergence of the TDOS with increasing cluster size N_c, we present our data of the TDOS for $N_c = 1, 4^3, 6^3$. Notice that $N_c = 1$ results for TDOS correspond to the single-site TMT of Dobrosavljević *et al.*, [100] and for average DOS they correspond to the ordinary CPA. As expected, [100, 105] for small disorder ($V_A = 0.15$) there is not much difference between the DCA ($N_c = 4^3$) and the TMDCA ($N_c = 4^3$) or between the CPA and TMT for $N_c = 1$ results. However, there are subtle differences between the results for finite $N_c = 4^3$ and single site $N_c = 1$ clusters due to incorporation of spatial correlations. As the disorder strength V_A is increased ($V_A = 0.6$), the typical density of states (TDOS) becomes smaller than the average DOS and is broader for the larger cluster. Moreover, the finite cluster introduce features in the DOS which are missing in the local $N_c = 1$ data. Regions where the TDOS is zero while the average DOS is finite indicate Anderson localized states, separated by the mobility edge (marked by arrows). For $N_c > 1$ these localized regions are wider which indicates that the localization edge is driven to higher frequencies. This is a consequence of the tendency of non-local corrections to suppress localization. For even larger disorder $V_A = 1$, a gap opens in both the TDOS and the average DOS leading to the formation of four localization edges, but again the region of extended states is larger for the finite cluster,

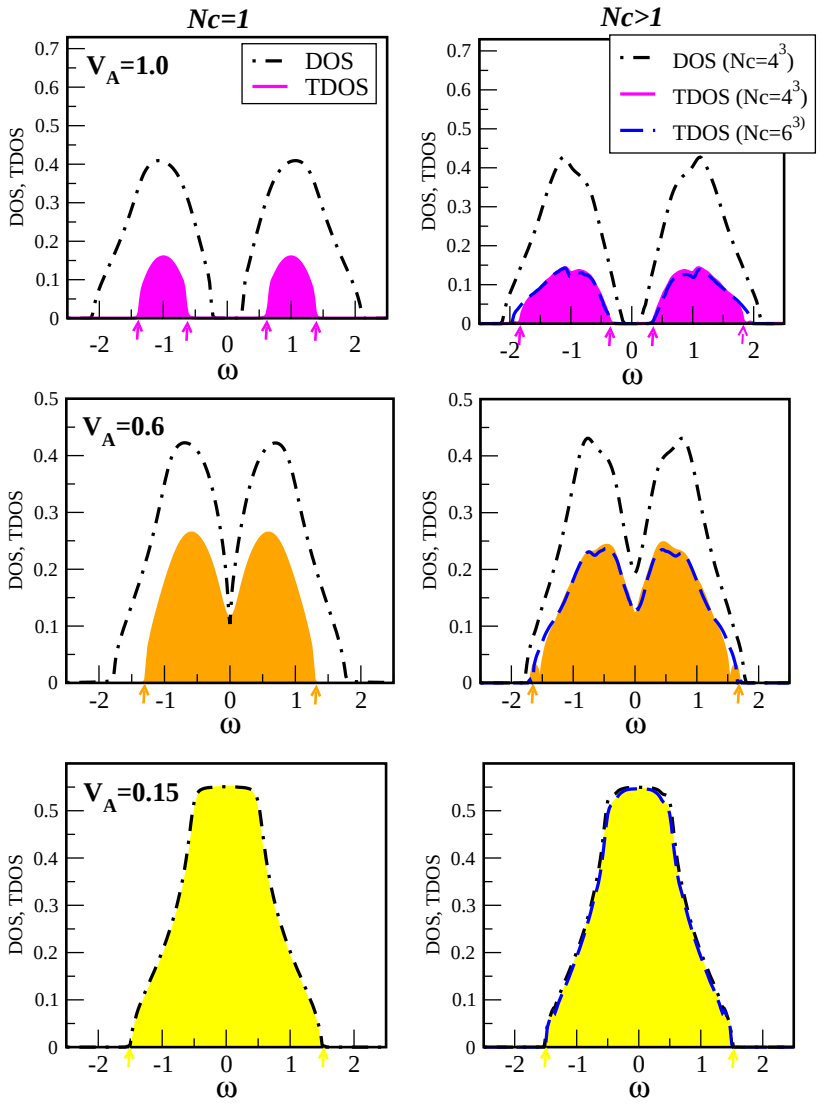

Figure 3.4: (Color online). Diagonal disorder case: The average density of states (dash-dotted line) calculated within the DCA for $N_c = 1$ (left panel) and $N_c = 4^3$ (right panel) and the typical density of states shown as shaded regions for $N_c = 1$ (left panel) and $N_c = 4^3$ (right panel) and dash-line for $N_c = 6^3$ (right panel) are calculated within the TMDCA for diagonal disorder $t^{AA} = t^{BB} = t^{AB} = t^{BA} = 1, c_A = 0.5$, and various values of the local potential $V_A = -V_B$. The TDOS is presented for several cluster sizes $N_c = 1$, $N_c = 4^3$ and $N_c = 6^3$ in order to show its systematic convergence with N_c. The average DOS converges for cluster sizes beyond $N_c = 4^3$. The TDOS is finite for the extended states and zero when the states are localized. The mobility edges extracted from the vanishing of the TDOS are marked by the arrows (we show arrows for $N_c = 4^3$ only). The extended states region with a finite TDOS is always narrower for $N_c = 1$ as compared to the results of $N_c > 1$ clusters, indicating that a single site TMT tends to overemphasize the localized states.

indicating that local TMT ($N_c = 1$) tends to underestimate the extended states region.

To further benchmark our results for the diagonal disorder, we show in Fig. 3.5 a comparison of the average and typical DOS calculated with the DCA and the TMDCA ($N_c = 4^3$) as compared with the kernel polynomial method (KPM). [109, 108, 92, 93] In the KPM analysis, instead of

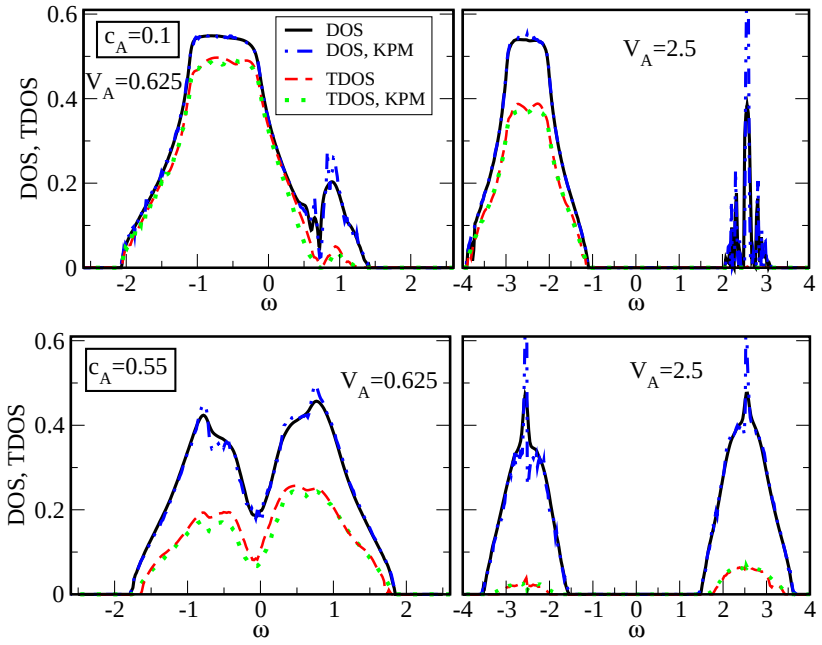

Figure 3.5: (Color online). Diagonal disorder case. Comparison of the average and typical DOS calculated with the DCA/TMDCA and Kernel polynomial methods (KPM) [108] for diagonal disorder with $t^{AA} = t^{BB} = t^{AB} = t^{BA} = 1$ at various values of local potential V_A and concentrations c_A for cluster size $N_c = 6^3$. The kernel polynomial method used 2048 moments on a 48^3 cubic lattice, and 200 independent realizations generated with 32 sites randomly sampled from each realization.

diagonalizing the Hamiltonian directly, the local DOS is expressed in term of an infinite series of Chebyshev polynomials. In practice, the truncated series leads to Gibbs oscillations. The KPM damps these oscillations by a modification of the expansion coefficients. Following previous studies on the Anderson model, the Jackson kernel is used. [109] The details of the implementation are well discussed in Ref. [109]. The parameters used in the KPM calculations are listed in the caption of Fig. 3.5. As it is evident from the plots, our TMDCA results reproduced those from the KPM nicely showing that our formalism offers a systematic way of studying the Anderson localization transition in binary alloy systems. Such good agreement indicates a successful benchmarking of the

TMDCA method. [105]

Typical medium analysis of off-diagonal disorder

Next, we explore the effects of the off-diagonal disorder. In Fig. 3.6, we compare the typical TDOS from the TMDCA and average DOS from the DCA for several values of the diagonal disorder strength V_A at fixed off-diagonal disorder amplitudes $t^{AA} = 1.5$, $t^{BB} = 0.5$, $t^{AB} = 1.0$. To show the effect of a finite cluster with respect to incorporation of non-local correlations, we present data for the single site $N_c = 1$ and finite clusters $N_c = 4^3$ and 5^3. The TMT ($N_c = 1$) again underestimates the extended states regime by having a narrower TDOS as compared to the $N_c > 1$. We also see that the mobility edge defined by the vanishing of the TDOS (marked by arrows for $N_c = 4^3$) systematically converges with increasing cluster size N_c. For small disorder V_A, both the DOS and the TDOS are practically the same. However, as V_A increases, significant differences start to emerge. Increasing V_A leads to the gradual opening of the gap which is more pronounced in the $N_c = 1$ case and for smaller disorder $V_A = 0.6$ is partially filled for the $N_c > 1$ clusters. As compared to the diagonal disorder case (cf. Fig. 3.4), the average DOS and TDOS become asymmetric with respect to zero frequency due to the off-diagonal randomness.

In Fig. 3.7 and Fig. 3.8 we present the disorder-energy phase diagram for both diagonal (Fig. 3.7) and off-diagonal (Fig. 3.8) disorder calculated using the single TMT ($N_c = 1$) and the non-local TMDCA ($N_c > 1$). To check the accuracy of the mobility edge trajectories extracted from our typical medium analysis, we compare our data with the results obtained with the transfer matrix method (TMM). The TMM [149, 150, 98] is a well established numerical method for calculating the correlation length and determining the mobility edge of the disorder Anderson model. Its main advantage is in its capability of capturing the effects from rather large system sizes. Thus, TMM provides good data for a finite size scaling analysis to capture the critical points and the corresponding exponents. In our calculations, the transmission of states down a three-dimensional bar of widths $M = [6, 12]$ and length $L = 2{\times}10^4 M$ are studied by adding the products of the transfer matrices with random initial states. The multiplication of transfer matrices is numerically unstable. To avoid this instability, we orthogonalized the transfer matrix product every five multiplications

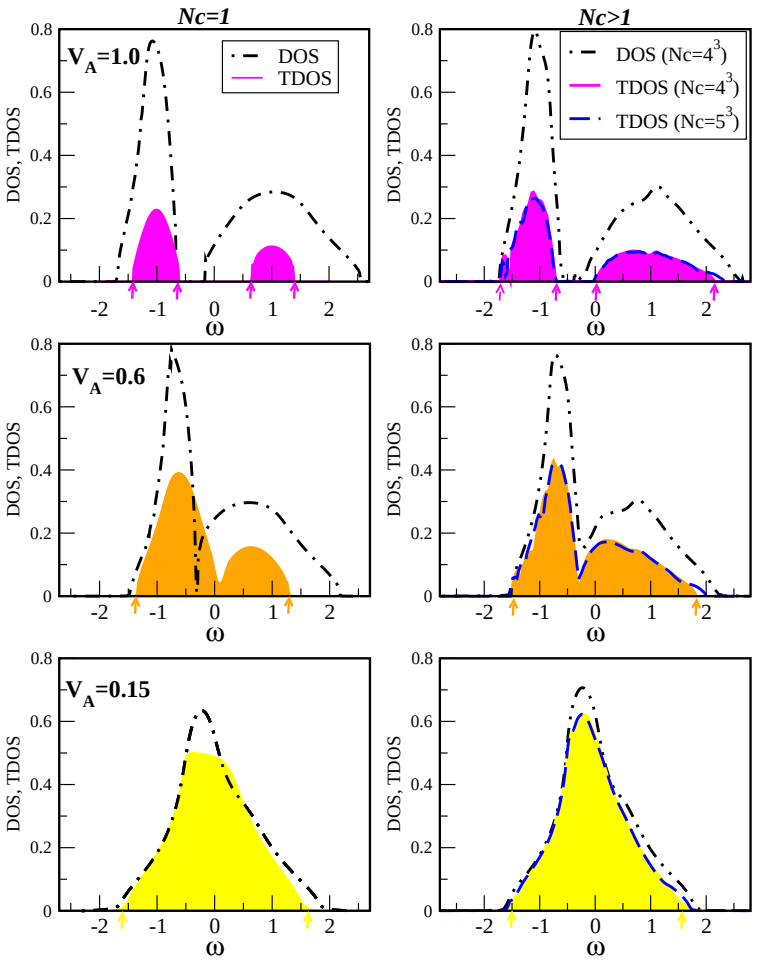

Figure 3.6: (Color online). Off-diagonal disorder case. The left panel displays results for $N_c = 1$ and the right panel for $N_c > 1$. The average density of states (dash-dotted line) and the typical density of states (shaded regions) for $N_c = 1$ (left panel), $N_c = 4^3$ (right panel) and blue dash lines for $N_c = 5^3$ (left panel) for various values of the local potential V_A with off-diagonal disorder parameters: $t^{AA} = 1.5$, $t^{BB} = 0.5$, $t^{AB} = 0.5(t^{AA} + t^{BB})$, and $c_A = 0.5$. As in Fig. 3.4, we show the TDOS for several cluster sizes $\mathrm{N}_c = 1, 4^3$, and $= 6^3$ in order to show its systematic convergence with increasing cluster size N_c. The average DOS converges for cluster sizes beyond $\mathrm{N}_c = 4^3$. The TDOS is finite for the extended states and zero for localized states. The mobility edges are extracted as described in Fig. 3.4.

using a Lapack QR decomposition. [50] The localization edge is obtained by calculating the Kramer-MacKinnon scaling parameter Λ_M. [149] This is a dimensionless quantity which should be invariant at the critical point, that is, Λ_M scales as a constant for $M \to \infty$. [150] Thus, we determine the boundary of the localization transition vis-à-vis the critical disorder strength [96] by performing a linear fit to Λ_M v. M data: localized states will have a negative slope and visa versa for extended

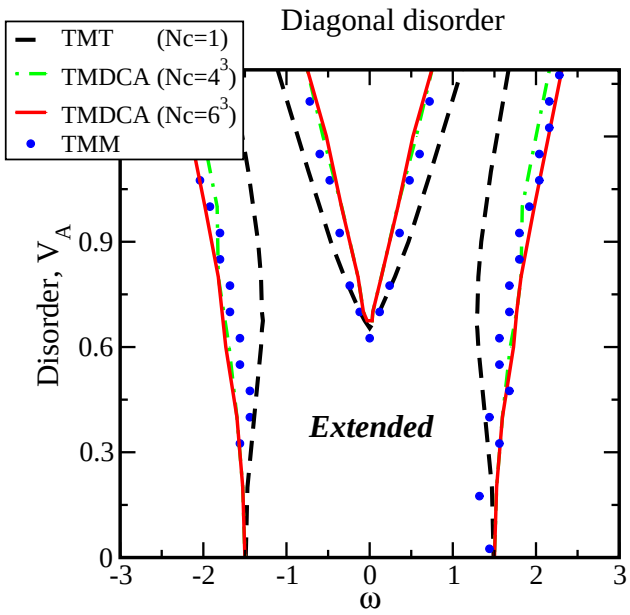

Figure 3.7: (Color online). Disorder-energy phase diagram for the diagonal disorder case. Parameters used are: $t^{AA} = t^{BB} = t^{AB} = 1.0$, and $c_A = 0.5$. We compare the mobility edges obtained from the TMT $N_c = 1$ (black dash line), TMDCA with $N_c = 4^3$ (green dot-dashed line) and $N_c = 6^3$ (red solid line), and the transfer-matrix method (TMM) (blue dotted line). The single site $N_c = 1$ results strongly underestimate the extended states region when compare with TMDCA results for $N_c > 1$. The mobility edges obtained from the finite cluster TMDCA ($N_c > 1$) show good agreement with those obtained from the TMM, in contrast to single site TMT. See the text for parameters and details of the TMM implementation.

states. The transfer-matrix method finite size effects are larger for weak disorder where the states decay slowly with distance and so have large values of Λ_M that carry a large variance in the data. Notice that the CPA and the DCA do not suffer such finite size effect limitation for small disorder and are in fact exact in this limit.

The mobility edges shown in Fig. 3.7 and Fig. 3.8 were extracted from the TDOS, with boundaries being defined by zero TDOS. As can be seen in Fig. 3.7 and Fig. 3.8, while the single-site TMT does not change much under the effect of off-diagonal disorder, the TMDCA results are significantly modified. The bands for a larger cluster become highly asymmetric with significant widening of the A subband. The local $N_c = 1$ boundaries are narrower than those obtained for $N_c > 1$ indicating that the TMT strongly underestimates the extended states regime in both diagonal and off-diagonal disorder. On the other hand, comparing the mobility edge boundaries for $N_c > 1$ with those obtained using TMM, we find very good agreement. This again confirms the validity of our

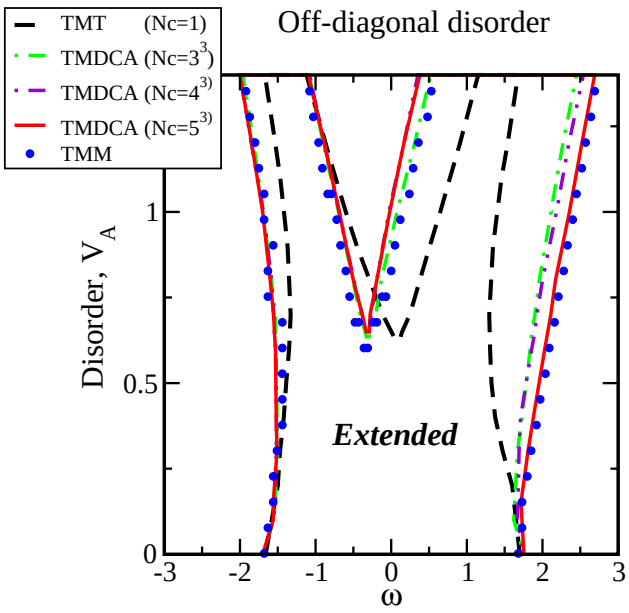

Figure 3.8: (Color online). Disorder-energy phase diagram for the off-diagonal disorder case. Parameters used are $t^{AA} = 1.5$, $t^{BB} = 0.5$, $t^{AB} = 1.0$, and $c_A = 0.5$. The mobility edges obtained from the TMT $N_c = 1$ (black dashed line), TMDCA $N_c = 3^3$ (green dot-dashed line), $N_c = 4^3$ (purple double-dot-dashed line) and $N_c = 5^3$ (red solid line), and the transfer-matrix method (TMM) (blue dotted line). The single site $N_c = 1$ strongly underestimates the extended states region especially for higher values of V_A. The mobility edges obtained from the finite cluster TMDCA ($N_c > 1$) converge gradually with increasing N_c and show good agreement with those obtained from the TMM, in contrast to single site TMT. See the text for parameters and details of the TMM implementation.

generalized TMDCA.

Next, we consider the effect of off-diagonal disorder for various concentrations c_A. In Fig. 3.9, we show the typical and average DOS for several values of c_A calculated with the TMDCA and the DCA, respectively. As expected, when $c_A \to 0$, we obtain a pure B subband contribution (the top panel). Upon gradual increase of the c_A concentration, the number of states in the A sub-band grows until B-subband becomes a minority for $c_A > 0.5$ and completely disappears at $c_A \to 1$ (the bottom panel). Again, we see that a finite cluster $N_c = 5^3$ provides a more accurate description (with finite details in DOS and broader regions of extended states in TDOS) in both average DOS and TDOS. The associated contour plots for the evolution of the TDOS in the concentration range $0 \leq c_A \leq 1$ are shown in Fig. 3.10.

The essence of these plots is to show the overall evolution of the typical DOS for a fixed local

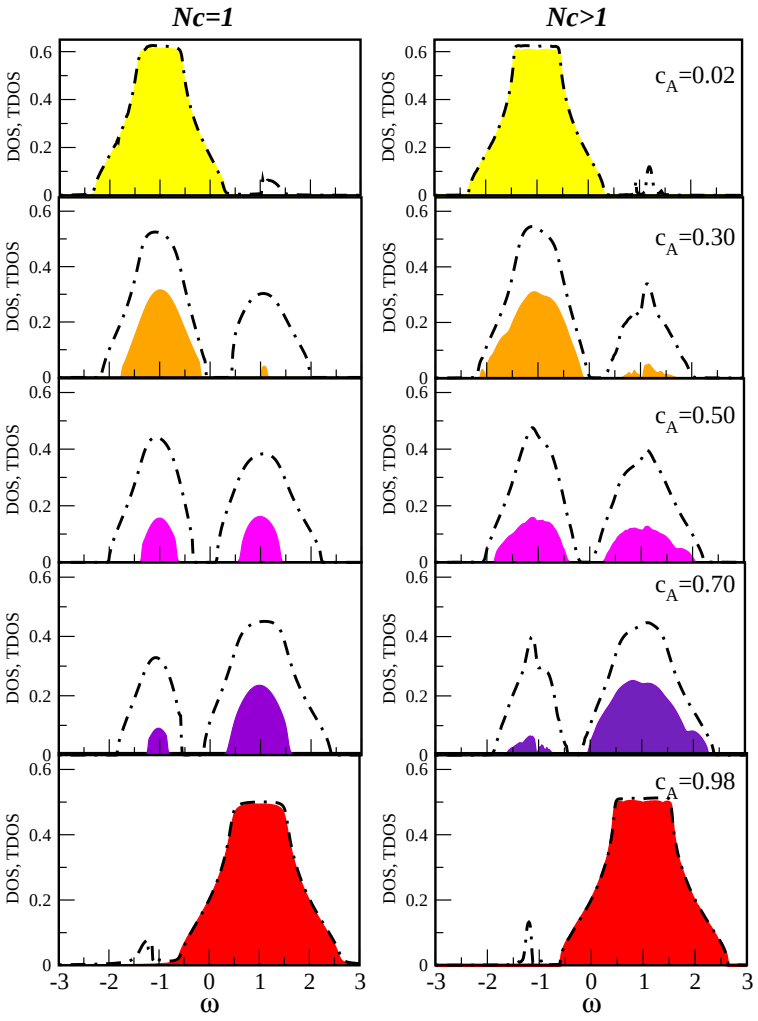

Figure 3.9: (Color online). The average DOS (dot-dashed lines) and the typical DOS (shaded regions) for various values of the concentration c_A with off-diagonal disorder parameters $t^{AA} = 1.1$, $t^{BB} = 0.9$ and $t^{AB} = 1.0$, at fixed local potential $V_A = 1.0$ for $N_c = 1$ (left panel) and $N_c = 5^3$ (right panel).

potential and off-diagonal disorder parameters as a function of the concentration c_A. In the limit of $c_A \to 0$, only the B-subband centered around $\omega = -V_A$ survives, and for $c_A \to 1$, only the A-subband centered around $\omega = V_A$ is present. For intermediate concentrations, we clearly have contributions to the total typical density of states from both species, as expected.

Finally, we would like to comment on the possible further development of the presented scheme. After certain generalizations our current implementation of the typical medium dynamical cluster approximation for off-diagonal disorder can serve as the natural formalism for multiband (multior-

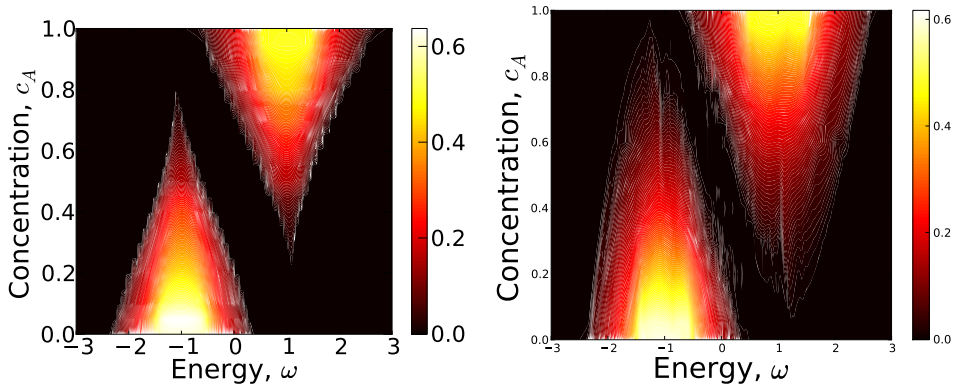

Figure 3.10: (Color online). The evolution of the typical density of states for $N_c = 1$ (left panel) and $N_c = 5^3$ (right panel) with the change in the concentration $0 < c_A < 1$ at fixed diagonal and off-diagonal disorder parameters: $t^{AA} = 1.1$, $t^{BB} = 0.9$, $t^{AB} = 1.0$ and $V_A = 1.0$

bital) systems. [60] Such an extension is crucial for studying disorder and localization effects in real materials. Further development towards this direction will be the subject of future publications.

3.4 Conclusion

A proper theoretical description of disordered materials requires the inclusion of both diagonal and off-diagonal randomness. In this paper, we have extended the BEB single site CPA scheme to a finite cluster DCA that incorporates the effect of non-local disorder. Applying the generalized DCA scheme to a single band tight binding Hamiltonian with configuration-dependent hopping amplitudes, we have considered the effects of non-local disorder and the interplay of diagonal and off-diagonal disorder on the average density of states. By comparing our results with those from exact numerical methods, we have established the accuracy of our method. We found that non-local multi-site effects lead to the development of finite structures in the density of states and the partial filling of the gap at larger disorder. Utilizing the self-energy, we show as a function of increasing disorder strengths, the importance of a finite cluster in characterizing the Anderson localization transition. For small disorder the single site and finite cluster results are essentially the same, indicating that the CPA is a good approximation in the small disorder regime. However, for a larger disorder we observe a significant momentum dependence in the self-energy resulting from the non-local correlations which are incorporated in the DCA.

Electron localization for off-diagonal disorder models had not been studied from the the typical medium perspective. The typical medium formalism did not exist for such disordered systems. In this paper, we generalized the TMDCA to systems with both diagonal and off-diagonal disorder. Our developed method can quantitatively and qualitatively be used to study the effects of disorder on the electron localization, effectively for systems with both diagonal and off-diagonal randomness.

We demonstrate that within the TMDCA, the typical DOS vanishes for localized states, and is finite for states which are extended. Employing the typical DOS as an order parameter for Anderson localization, we have constructed the disorder-energy phase diagram for systems with both diagonal and off-diagonal disorder. We have also demonstrated the inability of the single site CPA and the TMT methods to accurately capture the localization and disorder effects in both the average and the typical DOS, respectively. We note that the single site TMT while being able to capture the behavior for the diagonal and off-diagonal disorder, strongly underestimates the extended regions. Also the TMT is less sensitive to the off-diagonal randomness with the mobility edges being only slightly modified as compared to the diagonal case. In contrast, the finite cluster TMDCA results are able to capture the considerable changes, with a pronounced asymmetry of the extended state region, in the disorder-energy phase diagram under the effect of the off-diagonal disorder as compared to the diagonal case. Most importantly, the TMDCA results are found to be in a quantitative agreement with exact numerical results. Comparing our results with kernel polynomial, exact diagonalization, and transfer-matrix methods we find a remarkably good agreement with our extended DCA and TMDCA. To the best of our knowledge, this is the first numerically accurate investigation of the Anderson localization in systems with off-diagonal disorder within the framework of the typical medium analysis. We believe that the extended TMDCA scheme presents a powerful tool for treating both diagonal and off-diagonal disorder on equal footing, and can be easily extended to study localization in multi-band systems.

Chapter 4

TMDCA Study of Multi-band Systems

Prior to this work, TMDCA calculations had been restriced to model calculations that involve only a single band. As real materials exhibit multiple bands, it is important to establish that TMDCA can capture the Anderson transition in a multiband system which is the result that will be presented in this chapter [1] . The density of states and predictions of the mobility edge are compared with the kernel polynomial method and the TMM for the model two-band system as seen in Fig.4.1. Also, the method is then applied to the real material $K_xFe_{2-y}Se_2$ and found to not be an Anderson insulator.

My contribution to this work was primarily in the figures which show the mobility edge comparisons with the TMM (Fig.4.6 and Fig.4.7). I extended my parallel TMM code to the multiband system described in this chapter below and performed finite size scaling analysis of the of the Kramer-MacKinnon scaling parameter as a function of disorder as seen in Fig.4.2.

[1] This chapter includes previously published work published by American Physical Society and appears in [38] and is reproduced here under term 3 of Author's rights of the APS Transfer of Copyright Agreement to "The right to use all or part of the Article, including the APS-prepared version without revision or modification ... for educational or research purposes."

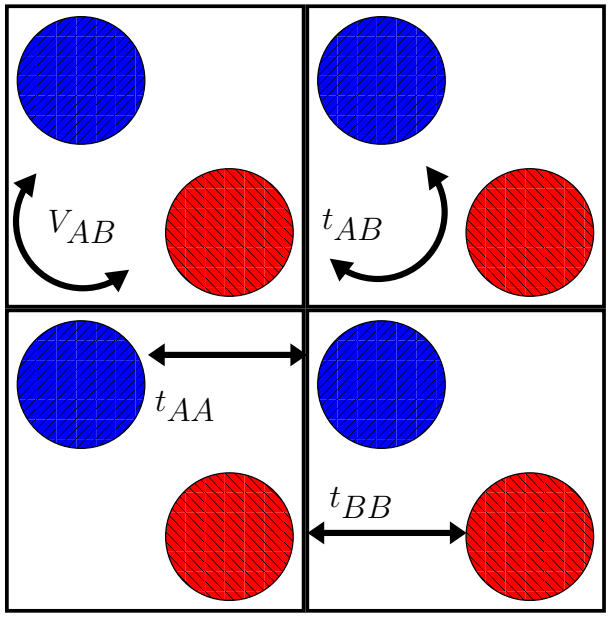

Figure 4.1: Simple two band model where each unit cell contains two orbitals with couplings as defined in [38].

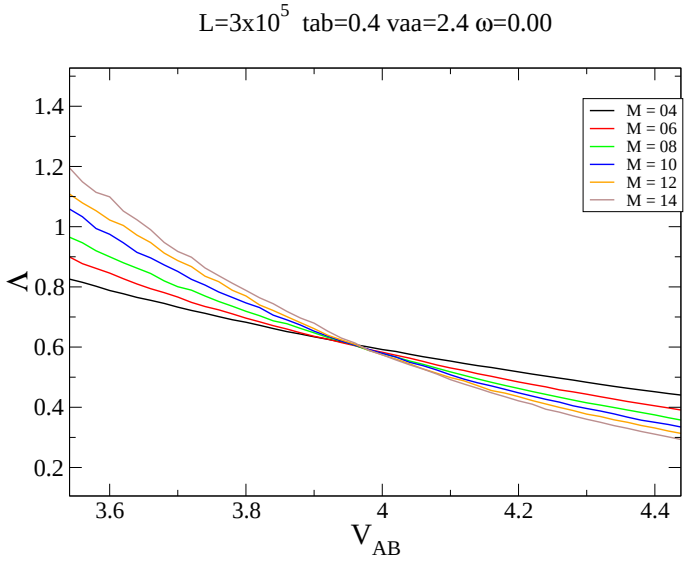

Figure 4.2: Krammer-Macinnon scaling parameter. The crossing denotes the critical disorder strength as the scaling parameter is invariant as a function of system size.

4.1 Introduction

The role of disorder (randomness) in materials has been at the forefront of current research [101, 102, 110] due to the new and improved functionalities that can be achieved in materials by carefully controlling the concentration of impurities in the host. At half-filling and in the absence of any spontaneous symmetry breaking field, disorder can induce a transition in a non-degenerate electronic three-dimensional system from a metal to an insulator (MIT) [103, 111]. This phenomenon, which occurs due to the multiple scattering of charge carriers off random impurities, is known as Anderson localization [103].

The most commonly used mean-field theory to study disordered systems is the coherent potential approximation (CPA) [112, 113, 114], which maps the original disordered lattice to an impurity embedded in an effective medium. The CPA successfully describes some one-particle properties, such as the average density of states (ADOS) in substitutional disordered alloys [112, 113, 114]. However, being a single-site approximation, the CPA by construction neglects all disorder-induced nonlocal correlations involving multiple scattering processes. To remedy this, cluster extensions of the CPA such as the dynamical cluster approximation (DCA) [115, 116, 117] and the molecular CPA [118] have been developed, where nonlocal effects are incorporated. Unfortunately, all of these methods fail to capture the Anderson localization transition since the ADOS utilized in these approaches is neither critical at the transition or distinguish the extended and the localized states.

In order to describe the Anderson transition in such effective medium theories, a proper order parameter has to be used. As noted by Anderson, the probability distribution of the local density of states (LDOS) must be considered, and the most probable or typical value would characterize it [103, 119]. It was found that the geometric mean of the LDOS is a good approximation of its typical value (TDOS) and it is critical at the transition [120, 106, 107], which makes it an appropriate order parameter to describe Anderson localization. Based on this idea, Dobrosavljevic *et al.*. [100] formulated a single-site typical medium theory (TMT) for Anderson localization which gives a qualitative description of the transition in three dimensions. In contrast to the CPA, the TMT uses the geometrical averaging over the disorder configuration in the self consistency loop. And thus, the typical not the average DOS is used as the order parameter. However, due to the single-site

nature of the TMT it neglects nonlocal correlations such as the effect of coherent back scattering. Thus, the TMT underestimates the critical disorder strength of the Anderson localization transition and fails to capture the reentrant behavior of the mobility edge (which separates the extended and localized states) for uniform box disorder.

Recently, a cluster extension of TMT was developed, named the typical medium dynamical cluster approximation (TMDCA) [105], which predicts accurate critical disorder strengths and captures the reentrant behavior of the mobility edge. The TMDCA was also extended to include off-diagonal in addition to diagonal disorder. [121]. However, like the TMT, the previous TMDCA implementations have only been developed for single-band systems, and in real materials, there are usually more than one band close to the Fermi level. Sen performed CPA calculation on two-band semiconducting binary alloys [122], and the electronic structure of disordered systems with multiple bands has also been studied numerically in finite systems [123, 124]. But a good effective medium theory to study Anderson localization transition in multiband systems is still needed to understand the localization phenomenon in real systems such as diluted doped semi-conductors, disordered systems with strong spin-orbital coupling, etc.

In this paper, we extend the TMDCA to multiple band disordered systems with both intra-band and inter-band hopping, and study the effect of intra-band disorder potential on electron localization. We perform calculations for both single-site and finite size clusters, and compare the results with those from numerically exact methods, including transfer matrix method (TMM) and kernel polynomial method (KPM). We show that finite sized clusters are necessary to include the nonlocal effects and produce more accurate results. Since these results show that the method is accurate and systematic, we then apply it to study the iron selenide superconductor $K_xFe_{2-y}Se_2$ with Fe vacancies, as an example to show that this method can be used to study localization effects in real materials. In addition, as an effective medium theory, our method is also able to treat interactions [125], unlike the TMM and KPM.

The paper is organized as follows. We present the model and describe the details of the formalism in Sec. 4.2. In Sec. 4.3.1, we present our results of the ADOS and TDOS for a two-band disordered system with various parameters, and use the vanishing of the TDOS to: determine the critical

disorder strength, extract the mobility edge and construct a complete phase diagram in the disorder-energy parameter space for different inter-band hopping. In Sec. 4.3.2, we discuss simulations of $K_xFe_{2-y}Se_2$ with Fe vacancies. We summarize and discuss future directions in Sec. 5.4. In Appendix 4.4, we provide justification for the use of our order parameter ansatz.

4.2 Formalism

4.2.1 Dynamical cluster approximation for multiband disordered systems

We consider the multiband Anderson model of non-interacting electrons with nearest neighbor hopping and random on-site potentials. The Hamiltonian is given by

$$\begin{aligned} H = &- \sum_{<ij>} \sum_{\alpha,\beta=1}^{l_b} t_{ij}^{\alpha\beta} (c_{i\alpha}^{\dagger} c_{j\beta} + c_{j\beta}^{\dagger} c_{i\alpha}) \\ &+ \sum_{i=1}^{N} \sum_{\alpha,\beta=1}^{l_b} (V_i^{\alpha\beta} - \mu\delta_{\alpha\beta}) n_i^{\alpha\beta} \end{aligned} \tag{4.1}$$

The first term provides a realistic multiband description of the host valence bands. The labels i, j are site indices and α, β are band indices. The operators $c_{i\alpha}^{\dagger}(c_{i\alpha})$ create (annihilate) a quasiparticle on site i and band α. The second part denotes the disorder, which is modeled by a local potential $V_i^{\alpha\beta}$ that is randomly distributed according to some specified probability distribution $P(V_i^{\alpha\beta})$, where $n_i^{\alpha\beta} = c_{i\alpha}^{\dagger} c_{i\beta}$, μ is the chemical potential, and $t_{ij}^{\alpha\beta}$ are the hopping matrix elements. Here we consider binary disorder, where the random on-site potentials $V_i^{\alpha\beta}$ obey independent binary probability distribution functions with the form

$$P(V_i^{\alpha\beta}) = x\delta(V_i^{\alpha\beta} - V_A^{\alpha\beta}) + (1-x)\delta(V_i^{\alpha\beta} - V_B^{\alpha\beta}). \tag{4.2}$$

In our model, there are l_b band indices so that both the hopping and disorder potential are $l_b \times l_b$

matrices. The random potential is

$$\underline{V_i} = \begin{pmatrix} V_i^{\alpha\alpha} & \cdots & V_i^{\alpha\beta} \\ . & . & . \\ . & . & . \\ . & . & . \\ V_i^{\alpha\alpha} & \cdots & V_i^{\beta\alpha} \end{pmatrix}, \tag{4.3}$$

while the hopping matrix is

$$\underline{t_{ij}} = \begin{pmatrix} t_{ij}^{\alpha\alpha} & \cdots & t_{ij}^{\alpha\beta} \\ . & . & . \\ . & . & . \\ . & . & . \\ t_{ij}^{\beta\alpha} & \cdots & t_{ij}^{\beta\beta} \end{pmatrix}, \tag{4.4}$$

where underbar denotes $l_b \times l_b$ matrix, $t^{\alpha\alpha}$ and $t^{\beta\beta}$ are intra-band hoppings, while $t^{\alpha\beta}$ and $t^{\beta\alpha}$ are inter-band hoppings. Similar definitions apply to the disorder potentials. If we restrict the matrix elements to be real, Hermiticity requires both matrices to be symmetric, i.e., $t^{\alpha\beta} = t^{\beta\alpha}$ and $V_i^{\alpha\beta} = V_i^{\beta\alpha}$.

To solve the Hamiltonian of Eq. 4.1, we first generalize the standard DCA to a multiband system. Within DCA the original lattice model is mapped onto a cluster of size $N_c = L^3$ with periodic boundary condition embedded in an effective medium. The first Brillouin zone is divided in N_c coarse grained cells [116], whose center is labeled by K, surrounded by points labeled by $\tilde{k}$ within the cell. Therefore, all the k-points are expressed as $k = K + \tilde{k}$. The effective medium is characterized by the hybridization function $\underline{\Delta(K,\omega)}$. The generalization of the DCA to a multiband system entails representing all the quantities in momentum space as $l_b \times l_b$ matrices.

The DCA self-consistency loop starts with an initial guess for the hybridization matrix $\underline{\Delta(K,\omega)}$,

which is given by

$$\underline{\Delta(K,\omega)} = \begin{pmatrix} \Delta^{\alpha\alpha}(K,\omega) & \cdots & \Delta^{\alpha\beta}(K,\omega) \\ . & . & . \\ . & . & . \\ . & . & . \\ \Delta^{\beta\alpha}(K,\omega) & \cdots & \Delta^{\beta\beta}(K,\omega) \end{pmatrix}. \tag{4.5}$$

For the disordered system, we must solve the cluster problem in real space. In that regard, for each disorder configuration described by the disorder potential V we calculate the corresponding cluster Green function which is now an $l_b N_c \times l_b N_c$ matrix

$$\underline{G_c}(V) = \left(\omega\mathbb{I} - \underline{t}^{(\alpha\beta)} - \underline{\Delta}'^{(\alpha\beta)} - \underline{V}^{\alpha\beta}\right)^{-1}. \tag{4.6}$$

Here, $\mathbb{I}$ is identity matrix and Δ'_{ij} is the Fourier transform (FT) of the hybridization, i.e.,

$$\Delta'^{\alpha\beta}_{ij} = \sum_K \Delta^{\alpha\beta}(K) exp[iK \cdot (r_i - r_j)]. \tag{4.7}$$

We then stochastically sample random configurations of the disorder potential V and average over disorder $\langle(\cdots)\rangle$ to get the $l_b N_c \times l_b N_c$ disorder averaged cluster Green function in real space

$$\underline{G_c(\omega)_{ij}} = \begin{pmatrix} \langle G_c^{\alpha\alpha}(\omega,V)\rangle_{ij} & \cdots & \left\langle G_c^{\alpha\beta}(\omega,V)\right\rangle_{ij} \\ . & . & . \\ . & . & . \\ . & . & . \\ \left\langle G_c^{\beta\alpha}(\omega,V)\right\rangle_{ij} & \cdots & \left\langle G_c^{\beta\beta}(\omega,V)\right\rangle_{ij} \end{pmatrix}. \tag{4.8}$$

We then Fourier transform to K space and also impose translational symmetry to construct the K-dependent disorder averaged cluster Green function $\underline{G_c(K,\omega)}$, which is a $l_b \times l_b$ matrix for each

K component

$$\underline{G_c(K,\omega)} = \begin{pmatrix} G_c^{\alpha\alpha}(K,\omega) & \cdots & G_c^{\alpha\beta}(K,\omega) \\ . & . & . \\ . & . & . \\ . & . & . \\ G_c^{\beta\alpha}(K,\omega) & \cdots & G_c^{\beta\beta}(K,\omega) \end{pmatrix}. \tag{4.9}$$

After the cluster problem is solved, we can calculate the coarse grained lattice Green function matrix

$$\begin{aligned} \underline{\overline{G}(K,\omega)} &= \begin{pmatrix} \overline{G}^{\alpha\alpha}(K,\omega) & \cdots & \overline{G}^{\alpha\beta}(K,\omega) \\ . & . & . \\ . & . & . \\ . & . & . \\ \overline{G}^{\beta\alpha}(K,\omega) & \cdots & \overline{G}^{\beta\beta}(K,\omega) \end{pmatrix} \\ &= \frac{N_c}{N} \sum_{\tilde{k}} \left(\underline{G_c(K,\omega)}^{-1} + \underline{\Delta(K,\omega)} - \underline{\varepsilon_k} + \underline{\overline{\epsilon}(K)} \right)^{-1}, \end{aligned} \tag{4.10}$$

where the overbar denotes cluster coarse-graining, and $\underline{\overline{\epsilon}(K)}$ is the cluster coarse-graining Fourier transform of the kinetic energy

$$\underline{\overline{\epsilon}(K)} = \underline{E_0} + \frac{N_c}{N} \sum_{\tilde{k}} \underline{\varepsilon_k} \tag{4.11}$$

where $E_0^{\alpha\beta}$ is a local energy, which is used to shift the bands. The diagonal components of Eq. 4.10 have the same normalization than a conventional, i.e., scalar, Green function.

The DCA self-consistency condition requires the disorder averaged cluster Green function equal the coarse grained lattice Green function

$$\underline{G_c(K,\omega)} = \underline{\bar{G}(K,\omega)}. \tag{4.12}$$

Then, we close our self-consistency loop by updating the hybridization function matrix using

linear mixing

$$\underline{\Delta_n(K,\omega)} = \underline{\Delta_o(K,\omega)} + \xi[\underline{G_c^{-1}(K,\omega)} - \underline{\bar{G}^{-1}(K,\omega)}], \tag{4.13}$$

where the subscript "o" and "n" denote old and new respectively, and ξ is a linear mixing factor $0 < \xi < 1$. The procedure above is repeated until the hybridization function matrix converges to the desirable accuracy $\underline{\Delta_n(K,\omega)} = \underline{\Delta_o(K,\omega)}$.

We can see that when the inter-band hopping, $t^{\alpha\beta}$, and disorder potential, $V^{\alpha\beta}$, vanish all the $l_b \times l_b$ matrices become diagonal, and the formalism reduces to single band DCA for l_b independent bands.

4.2.2 Typical medium theory for multiband disordered systems

To study localization in multiband systems, we generalize the recently developed TMDCA [105] where the TDOS is used as the order parameter of the Anderson localization transition, so the electron localization is captured by the vanishing of the TDOS. We will use this TMDCA formalism to address the question of localization and mobility edge evolution in the multiband model.

Unlike the standard DCA, where the Green function is averaged over disorder algebraically, the TMDCA calculates the typical (geometrically) averaged cluster density of states in the self-consistency loop as

$$\rho_c^{typ}(K,\omega) = e^{\frac{1}{Nc}\sum_i \langle \log \rho_{ii}(\omega)\rangle} \left\langle \frac{\rho(K,\omega)}{\frac{1}{Nc}\sum_i \rho_{ii}(\omega)} \right\rangle, \tag{4.14}$$

which is constructed as a product of the geometric average of the local density of states, $\rho_{ii} = -\frac{1}{\pi} ImG_{ii}(\omega)$, and the linear average of the normalized momentum resolved density of states $\rho(K,\omega) = -\frac{1}{\pi} ImG_c(K,\omega)$. The cluster-averaged typical Green function is constructed via the Hilbert transformation

$$G_c^{typ}(K,\omega) = \int d\omega' \frac{\rho_c^{typ}(K,\omega')}{\omega - \omega'}. \tag{4.15}$$

Generalization of the TMDCA to the multiband case is not straightforward since the off-diagonal LDOS $\rho_{ii}^{\alpha\beta}(\omega) = -\frac{1}{\pi} G_{ii}^{\alpha\beta}(\omega)$ is not positive definite. We construct the $l_b \times l_b$ matrix for the typical

density of states as

$$\underline{\rho^c_{typ}(K,\omega)} = \begin{pmatrix} e^{\frac{1}{Nc}\sum_i \left\langle ln\rho^{\alpha\alpha}_{ii}(\omega)\right\rangle} \left\langle \frac{\rho^{\alpha\alpha}(K,\omega)}{\frac{1}{Nc}\sum_i \rho^{\alpha\alpha}_{ii}(\omega)} \right\rangle & \cdots & e^{\frac{1}{Nc}\sum_i \left\langle ln|\rho^{\alpha\beta}_{ii}(\omega)|\right\rangle} \left\langle \frac{\rho^{\alpha\beta}(K,\omega)}{\frac{1}{Nc}\sum_i |\rho^{\alpha\beta}_{ii}(\omega)|} \right\rangle \\ . & . & . \\ . & . & . \\ . & . & . \\ e^{\frac{1}{Nc}\sum_i \left\langle ln|\rho^{\beta\alpha}_{ii}(\omega)|\right\rangle} \left\langle \frac{\rho^{\beta\alpha}(K,\omega)}{\frac{1}{Nc}\sum_i |\rho^{\beta\alpha}_{ii}(\omega)|} \right\rangle & \cdots & e^{\frac{1}{Nc}\sum_i \left\langle ln\rho^{\beta\beta}_{ii}(\omega)\right\rangle} \left\langle \frac{\rho^{\beta\beta}(K,\omega)}{\frac{1}{Nc}\sum_i \rho^{\beta\beta}_{ii}(\omega)} \right\rangle \end{pmatrix}. \tag{4.16}$$

The diagonal part takes the same form as the single-band TMDCA ansatz, and the off-diagonal part takes a similar form but involves the absolute value of the off-diagonal 'local' density of states.

We construct the typical cluster Green function through a Hilbert transformation

$$\underline{G^c_{typ}(K,\omega)} = \begin{pmatrix} \int d\omega' \frac{\rho^{\alpha\alpha}_{typ}(K,\omega')}{\omega-\omega'} & \cdots & \int d\omega' \frac{\rho^{\alpha\beta}_{typ}(K,\omega')}{\omega-\omega'} \\ . & . & . \\ . & . & . \\ . & . & . \\ \int d\omega' \frac{\rho^{\beta\alpha}_{typ}(K,\omega')}{\omega-\omega'} & \cdots & \int d\omega' \frac{\rho^{\beta\beta}_{typ}(K,\omega')}{\omega-\omega'} \end{pmatrix}, \tag{4.17}$$

which plays the same role as $\underline{G_c(K,\omega)}$ in the DCA loop. Once $\underline{G_{typ}}$ is calculated from Eq. 4.17, the self-consistency steps are the same as those in the multiband DCA described in the previous section: we calculate the coarse grained lattice Green function using Eq. 4.10, and use it to update the hybridization function matrix of the effective medium via Eq. 4.13.

The proposed ansatz Eq. 4.16 has the following properties. When the inter-band hopping $t^{\alpha\beta}$ and disorder potential $V^{\alpha\beta}$ vanish, it reduces to single-band TMDCA for l_b independent bands, since all the off-diagonal elements of the Green functions vanish. When disorder is weak, all the $V^{\alpha\alpha}$ are small so the distribution of the LDOS becomes Gaussian with equal linear and geometric average so it reduces to DCA for a multiband disordered system.

When convergence is achieved, we use the total TDOS $\rho^{tot}_{typ}(\omega)$ to determine the mobility edge

which is calculated as the trace of the local TDOS matrix

$$\rho_{typ}^{tot}(\omega) = Tr\left[\frac{1}{N_c}\sum_{K}\underline{\rho_{typ}(K,\omega)}\right] = \sum_{\forall\alpha=\beta}\rho_{typ}^{\alpha\beta}(\omega). \tag{4.18}$$

This construction of the order parameter may not seem very physical as the typical value of the LDOS should serve as the order parameter [103, 119], and the LDOS for the multiband system is the sum of the l_b bands in the local site basis $\rho_i^{tot} = \sum_{\alpha=\beta}\rho_i^{\alpha\beta}(\omega)$. Therefore, the real order parameter should be the typical value of ρ_i^{tot} defined as the geometric average of the total LDOS, $\exp\left(\frac{1}{N_c}\sum_i \log\rho_i^{tot}\right)$ which is invariant under local unitary transformations and is not equal to the ρ_{typ}^{tot} defined in Eq. 4.18.

However, Eq. 4.18 should also be a correct order parameter as long as it vanishes simultaneously with the typical value of ρ_i^{tot}, and we show this in Appendix 4.4. By considering the distribution of the LDOS in each band, Appendix 4.4 shows that when localized states mix with extended states the system is still extended, which is consistent with Mott's insight about the mobility edge [126]. Intuitively, this makes sense as when all the distributions of $\rho_i^{\alpha\alpha}$ are critical then the typical values must behave as $|V - V_c|^{\beta_\nu}$ near the transition, and so their sum must as well. If one is not critical (on the metallic side) then Eq. 4.18 will not vanish as $|V - V_c|^{\beta_\nu}$, as expected.

To test our multiband typical medium dynamical cluster approximation formulation, we apply it to the specific case of a two band model, unless otherwise stated in Sec. 5.3. Throughout the discussion of our results below, we denote α as a and β as b.

4.3 Results

4.3.1 Two band model

As a specific example, we test the generalized DCA and TMDCA algorithms for a three-dimensional system with two degenerate bands (ab) described by Eq. 4.1. In this case, both the hopping and

disorder potential are 2×2 matrices in the band basis given by

$$\underline{t_{ij}} = \underline{t} = \begin{pmatrix} t^{aa} & t^{ab} \\ t^{ba} & t^{bb} \end{pmatrix}, \tag{4.19}$$

and

$$\underline{V_i} = \begin{pmatrix} V_i^{aa} & V_i^{ab} \\ V_i^{ba} & V_i^{bb} \end{pmatrix}, \tag{4.20}$$

respectively. The intra-band hopping is set as $t^{aa} = t^{bb} = 1$, with finite inter-band hopping t^{ab}. Here, the hopping matrix is defined as dimensionless so that the bare dispersion can be written as $\underline{\varepsilon_k} = \underline{t}\varepsilon_k$ with $\varepsilon_k = -2t[\cos(k_x) + \cos(k_y) + \cos(k_z)]$ in three dimensions. We choose $4t = 1$ to set the units of energy. We consider the two bands orthogonal to each other, where the local inter-band disorder $V_i^{\alpha\beta}$ vanishes and the randomness comes from the local intra-band disorder potential $V_i^{\alpha\alpha}$ that follow independent binary probability distribution functions with equal strength, $V^{aa} = V^{bb}$. Since the two bands are degenerate and the disorder strength for each band is also identical, the calculated average DOS will be the same for each band, so we only plot the quantities for one of the bands in the following results, as it is enough to characterize the properties of the system.

In our formalism, in order to disorder average instead of performing the very expensive enumeration of all disorder configurations, which scales as 2^{2N_c}, we perform a stochastic sampling of configurations which greatly reduces the computational cost [127]. This is so we can study larger systems. For a typical $N_c = 64$ calculation, 500 disorder configurations are enough to produce reliable results and this number decreases with increasing cluster size.

We first compare the ADOS and TDOS at various disorder strengths $V^{aa}(V^{bb})$, with a fixed inter-band hopping $t^{ab} = 0.3$, for different cluster sizes N_c in Fig. 4.3. Our TMDCA scheme for $N_c = 1$ corresponds to the analog of the TMT for two-band systems, and the ADOS is calculated with the two-band DCA. To show the effects of non-local correlations introduced by finite clusters, we present data for both $N_c = 1$ and $N_c > 1$. We can clearly see that the TDOS, which can be viewed as the the order parameter of the Anderson localization transition, gets suppressed as the disorder increases . By comparing the width of the extended state region, where the TDOS is finite,

we can see that single site TMT overestimates localization.

From Fig. 4.3, we see that the results of TMDCA for $N_c = 64$ and $N_c = 216$ are almost on top of each other, showing a quick convergence with the increase of cluster size. To see this more

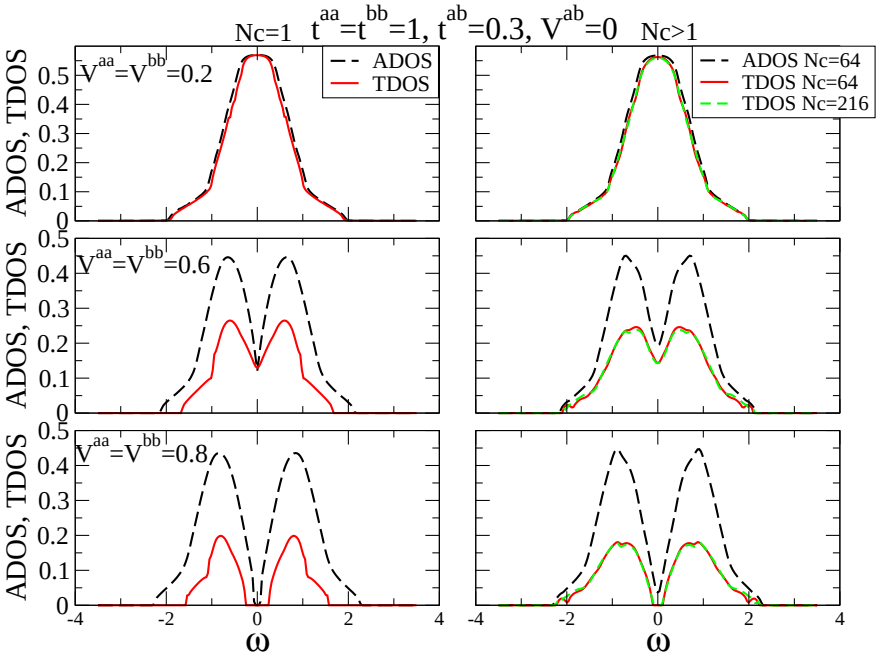

Figure 4.3: Evolution of the ADOS and TDOS at different disorder strengths $V^{aa}(V^{bb})$, for $N_c = 1$ (left panel) and $N_c > 1$ (right panel) for fixed $t^{ab} = 0.3$. For small disorder, the ADOS and TDOS are almost identical. The TDOS is suppressed as the disorder increases. The extended states region with finite TDOS for $N_c = 1$ is narrower than the results of $N_c > 1$ which indicates that the single-site TMT overemphasizes localization.

clearly, we plot in Fig. 4.4 the TDOS at the band center for two different disorder strengths and various cluster sizes. We see that the results for both cases converge quickly with cluster size. Faster convergence (around $N_c = 38$) is reached for the case further away from the critical region ($V^{aa} = V^{bb} = 0.6$) than for the one closer ($V^{aa} = V^{bb} = 0.7$) where convergence is reached around $N_c = 98$. This is expected due to the critical slowing down close to the transition. To further study the convergence, we also plot in Fig. 4.5 the TDOS at the band center as a function of disorder strength ($V^{aa} = V^{bb}$) for several N_c. The critical disorder strength is defined by the vanishing of the TDOS($\omega = 0$). The results show a systematic increase of the critical disorder strength as N_c increases, and the convergence is reached at $N_c = 98$ with the critical value of 0.74.

To study the effect of inter-band hopping t^{ab}, we calculate the disorder-energy phase diagram

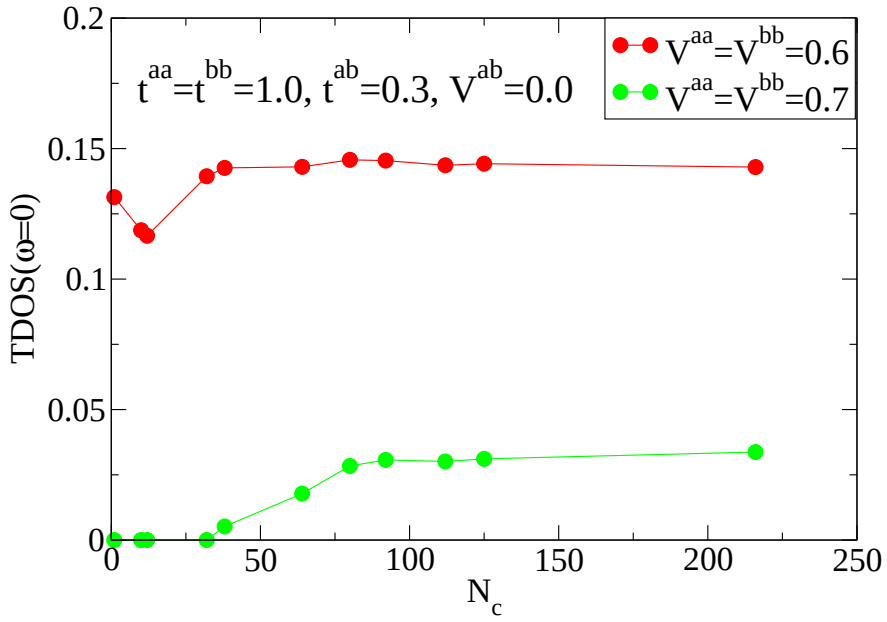

Figure 4.4: Evolution of the TDOS at the band center ($\omega = 0$) with increasing cluster size for two different sets of parameters with $t^{aa} = t^{bb} = 1.0$, $t^{ab} = 0.3$, $V^{ab} = 0.0$, $V^{aa} = V^{bb} = 0.6, 0.7$. The former has faster convergence (around $N_c = 38$) than the latter (around $N_c = 98$), due to the critical slowing down closer to the transition region.

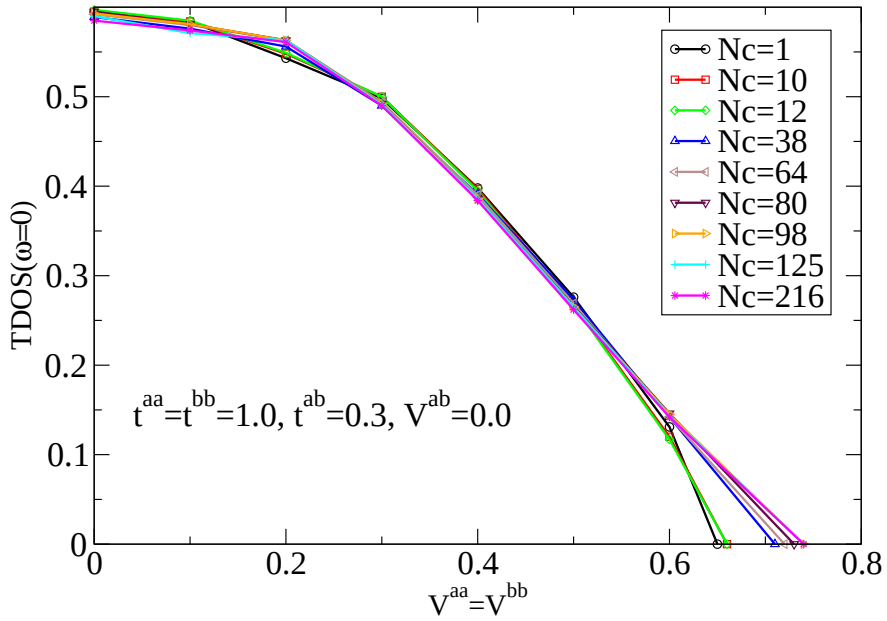

Figure 4.5: The TDOS at the band center ($\omega = 0$) vs. $V^{aa} = V^{bb}$ with increasing cluster size, for $t^{aa} = t^{bb} = 1.0$, $t^{ab} = 0.3$, $V^{ab} = 0.0$. For $N_c = 1$, the critical disorder strength is 0.65 and as N_c increases, it increases and converges to 0.74 for $N_c = 98$.

for the case with vanishing t^{ab} and finite $t^{ab} = 0.3$ in Fig. 4.6. The mobility edge is determined

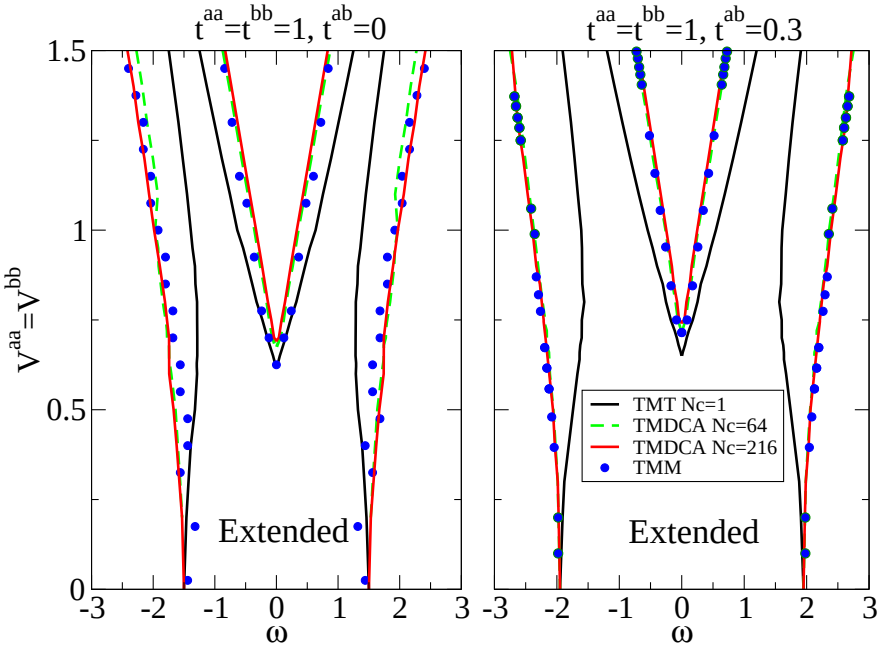

Figure 4.6: Disorder-energy phase diagram for vanishing t^{ab} (left panel) and finite $t^{ab} = 0.3$ (right panel). We compare the mobility edge obtained from the TMT ($N_c = 1$), TMDCA ($N_c = 64$ and 216) and TMM. Parameters for the TMM data are given in the text (the TMM data for $t_{ab} = 0.0$ is reproduced from [121]). A finite t^{ab} increases the critical disorder strength, indicating that t^{ab} results in a delocalizing effect. The single site TMT overestimates the localized region.

by the energy where the TDOS vanishes. By comparing the left and right panels, we can see that introducing a finite t^{ab} makes the system more difficult to localize, causing an upward shift of the mobility edge. The single site TMT overestimates the localized region compared to finite cluster results. We also compare our results with those from the TMM [98, 149, 150] to check the accuracy of the mobility edge calculated from TMDCA. For the TMM, the Schrödinger equation is written in terms of wavefunction amplitudes for adjacent layers in a quasi-one dimensional system, and the correlation (localization) length is computed by accumulating the Lyapunov exponents of successive transfer matrix multiplications that describe the propagation through the system. All TMM data is for a 3d system of length $L = 10^6$ and the Kramer-MacKinnon scaling parameter $\Lambda(V, M)$ is computed for a given disorder strength V and "bar" width M. The transfer matrix is a $2Ml_b \times 2Ml_b$ matrix. The system widths used were $M = [4 - 12]$. The critical point is found by identifying the crossing of the $\Lambda(M)$vs.V curves for different system sizes. The transfer matrix

product is reorthogonalized after every five multiplications.

To see the effect of inter-band hopping more directly, we now consider increasing t^{ab} while keeping the disorder strength fixed ($V^{aa} = V^{bb} = 0.71$), and study the evolution of the mobility edge (Fig. 4.7). The localized region around the band center starts to shrink as t^{ab} is increased, leading to a small dome-like shape with the top located at $t^{ab} = 0.2$. This shows that increasing t^{ab} delocalizes the system which is reasonable since increasing t^{ab} effectively increases the bare bandwidth.

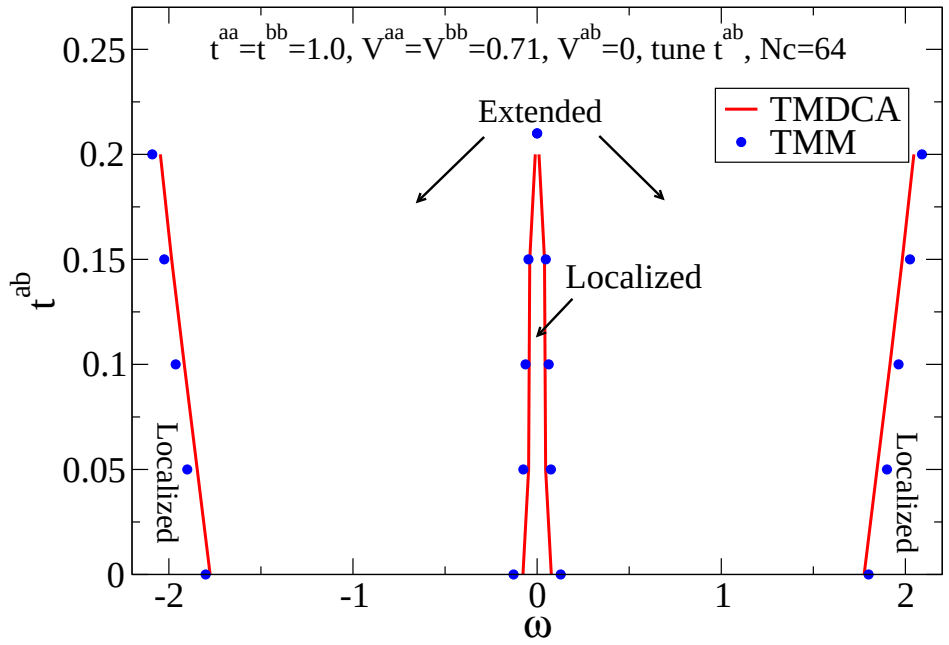

Figure 4.7: Evolution of the mobility edge as t^{ab} increases, while V^{aa} and V^{bb} are fixed. The results are calculated for $N_c = 64$. A dome-like shape shows up around the band center, signaling the closing of the TDOS gap. Parameters for the TMM data are given in the text.

To further benchmark our algorithms, we plot the ADOS and TDOS calculated with two-band DCA and TMDCA together with those calculated by the KPM [108, 109, 128, 129] (Fig. 4.8). In the KPM analysis, the LDOS is expanded by a series of Chebyshev polynomials, so that the ADOS and TDOS can be evaluated. The details for the implementation of KPM are well discussed in Ref. [109] and the parameters used in the KPM calculations are listed in the caption of Fig. 4.8. The Jackson kernel is used in the calculations [109]. As shown in the plots, the results from the generalized DCA and TMDCA match nicely with those calculated from the KPM.

The excellent agreement of the TMDCA results with those from more conventional numerical methods, like KPM and TMM, suggest that the method may be used for the accurate study of real materials.

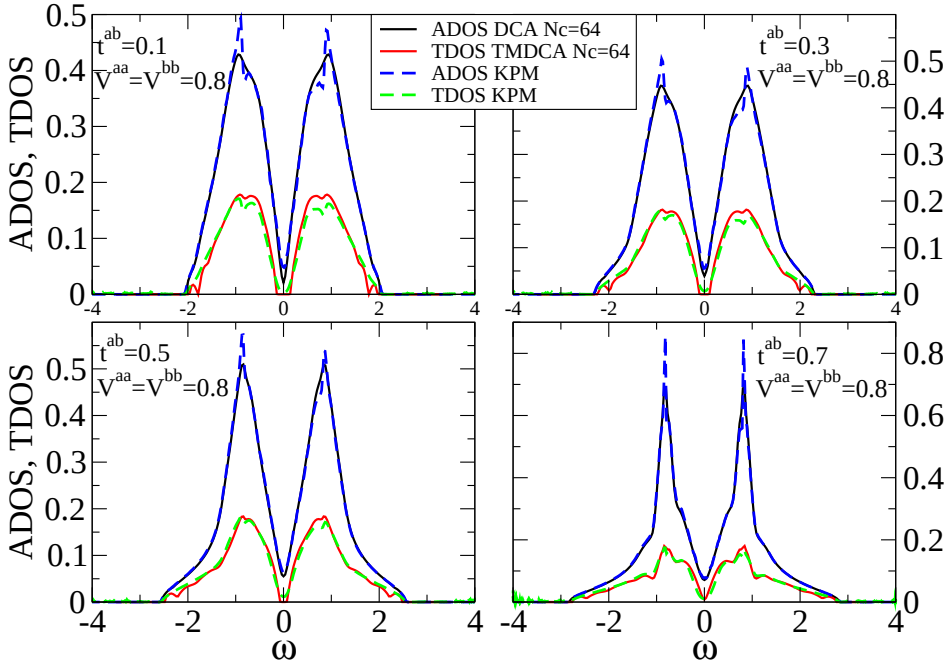

Figure 4.8: Comparison of ADOS and TDOS calculated with DCA, TMDCA and KPM with fixed disorder strength $V^{aa} = V^{bb} = 0.8$ and various values of inter-band hopping t^{ab}. The KPM uses 2048 moments on a cubic lattice of size 48^3 and 200 independent realizations generated with 32 sites randomly sampled from each realization.

4.3.2 Application to $K_yFe_{2-x}Se_2$

Next, we demonstrate the method with a case study of Fe vacancies in the Fe-based superconductor $K_xFe_{2-y}Se_2$, which has been studied intensely because of its peculiar electronic and structural properties. Early on it was found that there is a strong $\sqrt{5} \times \sqrt{5}$ ordering of Fe vacancies [130]. Later it was discovered that this material also contains a second phase[131, 132]. It is commonly speculated that the second phase is the one that hosts the superconducting state and the phase with the $\sqrt{5} \times \sqrt{5}$ vacancy ordering is an antiferromagnetic (AFM) insulator. Recent measurements of the local chemical composition [133, 134] have determined that the second phase also contains a large concentration of Fe vacancies (up to 12.5%). However, these Fe vacancies are not well ordered

since no strong reconstruction of the Fermi surface [135, 136, 137] was observed by angle-resolved photoelectron spectroscopy (ARPES) experiments [138, 139].

Interestingly, with such a disordered structure, this material hosts a relatively high superconducting transition temperature of 31 K at ambient pressure [140]. It was the first Fe-based superconductor that was shown from ARPES [138, 139] to have a Fermi surface with electron pockets only and no hole pockets, apparently disfavoring the widely discussed $S^{\pm}$ pairing symmetry [141] in the Fe-based superconductors. $K_xFe_{2-y}Se_2$ is also the only Fe-based superconductor whose parent compound (with perfectly ordered Fe vacancy) is an AFM insulator [142] rather than a AFM bad metal. Furthermore from neutron scattering [130], it has been observed that the anti-ferromagnetism has a novel block type structure with a record high Neel temperature of $T_N = 559K$ and magnetic moment of $3.31\mu_B$/Fe. Such a special magnetic structure is obviously not driven from the nesting of the simple Fermi surface, but requires the interplay between local moments and itinerant carriers present in the normal state [143, 144].

Given that Fe vacancies are about the strongest possible type of disorder that can exist in Fe-based superconductors and given that the Fe-based superconductors are quasi two-dimensional materials, it is natural to speculate how close the second phase is to an Anderson insulator. If it is indeed close, this would have interesting implications for the strong correlation physics and the non-conventional superconductivity in these compounds.

To investigate the possibility of Anderson localization in the second phase of $K_xFe_{2-y}Se_2$ we will employ TMDCA on a realistic first principles model. To this end we use Density Functional Theory (DFT) in combination with the projected Wannier function technique [145] to extract the low energy effective Hamiltonian of the Fe-d degrees of freedom. Specifically we applied the WIEN2K [146] implementation of the full potential linearized augmented plane wave method in the local density approximation. The k-point mesh was taken to be $10\times10\times10$ and the basis set size was determined by RKmax=7. The lattice parameters of the primitive unit cell (c.f. Fig. 4.9(b)) are taken from Ref. [130]. The subsequent Wannier transformation was defined by projecting the Fe-d characters on the low energy bands within the interval [-3,2] eV. For numerical convenience, we use the conventional unit cell shown in Fig. 4.9(a) which contains 4 Fe atoms. Since there are 5 d orbitals per Fe atom,

we are dealing with a 20-band problem. To simulate the effect of Fe vacancies we add a local binary disorder with strength V and Fe vacancy concentration c_a:

$$P(V_i) = c_a\delta(V_i - V) + (1 - c_a)\delta(V_i). \tag{4.21}$$

We set the disorder strength to be $V = 20eV$, much larger than the Fe-d bandwidth, such that it effectively removes the corresponding Fe-d orbitals from the low energy Hilbert space. This will capture the most dominant effect of the Fe vacancies. The Fe concentration is taken to be $c_a = 12.5\%$, which is the maximum value found in the experiments.

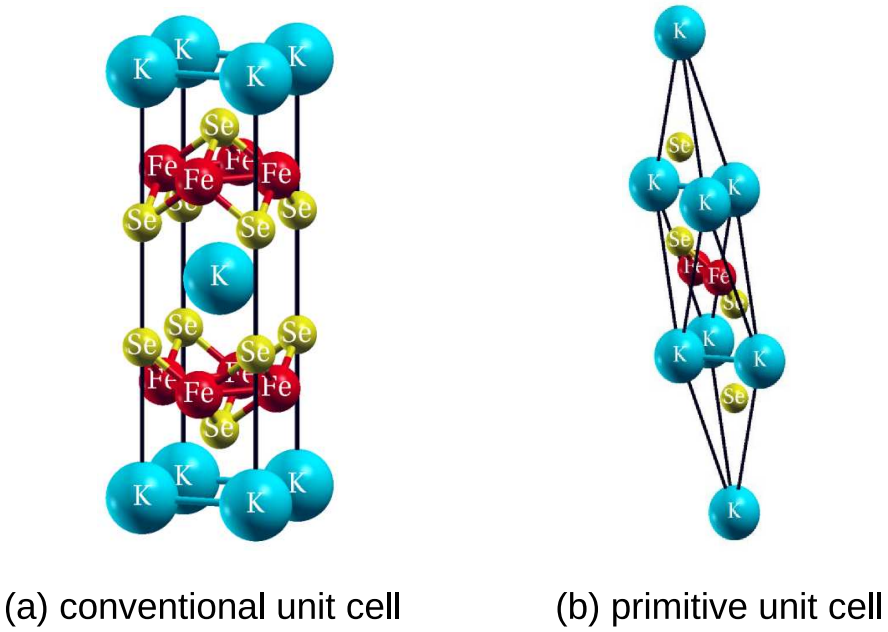

Figure 4.9: Crystal structure of KFe_2Se_2.

Fig. 4.10 presents the ADOS and TDOS, obtained from our multiband TMDCA for which we considered two cluster sizes $N_c = 1$ and $N_c = 2\sqrt{2} \times 2\sqrt{2} \times 2 = 16$. Consistent with the model calculations presented in the previous sections, we find that the TMT ($N_c = 1$) tends to overestimate the localization effects compared to TMDCA results ($N_c = 16$). While the TMT shows localized states within [0.6,1.1] eV, the TMDCA for $N_c = 16$ finds localized states in the much smaller energy region [1.0,1.1] eV instead. Apparently a concentration of $c_a = 12.5\%$ is still too small to cause

any significant localization effects despite the strong impurity potentials of the Fe vacancies and the material being quasi-two dimensional. To determine the chemical potential we consider two fillings. The first filling of 6.0 electrons per Fe corresponds to the reported $K_2Fe_7Se_8$ phase [134]. Since strong electron doping has been found in ARPES experiments [138, 139], we also consider a filling of 6.5 electrons per Fe. The latter would correspond to the extreme case of no vacancies. Clearly for both fillings the chemical potential remains energetically very far from the mobility edge, and thus far from Anderson insulating.

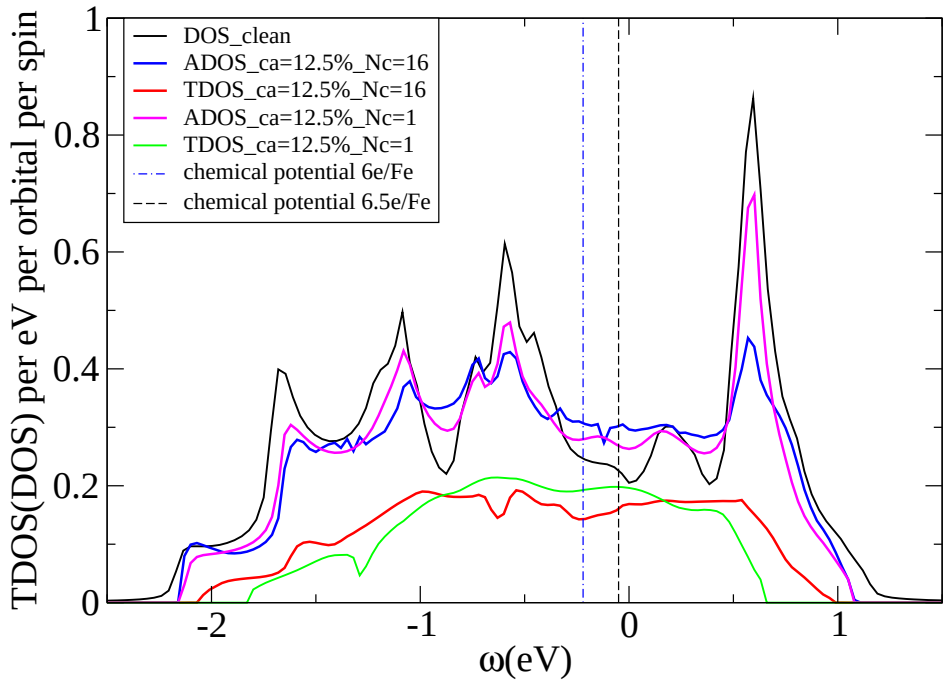

Figure 4.10: The average and typical density of states of KFe_2Se_2 with 12.5% Fe vacancy concentration calculated by multiband DCA and TMDCA with cluster size $N_c = 1$ and $N_c = 16$, compared with the average density of states of the clean (no vacancy) KFe_2Se_2.

4.4 Conclusion

We extend the single-band TMDCA to multiband systems and study electron localization for a two-band model with various hopping and disorder parameters. We benchmark our method by comparing our results with those from other numerical methods (TMM and KPM) and find good agreement. We find that the inter-band hopping leads to a delocalization effect, since it gradually

closes the $\omega = 0$ disorder induced gap on the TDOS. A direct application of our extended TMDCA could be done for disordered systems with strong spin-orbital coupling. Combined with electronic structure calculations, our method can be used to study the electron localization phenomenon in real materials. To show this, we apply this approach to the iron selenide superconductors $K_xFe_{2-y}Se_2$ with Fe vacancies. By calculating the TDOS around the chemical potential, we conclude that the insulating behavior of its normal state is unlikely due to Anderson localization. This method also has the ability to include interactions [125], and future work will involve real material calculations that fully treat both disorder and interactions.

Acknowledgments– This work is supported in part by the National Science Foundation under the NSF EPSCoR Cooperative Agreement No. EPS-1003897 with additional support from the Louisiana Board of Regents (YZ, HT, CM, CE, KT, JM, and MJ). Work by TB was performed at the Center for Nanophase Materials Sciences, a DOE Office of Science user facility. This manuscript has been authored by UT-Battelle, LLC under Contract No. DE-AC05-00OR22725 with the U.S. Department of Energy. WK acknowledges support from U.S. Department of Energy, Office of Basic Energy Science, Contract No. DEAC02-98CH10886. This work used the high performance computational resources provided by the Louisiana Optical Network Initiative (http://www.loni.org), and HPC@LSU computing. The United States Government retains and the publisher, by accepting the article for publication, acknowledges that the United States Government retains a non-exclusive, paid-up, irrevocable, world-wide license to publish or reproduce the published form of this manuscript, or allow others to do so, for United States Government purposes. The Department of Energy will provide public access to these results of federally sponsored research in accordance with the DOE Public Access Plan (http://energy.gov/downloads/doepublic- access-plan).

The order parameter defined in Eq. 4.18

We know the system is localized if the distribution of the total LDOS is critical, having a probability distribution $p(\rho_i^{aa} + \rho_i^{bb})$ which is highly skewed with a typical value close to zero. So if we can show that this is true if and only if both ρ_i^{aa} and ρ_i^{bb} are critical, then the critical behavior is basis independent and we can choose any particular basis and use the order parameter defined by Eq. 4.18

to study the localization transition.

To show this is true, we consider two probability distribution functions $p_1(x_1)$ and $p_2(x_2)$. The probability distribution function for $X = x_1 + x_2$ is

$$P(X) = \int_0^X p_1(x)p_2(X-x)dx, \tag{4.22}$$

and we want to show $P(X)$ is critical if and only if both $p_1(x_1)$ and $p_2(x_2)$ are critical.

4.4.1 Sufficiency

If both $p_1(x)$ and $p_2(x)$ are critical, then both $p_1(x)$ and $p_2(x)$ are dominated by the region $0 < x < \delta$ where $\delta \to 0^+$. The contribution to the integral in $P(X)$ mainly comes from the region $0 < x < \delta$ and $0 < X - x < \delta$ which is $max(X-\delta, 0) < x < min(\delta, X)$. Since δ is infinitesimal, we can assume $X > \delta$, and then we have $X - \delta < x < \delta$. To maximize $P(X)$, we want this region to be as big as possible, so we want $\delta - (X - \delta) = 2\delta - X$ to be as big as possible which means X must be smaller than $2\delta \to 0^+$. Thus, $P(X)$ is also critical with the typical value around 2δ which is infinitesimal.

4.4.2 Necessity

We now consider the case where one of the distributions is not critical. Without loss of generality, we assume $p_2(x)$ is not critical and is peaked at some finite value x_0. We calculate

$$\begin{aligned} P(x_0) - P(\delta) &= \int_0^{x_0} p_1(x)p_2(x_0-x)dx - \int_0^{\delta} p_1(x)p_2(\delta-x)dx \\ &= \int_0^{\delta} p_1(x)[p_2(x_0-x) - p_2(\delta-x)]dx + \int_{\delta}^{x_0} p_1(x)p_2(x_0-x)dx. \end{aligned} \tag{4.23}$$

The first term is positive since $p_2(x)$ is peaked around x_0 and $\delta \ll x_0$. The second term is positive obviously, so $P(x_0) > P(\delta)$. Therefore, $P(X)$ is not critical.

In this way we argue that $P(X)$ is critical if and only if both $p_1(x_1)$ and $p_2(x_2)$ are critical. In other words, when the localized states hybridize with extended states, only extended states remain which is exactly Mott's insight about the mobility edge [126]. The generalization to the multiple band case is trivial.

Chapter 5

Multifractal Study of Quasiparticle Localization in Disordered Superconductors

In addition to off-diagonal disorder and multiple bands, materials can also be superconducting. This adds much complication to the interpretation of localization in the Anderson sense as one can not only consider localization of the charge carriers (resulting in a standard metal to insulator transition as has so far been considered in this thesis), but of any quasiparticle excitations and it is an open question if the "traditional" methods of numerical analysis of disordered systems can be applied to capture such a localization transition. The purpose of this work was to apply the multifractal analysis that has been applied to the Anderson model to a model of a disordered superconductor to establish it can also capture the localization of bogolons (the excitations of this Hamiltonian), and the application of TMDCA to such a model is considered for future work.

My contribution to this work that was made in collaboration with K.-M. Tam, Yi Zhang, and M. Jarrell that has been submitted to Physical Review B was to first determine the critical parameters (the critical disorder strength W_c and correlation exponent ν) with a TMM code for a superconductor with extended s-wave pairing. The reason for this choice of pairing was to avoid the problem of not being able to "target" the lowest energy excitations with the TMM in the presence of a gap in the spectrum which a more conventional pairing realization would have . I then implemented a large scale diagonalization code in order to compute the bogolon wave function $|\psi_i|^2 = |u_i|^2 + |v_i|^2$ and applied multifractal finite size scaling to also compute the critical parameters and find agreement with TMM, establishing the ability of the method to capture localization of excitations in disordered superconductors.

5.1 Introduction

Anderson localization involves the localization of single-particle electronic states in a disordered metal[147]. Although this has proved to be a challenging and complex problem[148], the basic interpretation of the transition is clear: it is a transition from a metallic phase where electrons are able to diffuse and transport over long distances to an insulating phase where this is prevented. Anderson localization occurs in normal electronic systems (most famously doped[152] and amorphous[153] semiconductors). The conducting electronic states are separated from the insulating states by a mobility edge in energy and disorder strength. Many features of the localization transition have been studied and much attention has been paid to two in particular: the multifractality of critical wave functions at the transition and the role played by the symmetries of the Hamiltonian [154, 155, 156, 158].

The Anderson transition was first and most studied for Hamiltonians of the three Wigner-Dyson[156] symmetry classes. The identification of additional symmetry classes (bringing the full number to ten[154]) has lead to the study of the effects of Anderson localization beyond the original three symmetry classes and the additional rich phenomena[159]. In this paper, we consider the question of quasiparticle localization in the Bogoliubov de Gennes class for three dimensions with time reversal and spin rotation symmetry (class CI) which we use to model a dirty superconductor with a finite density of states at the Fermi level. The excitations of this class are Bogoliubov quasiparticles[160] (also referred to as bogolons in this paper) with no definite charge as they are a superposition of electron and hole excitations [161], so this is different from the case of the Anderson model where the excitations have a well defined charge. In this case, the localization transition is interpreted as localization of bogolons that occurs within the superconducting phase. The two phases are refereed to as a "thermal metal" where the bogolons are extended and a "thermal insulator" where they are localized[162]. As mentioned above, the quasiparticles do not transport charge and so there is no Weidemann-Franz law between the thermal and electric transport, but there is still thermal transport and so on the localized side of the transition the system will be thermally insulating and on the extended side it will be thermally metallic [162].

The idea of multifractality was introduced by Mandlebrot[164, 165] and describes spatial struc-

tures that have a complicated distribution and require an infinite number of critical exponents to describe the scaling of their moments. The multifractal nature of the wavefunction at criticality was realized for Anderson transitions [166, 158] and is now recognized as a defining characteristic. A proposed generalization of the multifractal analysis can be used to calculate the critical parameters of the Anderson transition[168, 167, 169] which has even been applied to calculations of doped semiconductors[170].

In this paper, we apply the generalized multifractal finite size scaling (MFSS) [168, 167] analysis to a simple model of a dirty superconductor. The model Hamiltonian and methods of extracting critical parameters which include transfer matrix method and multifractal analysis are described in Sec.5.2. We will demonstrate that the multifractal analysis can be used to extract the critical disorder strength by showing agreement with transfer matrix method calculations and confirms that this transition falls outside the Wigner-Dyson symmetry class. Also, we will argue that the multifractal character of the wavefunctions can possibly explain some experimental findings on dirty superconductors, such as the increase in T_c with disorder. These results are presented in Sec.5.3 and discussed in Sec.5.3.1. We conclude in Sec. 5.4

5.2 Model and Methods

5.2.1 Model of Dirty Superconductor

We study our model of a dirty superconductor within the mean field Bogoliubov-de Gennes approximation, and so the Hamiltonian is given by

$$H = \sum_{i,j}[t_{i,j} \sum_{\sigma=\uparrow,\downarrow} (c^{\dagger}_{i,\sigma} c_{j,\sigma} + H.c) + \Delta_{i,j}(c^{\dagger}_{i,\uparrow} c^{\dagger}_{j,\downarrow} + H.c.)]. \tag{5.1}$$

The annihilation operator for site i with spin σ is given by $c_{i,\sigma}$, and similarly for the creation operators. We only consider spin one-half fermions in this study, so $\sigma =\uparrow$ or $\downarrow$. $t_{i,j}$ and $\Delta_{i,j}$ are the hopping and pairing between site i and j respectively.

Previous studies of dirty superconductors predominately focused on the pairing with conventional s-wave symmetry with on-site pairing which has a spectral gap at the band center. With-

out disorder, the spectral function is given by $E(\mathbf{k}) = \sqrt{\Delta(\mathbf{k})^2 + \epsilon(\mathbf{k})^2}$, and for a cubic lattice $\epsilon(\mathbf{k}) = -2t\sum_{i=x,y,z}\cos(k_i)$. For the case of conventional s-wave pairing, we have $\Delta(\mathbf{k}) = \Delta_0$ a constant. Since we do not expect for gap formation to be required for multifractal behavior of the wavefunction, we instead focus on a gapless superconductor. A simple choice is one with extended s-wave pairing with the same nodal structure as that of the bare dispersion $\epsilon(\mathbf{k})$ [163], in which $\Delta(\mathbf{k}) = \Delta_0\sum_{i=x,y,z}\cos(k_i)$.

Random disorder is introduced via two independent terms, one for the on-site local potential and the other for the on-site pairing. Following the convention in Ref. [163], the total Hamiltonian may be written as

$$H = H_0 + H_{dis}, \tag{5.2}$$

$$H_0 = \sum_{<i,j>}[\frac{1}{\sqrt{2}}\sum_{\sigma=\uparrow,\downarrow}(c^\dagger_{i,\sigma}c_{j,\sigma} + H.c) + \frac{1}{\sqrt{2}}(c^\dagger_{i,\uparrow}c^\dagger_{j,\downarrow} + H.c.)], \tag{5.3}$$

$$H_{dis} = \sum_i[\epsilon_i\sum_{\sigma=\uparrow,\downarrow}(c^\dagger_{i,\sigma}c_{i,\sigma} + H.c) + \Delta_i(c^\dagger_{i,\uparrow}c^\dagger_{i,\downarrow} + H.c.)]. \tag{5.4}$$

The disorder in onsite potential and onsite pairing is assumed to be uniformly distributed from $-W$ to W, and so $P(\epsilon_i) = P(\Delta_i) = 1/2W\ \forall\ -W < \epsilon_i, \Delta_i < W$. The Hamiltonian possesses time reversal symmetry, spin rotation symmetry and particle-hole symmetry which dictates that eigenstates always come in pairs with energy E and $-E$. These symmetries put the Hamiltonian into the CI class [154].

5.2.2 Transfer Matrix Method

We first locate the critical point of the model and its localization length exponent using the transfer matrix method. The three dimensional system has a width and height equal to M for each slice of a N-slice cuboid, forming a "bar" of length N. The Hamiltonian can be decomposed into the form

$$H = \sum_i H_i + \sum_i (H_{i,i+1} + H.c.), \tag{5.5}$$

where H_i describes the Hamiltonian for slice i and $H_{i,i+1}$ is the coupling terms between the i and $i+1$ slices. The Schrödinger equation can be written in the form

$$H_{n,n+1}c_{n+1} = (E - H_n)c_n - H_{n,n-1}c_{n-1} \tag{5.6}$$

where c_i is the M^2 components wavefunction of the slice i. We introduce the transfer matrix

$$T_i = \begin{bmatrix} H_{i,i+1}^{-1}(E - H_i) & -H_{i,i+1}^{-1}H_{i-1,i} \\ 1 & 0 \end{bmatrix} \tag{5.7}$$

and Eq.5.6 can be interpreted as the iteration of

$$\begin{bmatrix} c_{i+1} \\ c_i \end{bmatrix} = T_i \times \begin{bmatrix} c_i \\ c_{i-1} \end{bmatrix}. \tag{5.8}$$

The goal of the transfer matrix method is to calculate the localization length, $\lambda_M(E)$, from the product of N transfer matricies

$$\tau_N \equiv \prod_{i=1}^{N} T_i. \tag{5.9}$$

The Lyapunov exponents of the matrix τ_N is given by the logarithm of its eigenvalues. The smallest exponent corresponds to the slowest exponential decay of the wavefunction and thus can be identified as corresponding to the localization length, $\lambda_M(E)$. The localization length is computed by repeated multiplication of T_i, but since the multiplication of matrices is numerically unstable periodic reorthogonalization is needed in the numerical implementation[150]. We use a QR decomposition for reorthogonalization implemented by LAPACK[151], and so at the s reorthogonalization step the matrix (corresponding to some intermediate L'th multiplication in calculating Eq.5.9) the matrix is decomposed

$$\tau_L = QR \tag{5.10}$$

where R is an upper triangular matrix and the Lyapunov exponents γ_s are calculated as

$$\gamma_s = \gamma_{s-1} + \log b_s \tag{5.11}$$

where b_s are the $2M^2$ diagonal elements of R for the s renormalization step. The multiplication of transfer matrices is then continued with the Q matrix. The slowest decaying exponent (γ_ℓ) is used to compute the localization length $\lambda_M(E) = 1/\gamma_\ell$ for a given width M and energy E.

The localization length is then used to calculate the the Kramer-Mackinnon[149] scaling parameter $\Lambda_M(E) = \lambda_M(E)/M$ which is expected to scale as

$$\Lambda_M = \frac{\lambda_M}{M} = f\left(\frac{M}{\xi}\right), \tag{5.12}$$

where $\xi \propto |W - W_c|^{-\nu}$. The scaling function f is Taylor expanded about the critical point W_c and the critical parameters W_c and ν enter as fitting parameters and so can be determined by a least-squares minimization.

5.2.3 Multifractal Analysis

We consider the multifractal properties of the bogolon wave-function $|\psi_i|^2 = |u_i|^2 + |v_i|^2$ for a three dimensional simple cubic lattice of linear size L. The method is based on the study of Anderson models in Wigner-Dyson class. [168, 167, 169] This cubic wavefunction is partitioned into boxes of linear size ℓ. We introduce the quantity $\lambda = \ell/L$ and so we have $N_b = \lambda^{-d}$ as the number of boxes where d is the dimensionality of the system. In this paper, we shall only consider $d = 3$. We introduce the "coarse grained" box measure

$$\mu_{b(\ell)} = \sum_{i \in b(\ell)} |\psi_i|^2 \tag{5.13}$$

where $b(\ell)$ indexes the N_b boxes for a given box size ℓ. We introduce for convenience[167] the quantity

$$\alpha \equiv \frac{\log \mu}{\log \lambda} \tag{5.14}$$

to work with instead of directly with the box measures given in Eq.5.13. Multifractility implies that the number of boxes that correspond to a given α (we denote as $N(\alpha)$) must scale as

$$N(\alpha) \sim \lambda^{-f(\alpha)} \tag{5.15}$$

where $f(\alpha)$ is some fractal dimension that depends on α. For the case where $|\psi|^2$ are distributed uniformly in space, one would expect there to be only a singular α and from the definition of λ above $f(\alpha) = d$. However, for finite λ a narrow distribution peaked around $f(\alpha) = d$ would be expected and so the above Eq.5.15 is only defined in the limit $\lambda \to 0$. The fact that there exists an α dependent *spectrum* $f(\alpha)$ characterizes a system as being multifractal[157].

We will want to consider the q-dependent moments of the distribution of α or $\alpha(q)$. We first introduce the generalized inverse participation ratios for the coarse grained distributions $P(\mu_{b(\ell)})$ as

$$R_q = \sum_{b(\ell)}^{N_b} \left(\mu_{b(\ell)}\right)^q \tag{5.16}$$

and assume (similarly to Eq.5.15) that the moments of the distribution of each box measure scale by the q dependent exponents $\tau(q)$ or

$$\langle R_q \rangle \sim \lambda^{\tau(q)} \tag{5.17}$$

where $\langle \cdots \rangle$ denotes an ensemble average. It can be shown[157] that $f(\alpha)$ and $\tau(q)$ can be related by a Legendre transform

$$f(\alpha) = -\tau(q) + q\alpha\,, \tag{5.18}$$

where

$$\alpha(q) = \frac{d\tau(q)}{dq}. \tag{5.19}$$

Carrying out the differentiation in Eq.5.19 and using the definition of $\tau(q)$ in Eq.5.17 leads to the expression

$$\alpha(q) = \lim_{\lambda \to 0} \frac{\langle S_q \rangle}{\log \lambda \langle R_q \rangle} \tag{5.20}$$

where

$$S_q = \sum_k^{N_b} \mu_k^q \log \mu_k. \tag{5.21}$$

As defined above, the multifractal exponents are only strictly defined in the limit of infinite system size ($\lambda \to 0$ as mentioned above) and at the critical point. However, they can be defined for fixed λ which we denote with a tilde as

$$\tilde{\alpha}_q = \frac{\langle S_q \rangle}{\log \lambda \langle R_q \rangle}. \tag{5.22}$$

The error in $\tilde{\alpha}_q$, $\sigma_{\tilde{\alpha}}$, is then estimated from standard propagation of uncertainty

$$\left(\frac{\sigma_{\tilde{\alpha}}}{\tilde{\alpha}}\right)^2 = \left(\frac{\sigma_{\langle S_q \rangle}}{\langle S_q \rangle}\right)^2 + \left(\frac{\sigma_{\langle R_q \rangle}}{\langle R_q \rangle}\right)^2 - 2\left(\frac{\sigma_{\langle R_q \rangle \langle S_q \rangle}}{\langle R_q \rangle \langle S_q \rangle}\right)^2$$

where the covariance term $\sigma_{\langle S_q \rangle \langle R_q \rangle}$ is kept to account for correlations as R_q and S_q are computed from the same data set.

The quantity $\tilde{\alpha}_q$ scales according to standard one parameter scaling for fixed λ in a relevant (ρ) and an irrelevant (η) scaling variable or [168, 167]

$$\tilde{\alpha}_q(W, L) = G(\rho L^{1/\nu}, \eta L^{-|y|}). \tag{5.23}$$

We expand the scaling function to first order in the irrelevant operator η

$$\tilde{\alpha}_q(W, L) = G^{(0)}(\rho L^{1/\nu}) + \eta L^{-|y|} G^{(1)}(\rho L^{1/\nu}), \tag{5.24}$$

where the sub-leading term is characterized by η, y, and $G^{(1)}$. The function $G^{(s)}$ (where $s = 0, 1$ from above) is expanded as a Taylor series

$$G^{(s)}(L^{1/\nu}) = \sum_{k=0}^{n_s} a_{sk} \rho^k L^{k/\nu}. \tag{5.25}$$

The scaling fields ρ and η are likewise expanded in terms of $w = (W - W_c)/W_c$ as

$$\rho(w) = w + \sum_{m=2}^{m_\rho} b_m w^m \tag{5.26}$$

and

$$\eta(w) = 1 + \sum_{m=1}^{m_\eta} c_m w^m. \tag{5.27}$$

The critical parameters (W_c, ν) and the irrelevant scaling exponent y are determined by fitting the data for $\tilde{\alpha}_q(W, L)$ to Eq.5.24. In addition, we have $n_0 + n_1 + m_\rho + m_\eta$ Taylor expansion parameters. The correlation length is $\xi = |\rho(\omega)|^{-\nu}$ and so the scaled $\tilde{\alpha}_q(W, L)$ data (which we denote as $\tilde{\alpha}_q^{\text{corr}}$) collapses onto two branches

$$\tilde{\alpha}_q^{\text{corr}} = G_q^{(0)}(\pm(L/\xi)^{1/\nu}) \tag{5.28}$$

5.3 Results

We employ the transfer matrix method to find the critical disorder strength by performing a finite size scaling analysis as shown in Fig.5.1. We will compare this result with that predicted by multifractal analysis of the bogolon wavefunction. The fitting is performed using the SciPy package which acts as a wrapper to MINPACK to perform the least squares minimization [178, 179]. The fitting range used in Fig.5.1 is determined by performing multiple fits and choosing the one that approximately provides the minimum for the sum of squares. This range is then used for 100 bootstrapped resamples of the data to estimate the error bars. Note however that there can still be error in choosing the fitting range so the error bars are most likely under-estimated. The calculation was performed for $E = 0$ as were are interested in only the lowest energy excitations which will also be the focus in the following multifractal analysis.

For the multifractal analysis of the bogolon wavefunctions, we use the JADAMALU package which implements a Jacobi-Davidson method with preconditioning[176, 177] to diagonalize the Hamiltonian. In contrast to that of the conventional Anderson model, the disorder terms for the present model appear in the off-diagonal elements. This poses as a challenge for attaining convergence by the iterative algorithm, both in term of the memory storage and floating point operation.

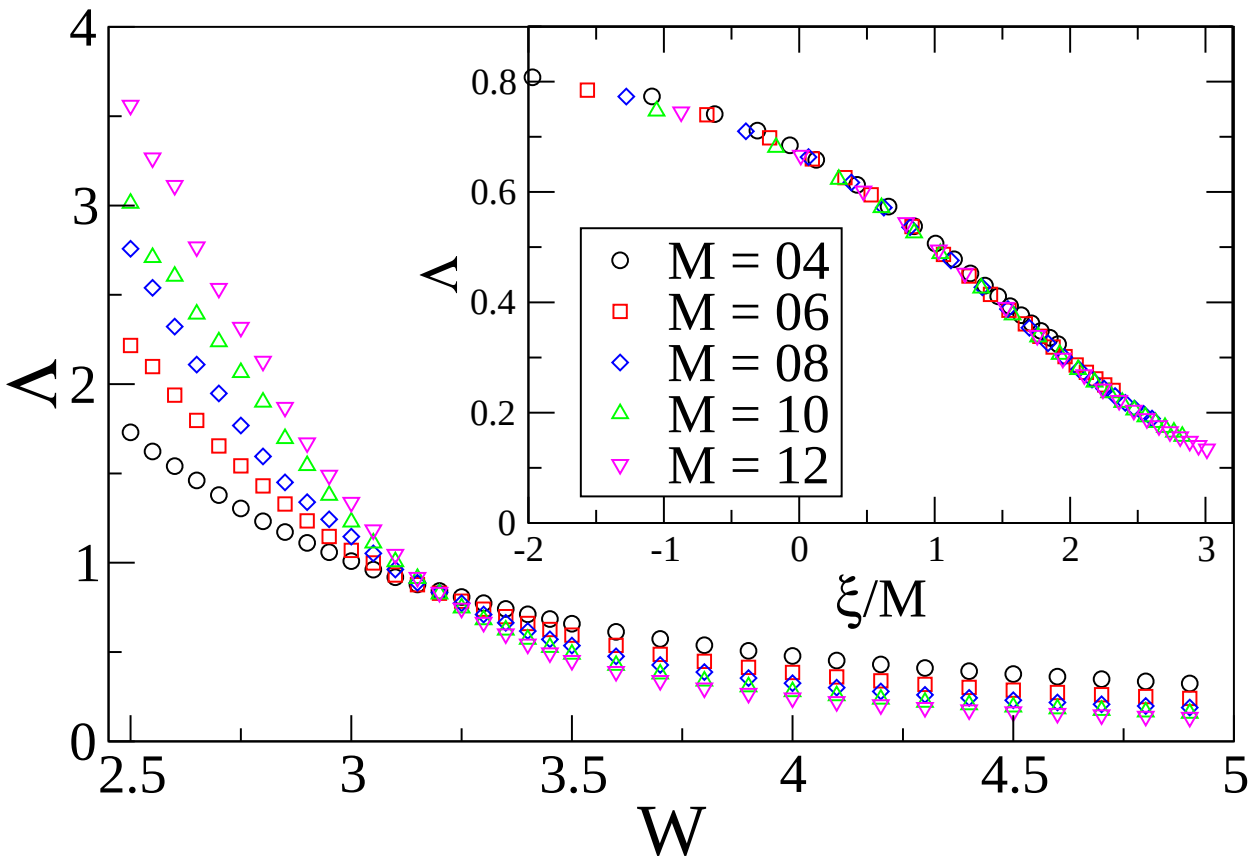

Figure 5.1: Kramer-Mackinnon scaling parameter as a function of disorder strength calculated with the transfer matrix method for a bar of length $N = 20000$, $E = 0$ and a QR reorthogonalization is performed after every 5 multiplications. Note the crossing indicating a critical disorder strength around $W = 3.2$. When the finite size scaling is performed as described in 5.2.2 the data collapses as is shown in the inset. A bootstrap re-sampling is performed to generate 100 data sets to estimate the fitting parameters yielding $W_c = 3.212 \pm 0.008$ and a critical exponent of $\nu = 1.01 \pm 0.05$.

Therefore the accessible system sizes are limited in comparison to that of the models with diagonal disorder terms. [168, 167] We keep only one state from each realization with the closest eigenvalue (and associated eigenvector) to zero. This is to prevent correlations in wavefunctions that come from the same realization of disorder. The wave function can then be coarse grained (as described in Sec.5.2.3) and the distribution of α is plotted in in Fig.5.2.

We can then calculate $\tilde{\alpha}_q$ for $q = 0$ (given by Eq.5.22 which we denote as $\tilde{\alpha}_0$) and is plotted in Fig.5.3 as a function of system size and disorder strength which is expected to show the characteristic finite size behavior and exhibit a crossing at the critical disorder strength[167][168]. We also carry out multifractal finite size scaling for fixed λ and we assume our data y_i (with uncertainty σ_i) is

uncorrelated (as we only consider fixed λ so each point is from it's own realization) and thus the χ^2 statistic for our model fits f_i is

$$\chi^2 = \sum_i \frac{(y_i - f_i)^2}{\sigma_i^2} \tag{5.29}$$

The order of expansion in n_0, n_1, m_η and m_ρ is determined by choosing the fit that keeps the χ^2 statistic small, keeps the order of expansion small and provides a "good" collapse of the data into two branches. Error bars in fitting parameters are determined by generating new values of $\langle S_q \rangle$ and $\langle R_q \rangle$ for each corresponding L and W by pulling from a Gaussian distribution with mean $\langle S_q \rangle$ and variance $\sigma_{\langle S_q \rangle}/\sqrt{N-1}$ where N is the number of samples of S_q and this is likewise done for $\langle R_q \rangle$. This allows for a new calculation of α_q. The result from this procedure yields $Wc = 3.208 \pm 0.007$ and $\nu = 0.97 \pm 0.06$ in agreement with the above transfer matrix study.

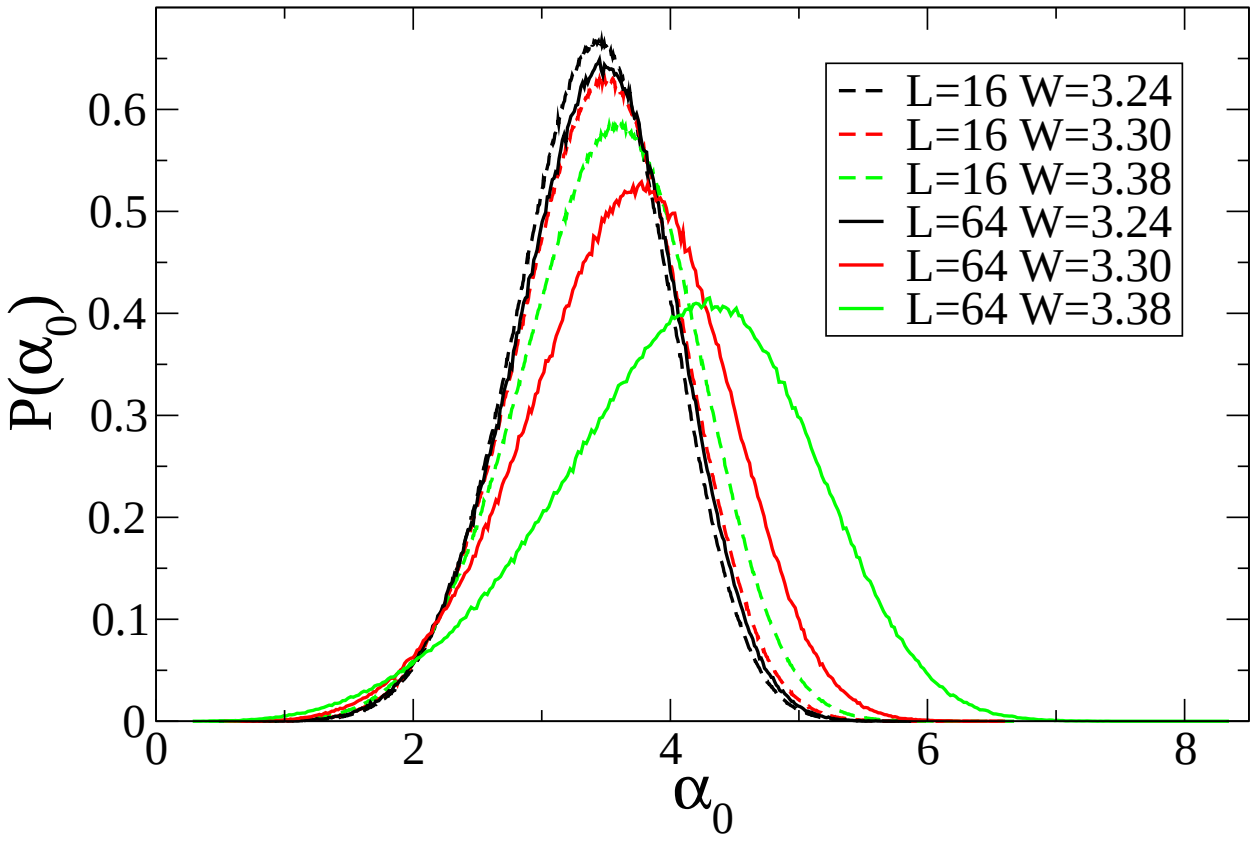

Figure 5.2: Distribution of the quantity α (defined in Eq.5.14) for a finite value of $\lambda = 1/8$ for various system sizes and two disorder strengths. The behavior of the distributions as a function of L motivates the application of the multifractal analysis in the Ref. [167] as when the transition is approached (~ 3.2) the distributions become more scale invariant (not depending on system size).

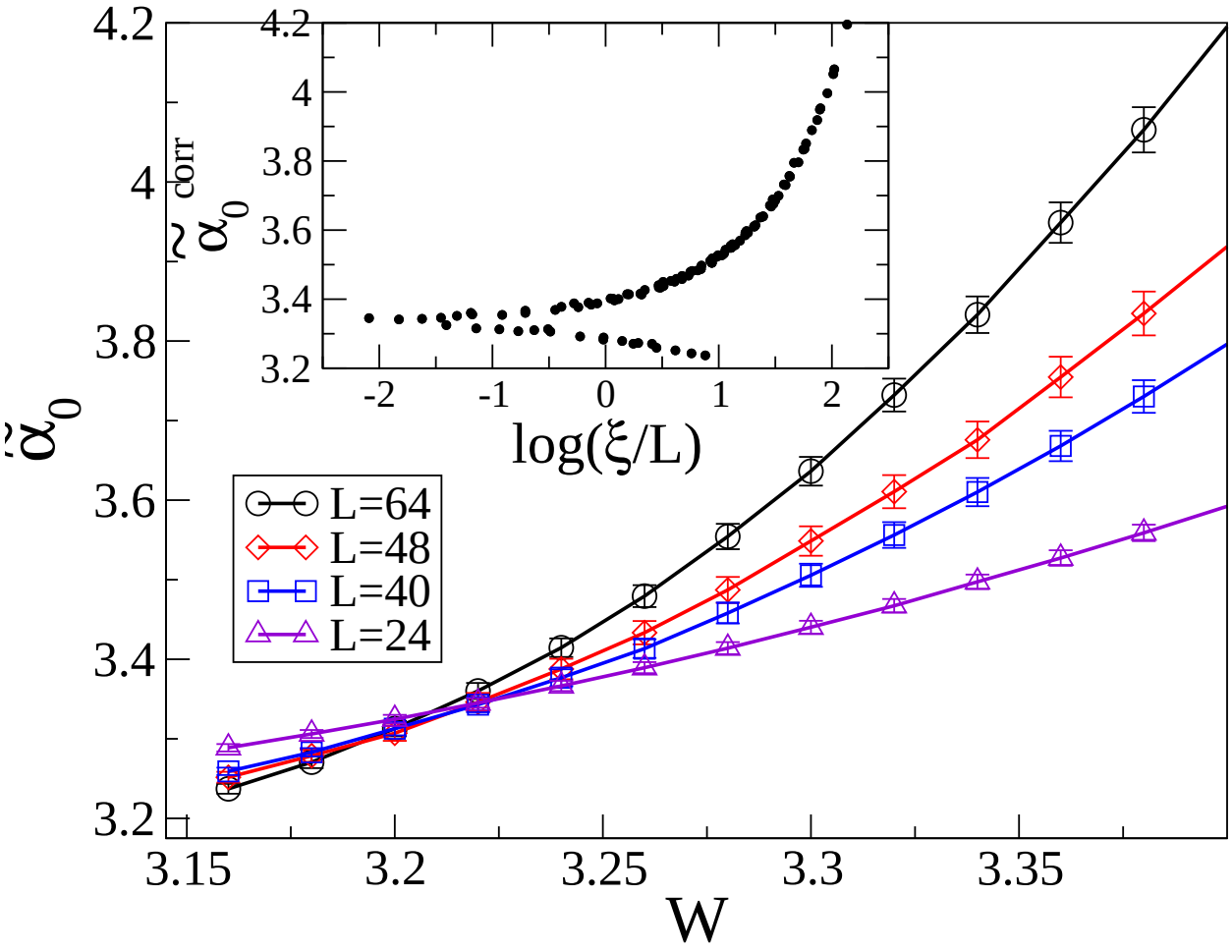

Figure 5.3: The multifractal exponent α_0 as a function of disorder strength W that exhibits scaling behavior around the critical disorder strength $W = 3.2$. The inset shows the data collapse into after performing the finite size scaling and plotting the scaling function for both branches of $\tilde{\alpha_0}$ in Eq. 5.28. The critical parameters used are $W_c = 3.21$, $\nu = 1.09$, $y = 15.94$. The orders of expansion used for $G^{(0)}, G^{(1)}, \rho$, and η are $n_0 = 2, n_1 = 2, m_\rho = 1$ and $m_\eta = 0$ respectively. The resulting $\chi^2 = 22$. The fit was chosen by keeping the order of expansion low and taking the smallest χ^2 for which the data collapse close to the fitting function $\tilde{\alpha_0}$.

5.3.1 Discussion

It has been established by the work of Ref.[163] that the exponent ν is much different than the Anderson model. We confirm this with our multifractal analysis, establishing that this falls outside the Wigner-Dyson (WD) symmetry class.

The motivation for studying models of disordered superconductors is the rich variety of unusual

properties they can exibit such as an enhanced single particle energy gap that persists even after superconductivity is destroyed [189]. Specific to this paper, the motivation for studying the multifractal character of the eigenstates is the proposal that multifractility can lead to enhancements of the critical temperature at which superconductivity is destroyed (T_c)[172, 171] which is observed in thin superconducting films that are weakly disordered, namely Al[193][192] wich is still not well understood. An explanation for the enhancement of T_c due to multifractility is that multifractility implies a broad distribution of exponents for the spatial correlations at the transition (given by $f(\alpha)$). This can be understood by the fact that there are regions of the system that have exponents that will decay off more slowly than if there were only a single one, implying stronger correlations among bogolon wavefunction $|\psi_i|^2$. It is known that the regions of large $|\psi_i|^2$ for the lowest excitations will correspond to regions of large local pairing amplitude Δ_i[174] [175], and so Δ_i will also realize multifractal correlations. The result of the longer range correlations would lead to stronger pairing correlations, resulting in an increase in T_c. Given the present calculations are done with a fixed distribution of Δ_i, we cannot address quantitatively the relation between the T_c and the disorder.

Furthermore, it is known that the presence of bogolon excitations is what dissipates momentum and disrupts the flow of super current, destroying superconductivity[191]. Therefore, a state in which the excitations are localized would help to "protect" superconductivity at finite temperatures and increase T_c. As the localization effect would be very strong in a quasi-2D system, when a superconducting film is made more thin the bogolons must become localized. The reason it is not observed for all thin films (it is more typical for T_c to decrease) is that if the disorder is strong this effect will not be observed because strong disorder is already destroying the superconductivity as it destroys the long range phase coherence[194].

Finally, we note that the multifractal analysis used here could be applied to models of conventional s-wave superconductivity with disorder which has been well studied [183, 182, 184, 173, 185, 186, 187, 188]. This is important because the transfer matrix method cannot be used to locate the localization transition if the pairing must be solved self-consistently as this creates a correlation between layers [190]. However, as all that is needed is the wavefunction for this method, the

multifractal finite size scaling analysis could be applied.

5.4 Conclusion

We conclude that the multifractal analysis that works for the Anderson model can also be used for models of disordered superconductors to find the localization transition of the quasi particle excitations. In addition, it also confirms that the thermal metal to thermal insulator is indeed in a separate universality class from the Anderson model. [163]

Future work would include addressing the question of the relation between multifractility of critical wavefunctions and the impact on T_c more directly by finding the transition temperature for a model of a conventional s-wave superconductor by solving the pairing field Δ_i self consistently for a given attraction interaction strength U. [175] The multifractal spectrum $f(\alpha)$ could then be compared as a function of interaction strength and T_c to quantitatively address the role played by multifractal eigenstates and coupling strength on the critical temperature. Also, the question of whether this method can detect the superconductor to insulator transition [183] would be of interest as this model could not be studied with transfer matrix due to the self consistency requirement on the pairing.

References

[1] Mott, N. F. Adv. in Phys. **16**, 49 (1967).

[2] Ashcroft, N.W. and Mermin N. D. *Solid State Physics*. Brooks/Cole. (1967).

[3] Ziman, J. M. *Principles of the Theory of Solids*. Cambridge University Press. (1972).

[4] R. Schneider, A. G. Zaitsev, D. Fuchs, H. v. Löhneysen. Phys. Rev. Lett. **108**, 257003 (2012).

[5] D. B. Haviland, Y. Liu, and A. M. Goldman. Phys. Rev. Lett. **62**, 2180 (1989).

[6] P.W. Adams, H. Nam, C.K. Shih, and G.Catelani. Phys. Rev. B. **95**, 094520 (2017).

[7] V. F. Gantmakher, V. T. Dolgopolov. Physics-Uspekhi **53**, (1) 1-49 (2010).

[8] A. M. Finkel'shtein. Pis'ma Zh. Eksp. Teor. Fix. **45**, No.1, 37-40 (1987).

[9] Onnes, Kamerlingh. *Leiden Comm.* 122b, 124c (1911).

[10] Bardeen, J. Cooper, L. N. and Schrieffer, J. R. Phys. Rev. **108**, 1175 (1957).

[11] L. N. Cooper. Phys. Rev. **104**, 1189 (1956).

[12] http://www.phys.lsu.edu/ jarrell/

[13] de Boer, J. H. and E. J. W. Verway. Proc. Phys. Soc. London, Sect. A 49, 59 (1937).

[14] Ying et al. Sci. Adv. **2**, e1501283 (2016).

[15] Y. L. Loh *et. al.* Phys. Rev. Lett. **107**, 067003 (2011).

[16] Beyer W. Phd Thesis Universität Marburg (1974).

[17] Mott N. F. and Davis E. A. *Electronic Processes in Non-Crystalline Materials* 2nd edn. Oxford. (1979).

[18] van den Dries L., ban Haesendonch C., Bruynseraede Y., Deutscher G. Phys Rev Lett. **46** 565 (1981).

[19] C. Van Haesendonck, L. van den Dries, Y. Bruynseraede and G. Deutscher. Phys Rev B. **25** 5090 (1982).

[20] Bergmann G. Phys Rev B. **28**, 515 (1983).

[21] B. Abeles, Roger W. Cohen and G. W. Cullen. Phys Rev Lett. **17**, 632 (1966).

[22] P. W. Anderson. J. Phys. Chem. Solid. **11**, 26 (1959).

[23] Paalanen M A., Thomas G A. Helv. Phys. Acta. **56**, 27 (1983).

[24] Kramer B., MacKinnon A. Rep. Prog. Phys. **56**, 1469 (1993).

[25] Yen LEE LOH and Nandini TRIVEDI. *Theoretical Studies of Superconductor-Insulator Transitions*
Conductor Insulator Phase Transitions. Oxford University Press. (2012).

[26] Dey, Poulumi and Basu, Saurabh. *Disordered Superconductors: A Simple Model Manifesting Pseudogap and BCS-BEC Crosssover.*
Condensed Matter Theories Vol. 24. (2009)

[27] A. MacKinnon and B. Kramer, Z. Phys. B - Condensed Matter **53**, 1–13 (1983).

[28] B. Kramer, A. MacKinnon, T. Ohtsuki, and K. Slevin, International Journal of Modern Physics B **24**(12n13), 1841–1854 (2010).

[29] P. W. Anderson, Phys. Rev. **109**, 1492–1505 (1958).

[30] V. Dobrosavljević, A. A. Pastor, and B. K. Nikolić, EPL **62**(1), 76 (2003).

[31] G Schubert. Phys Rev B **81**, 155106 (2010).

[32] P. Soven, Phys. Rev. **156**, 809–813 (1967).

[33] M. H. Hettler, A. N. Tahvildar-Zadeh, M. Jarrell, T. Pruschke, and H. R. Krishnamurthy, Phys. Rev. B **58**, R7475–R7479 (1998).

[34] M. H. Hettler, M. Mukherjee, M. Jarrell, and H. R. Krishnamurthy, Phys. Rev. B **61**, 12739–12756 (2000).

[35] M. Jarrell and H. R. Krishnamurthy, Phys. Rev. B **63**, 125102 (2001).

[36] P. Markoš, Acta Physica Slovaca **56**, 561–685 (2006).

[37] H. Terletska, C. E. Ekuma, C. Moore, K.-M. Tam, J. Moreno, M. Jarrell. PRB **90** 094208 (2014).

[38] Yi Zhang, Hanna Terletska, C. Moore, Chinedu Ekuma, Ka-Ming Tam, Tom Berlijn, Wei Ku, Juana Moreno, Mark Jarrell. PRB **92**, 205111 (2015).

[39] C Castellani, L Peliti. J Phys A **19**, L429 (1986).

[40] A Rodriguez *et. al.* Phys Rev B **84**, 134209 (2011).

[41] R Murcio *et. al.* Phys Rev E 9**2**, 06130 (2015).

[42] J Mayoh and M Garcia-Garcia. Phys Rev B **92**, 174526 (2015).

[43] I S Burmistrov. Phys Rev Lett **108**, 017002 (2012) .

[44] P. A. Lee and T. V. Ramakrishnan, Rev. Mod. Phys. **57**, 287–337 (1985).

[45] D. Belitz and T. R. Kirkpatrick, Rev. Mod. Phys. **66**, 261–380 (1994).

[46] P. W. Anderson, Phys. Rev. **109**, 1492–1505 (1958).

[47] E. Abrahams, P. W. Anderson, D. C. Licciardello, and T. V. Ramakrishnan, Phys. Rev. Lett. **42**, 673–676 (1979).

[48] B. Bulka, B. Kramer, and A. MacKinnon, Z. Phys. B **60**, 13–17 (1985).

[49] B. Bulka, M. Schreibe, and B. Kramer, Z. Phys. B **66**, 21–30 (1987).

[50] K. Slevin and T. Ohtsuki, New J. Phys. **16**, 015012 (2014).

[51] K. Slevin and T. Ohtsuki, Phys. Rev. Lett. **78**, 4083–4086 (1997).

[52] K. Slevin and T. Ohtsuki, Phys. Rev. Lett. **82**, 382–385 (1999).

[53] A. Rodriguez, L. J. Vasquez, K. Slevin, and R. A. Römer, Phys. Rev. Lett. **105**, 046403 (2010).

[54] A. Rodriguez, L. J. Vasquez, K. Slevin, and R. A. Römer, Phys. Rev. B **84**, 134209 (2011).

[55] T. Nakayama and K. Yakubo, *Fractal Concepts in Condensed Matter Physics* (Springer-Verlag Berlin Heidelberg, 2003).

[56] P. Markoš, Acta Physica Slovaca **56**, 561–685 (2006).

[57] P. Markoš, J. Phys. A **33**, L393 (2000).

[58] A. Gonis, *Green functions for ordered and disordered systems* (North-Holland Amsterdam, 1992).

[59] P. Soven, Phys. Rev. **156**, 809–813 (1967).

[60] K. Koepernik, B. Velický, R. Hayn, and H. Eschrig, Phys. Rev. B **58**, 6944–6962 (1998).

[61] P. D. Antoniou and E. N. Economou, Phys. Rev. B **16**, 3768–3781 (1977).

[62] K. Kumar, D. Kumar, and S. K. Josh, J. Phys.: Condens. Matter **10**, 1741 (1977).

[63] G. X. Tang and W. Nolting, Phys. Rev. B **73**, 024415 (2006).

[64] D. C. Licciardello and E. N. Economou, Phys. Rev. B **11**, 3697–3717 (1975).

[65] G. Theodorou and M. H. Cohen, Phys. Rev. B **13**, 4597–4601 (1976).

[66] E. R. Mucciolo and C. H. Lewenkopf, J. Phys.: Condens. Matter **22**, 273201 (2010).

[67] S.-J. Xiong and Y. Xiong, Phys. Rev. B **76**, 214204 (2007).

[68] A. Alam, B. Sanyal, and A. Mookerjee, Phys. Rev. B **86**, 085454 (2012).

[69] J. A. Blackman, D. M. Esterling, and N. F. Berk, Phys. Rev. B **4**, 2412–2428 (1971).

[70] A. Gonis and J. W. Garland, Phys. Rev. B **18**, 3999–4009 (1978).

[71] A. Gonis and J. W. Garland, Phys. Rev. B **16**, 1495–1502 (1977).

[72] M. H. Hettler, A. N. Tahvildar-Zadeh, M. Jarrell, T. Pruschke, and H. R. Krishnamurthy, Phys. Rev. B **58**, R7475–R7479 (1998).

[73] M. H. Hettler, M. Mukherjee, M. Jarrell, and H. R. Krishnamurthy, Phys. Rev. B **61**, 12739–12756 (2000).

[74] M. Jarrell and H. R. Krishnamurthy, Phys. Rev. B **63**, 125102 (2001).

[75] H. Shiba, Prog. Theor. Phys. **46**, 77 (1971).

[76] A. Brezini, M. Sebbani, and L. Dahmani, Phys. Status Solidi B **137**, 667 (1986).

[77] F. Hamdache and A. Brezini, Phys. Status Solidi B **172**, 635 (1992).

[78] C. E. Ekuma, H. Terletska, K.-M. Tam, Z.-Y. Meng, J. Moreno, and M. Jarrell, Phys. Rev. B **89**, 081107 (2014).

[79] D. J. Thouless, Phys. Rep. **17**, 93–142 (1974).

[80] A. Abou-Chacra, D. J. Thouless, and P. W. Anderson, J. Phys. C **6**, 1734 (1973).

[81] P. W. Anderson, Reviews of Modern Physics **50**(2), 191–201 (1978).

[82] A. D. Mirlin and Y. V. Fyodorov, Phys. Rev. Lett. **72**, 526–529 (1994).

[83] K. Byczuk, W. Hofstetter, and D. Vollhardt, Int. J. Mod. Phys. B **24**, 1727 (2010).

[84] G. Schubert, J. Schleede, K. Byczuk, H. Fehske, and D. Vollhardt, Phys. Rev. B **81**, 155106 (2010).

[85] M. Janssen, Phys. Rep. **295**, 1–91 (1998).

[86] E. Crow and K. Shimizu (eds.) *Log-Normal Distribution–Theory and Applications* (Marcel Dekker, NY, 1988).

[87] B. Derrida, Physics Reports **103**(1-4), 29 – 39 (1984).

[88] V. Dobrosavljević, A. A. Pastor, and B. K. Nikolić, EPL (Europhysics Letters) **62**(1), 76 (2003).

[89] A. Alvermann, G. Schubert, A. Weiße, F. X. Bronold, and H. Fehske, Physica B Condensed Matter **359**, 789–791 (2005).

[90] G. Schubert and H. Fehske, *in:* B. K. Chakrabarti, K. K. Bardhan, and A. K. Sen (eds.) *Quantum and Semi-classical Percolation and Breakdown in Disordered Solids*, *Lecture Notes in Physics*, vol. 762, 1–28 Springer Berlin Heidelberg. (2009).

[91] A. Weiße, G. Wellein, A. Alvermann, and H. Fehske, Rev. Mod. Phys. **78**, 275–306 (2006).

[92] G. Schubert, A. Weiße, and H. Fehske, Phys. Rev. B **71**, 045126 (2005).

[93] G. Schubert and H. Fehske, Phys. Rev. B **77**, 245130 (2008).

[94] A. MacKinnon and B. Kramer, Z. Phys. B - Condensed Matter **53**, 1–13 (1983).

[95] B. Kramer, A. MacKinnon, T. Ohtsuki, and K. Slevin, International Journal of Modern Physics B **24**(12n13), 1841–1854 (2010).

[96] I. Plyushchay, R. Römer, and M. Schrieber, Phys. Rev. B **68**, 064201 (2003).

[97] B. Kramer, A. MacKinnon, T. Ohtsuki, and K. Slevin, "Finite size scaling analysis of the anderson transition," *Int. J. Mod. Phys. B*, vol. 24, pp. 1841–1854. (2010).

[98] P. Markoš, "Numerical analysis of the anderson localization," *Acta Physica Slovaca*, vol. 56, pp. 561–685, (2006).

[99] A. MacKinnon and B. Kramer, "The scaling theory of electrons in disordered solids: Additional numerical results," *Z. Phys. B*, vol. 53, pp. 1–13, 1983.

[100] V. Dobrosavljević, A. A. Pastor, and B. K. Nikolić, "Typical medium theory of anderson localization: A local order parameter approach to strong-disorder effects," *EPL*, vol. 62, no. 1, p. 76, 2003.

[101] P. A. Lee and T. V. Ramakrishnan, "Disordered electronic systems," *Rev. Mod. Phys.*, vol. 57, pp. 287–337, Apr 1985.

[102] D. Belitz and T. R. Kirkpatrick, "The anderson-mott transition," *Rev. Mod. Phys.*, vol. 66, pp. 261–380, Apr 1994.

[103] E. Abrahams, P. W. Anderson, D. C. Licciardello, and T. V. Ramakrishnan, "Scaling theory of localization: Absence of quantum diffusion in two dimensions," *Phys. Rev. Lett.*, vol. 42, pp. 673–676, Mar 1979.

[104] B. Bulka, B. Kramer, and A. MacKinnon, "Mobility edge in the three dimensional anderson model," *Z. Phys. B*, vol. 60, pp. 13–17, 1985.

[105] C. E. Ekuma, H. Terletska, K.-M. Tam, Z.-Y. Meng, J. Moreno, and M. Jarrell, "Typical medium dynamical cluster approximation for the study of anderson localization in three dimensions," *Phys. Rev. B*, vol. 89, p. 081107, Feb 2014.

[106] K. Byczuk, W. Hofstetter, and D. Vollhardt, "Anderson localization vs. mott-hubbard metal-insulator transition in disordered, interacting lattice fermion systems," *Int. J. Mod. Phys. B*, vol. 24, p. 1727, 2010.

[107] E. Crow and K. Shimizu, eds., *Log-Normal Distribution–Theory and Applications.* Marcel Dekker, NY, Jan 1988.

[108] G. Schubert and H. Fehske, "Quantum percolation in disordered structures," in *Quantum and Semi-classical Percolation and Breakdown in Disordered Solids* (B. K. Chakrabarti, K. K. Bardhan, and A. K. Sen, eds.), vol. 762 of *Lecture Notes in Physics*, pp. 1–28, Springer Berlin Heidelberg, 2009.

[109] A. Weiße, G. Wellein, A. Alvermann, and H. Fehske, "The kernel polynomial method," *Rev. Mod. Phys.*, vol. 78, pp. 275–306, Mar 2006.

[110] E. Abrahams, ed., *50 Years of Anderson Localization*. World Scientific, 2010.

[111] B. Kramer and A. MacKinnon, "Localization: theory and experiment," *Rep. Prog. Phys.*, vol. 56, no. 12, p. 1469, 1993.

[112] P. Soven, "Coherent-potential model of substitutional disordered alloys," *Phys. Rev.*, vol. 156, pp. 809–813, Apr 1967.

[113] B. Velický, S. Kirkpatrick, and H. Ehrenreich, "Single-site approximations in the electronic theory of simple binary alloys," *Phys. Rev.*, vol. 175, pp. 747–766, Nov 1968.

[114] S. Kirkpatrick, B. Velický, and H. Ehrenreich, "Paramagnetic NiCu alloys: Electronic density of states in the coherent-potential approximation," *Phys. Rev. B*, vol. 1, pp. 3250–3263, Apr 1970.

[115] M. H. Hettler, M. Mukherjee, M. Jarrell, and H. R. Krishnamurthy, "Dynamical cluster approximation: Nonlocal dynamics of correlated electron systems," *Phys. Rev. B*, vol. 61, pp. 12739–12756, May 2000.

[116] M. Jarrell and H. R. Krishnamurthy, "Systematic and causal corrections to the coherent potential approximation," *Phys. Rev. B*, vol. 63, p. 125102, Mar 2001.

[117] M. Jarrell, T. Maier, C. Huscroft, and S. Moukouri, "Quantum monte carlo algorithm for non-local corrections to the dynamical mean-field approximation," *Phys. Rev. B*, vol. 64, p. 195130, Oct 2001.

[118] M. Tsukada, "A New Method for the Electronic Structure of Random Lattice -the Coexistence of the Local and the Band Character-," *J. Phys. Soc. Jpn.*, vol. 26, pp. 684–696, 1969.

[119] P. W. Anderson, "Local moments and localized states," *Rev. Mod. Phys.*, vol. 50, pp. 191–201, Apr 1978.

[120] M. Janssen, "Statistics and scaling in disordered mesoscopic electronic systems," *Phys. Rep.*, vol. 295, pp. 1–91, 1998.

[121] H. Terletska, C. E. Ekuma, C. Moore, K.-M. Tam, J. Moreno, and M. Jarrell, "Study of off-diagonal disorder using the typical medium dynamical cluster approximation," *Phys. Rev. B*, vol. 90, p. 094208, Sep 2014.

[122] P. N. Sen, "Coherent-potential approximation in a two-band model: Electronic and transport properties of semiconducting binary alloys," *Phys. Rev. B*, vol. 8, pp. 5613–5623, Dec 1973.

[123] H. Aoki, "Electronic structure of disordered intrinsic semiconductor and s-d systems: Two-band localisation," *Journal of Physics C: Solid State Physics*, vol. 14, no. 20, p. 2771, 1981.

[124] H. Aoki, "Electronic structure of disordered systems with multi-orbitals," *Journal of Physics C: Solid State Physics*, vol. 18, no. 10, p. 2109, 1985.

[125] C. E. Ekuma, S.-X. Yang, H. Terletska, K.-M. Tam, N. S. Vidhyadhiraja, J. Moreno, and M. Jarrell, "Metal-Insulator-Transition in a Weakly interacting Disordered Electron System," *ArXiv e-prints*, Feb. 2015.

[126] N. Mott, "The mobility edge since 1967," *J. Phys C*, vol. 20, no. 21, p. 3075, 1987.

[127] C. E. Ekuma, C. Moore, H. Terletska, K.-M. Tam, J. Moreno, M. Jarrell, and N. S. Vidhyadhiraja, "Finite-cluster typical medium theory for disordered electronic systems," *Phys. Rev. B*, vol. 92, p. 014209, Jul 2015.

[128] G. Schubert, A. Weiße, and H. Fehske, "Localization effects in quantum percolation," *Phys. Rev. B*, vol. 71, p. 045126, Jan 2005.

[129] G. Schubert and H. Fehske, "Dynamical aspects of two-dimensional quantum percolation," *Phys. Rev. B*, vol. 77, p. 245130, Jun 2008.

[130] B. Wei, H. Qing-Zhen, C. Gen-Fu, M. A. Green, W. Du-Ming, H. Jun-Bao, and Q. Yi-Ming, "A novel large moment antiferromagnetic order in k 0.8 fe 1.6 se 2 superconductor," *Chinese Physics Letters*, vol. 28, no. 8, p. 086104, 2011.

[131] A. Ricci, N. Poccia, G. Campi, B. Joseph, G. Arrighetti, L. Barba, M. Reynolds, M. Burghammer, H. Takeya, Y. Mizuguchi, Y. Takano, M. Colapietro, N. L. Saini, and A. Bianconi, "Nanoscale phase separation in the iron chalcogenide superconductor $k_{0.8}fe_{1.6}se_2$ as seen via scanning nanofocused x-ray diffraction," *Phys. Rev. B*, vol. 84, p. 060511, Aug 2011.

[132] Z. Wang, Y. J. Song, H. L. Shi, Z. W. Wang, Z. Chen, H. F. Tian, G. F. Chen, J. G. Guo, H. X. Yang, and J. Q. Li, "Microstructure and ordering of iron vacancies in the superconductor system $k_yfe_xse_2$ as seen via transmission electron microscopy," *Phys. Rev. B*, vol. 83, p. 140505, Apr 2011.

[133] S. Landsgesell, D. Abou-Ras, T. Wolf, D. Alber, and K. Prokeš, "Direct evidence of chemical and crystallographic phase separation in $k_{0.65}fe_{1.74}se_2$," *Phys. Rev. B*, vol. 86, p. 224502, Dec 2012.

[134] X. Ding, D. Fang, Z. Wang, H. Yang, J. Liu, Q. Deng, G. Ma, C. Meng, Y. Hu, and H.-H. Wen *Nat. Comm. 4*, vol. 4, p. 1897, 2013.

[135] C.-H. Lin, T. Berlijn, L. Wang, C.-C. Lee, W.-G. Yin, and W. Ku, "One-fe versus two-fe brillouin zone of fe-based superconductors: Creation of the electron pockets by translational symmetry breaking," *Phys. Rev. Lett.*, vol. 107, p. 257001, Dec 2011.

[136] T. Berlijn, P. J. Hirschfeld, and W. Ku, "Effective doping and suppression of fermi surface reconstruction via fe vacancy disorder in $\mathbf{k}_xfe_{2-y}se_2$," *Phys. Rev. Lett.*, vol. 109, p. 147003, Oct 2012.

[137] C. Cao and F. Zhang. Phys. Rev. B. **87**, 161105 (2013).

[138] F. Chen, M. Xu, Q. Q. Ge, Y. Zhang, Z. R. Ye, L. X. Yang, J. Jiang, B. P. Xie, R. C. Che, M. Zhang, A. F. Wang, X. H. Chen, D. W. Shen, J. P. Hu, and D. L. Feng. Phys. Rev. X. **1**, 021020 (2011).

[139] Y. Zhang, L. X. Yang, M. Xu, Z. R. Ye, F. Chen, C. He, H. C. Xu, J. Jiang, B. P. Xie, J. J. Ying, X. F. Wang, X. H. Chen, J. P. Hu, M. Matsunami, S. Kimura, and D. L. Feng, "Nodeless superconducting gap in $A_xFe_2Se_2$ (A=K,Cs) revealed by angle-resolved photoemission spectroscopy," *Nat Mater*, vol. 10, pp. 273–277 (2011).

[140] J. Guo, S. Jin, G. Wang, S. Wang, K. Zhu, T. Zhou, M. He, and X. Chen. Phys. Rev. B. **82**, 180520 Nov (2010).

[141] I. I. Mazin, D. J. Singh, M. D. Johannes, and M. H. Du. Phys. Rev. Lett. **101**, 057003 (2008).

[142] M.-H. Fang, H.-D. Wang, C.-H. Dong, Z.-J. Li, C.-M. Feng, J. Chen, and H. Q. Yuan, "Fe-based superconductivity with T_c =31K bordering an antiferromagnetic insulator in $(Tl,K)Fe_xSe_2$," *EPL (Europhysics Letters)*, vol. 94, no. 2, p. 27009, 2011.

[143] W.-G. Yin, C.-C. Lee, and W. Ku. Phys. Rev. Lett. **105**, 107004 (2010).

[144] Y.-T. Tam, D.-X. Yao, and W. Ku. Phys. Rev. Lett. **115**, 117001 (2015).

[145] W. Ku, H. Rosner, W. E. Pickett, and R. T. Scalettar, "Insulating ferromagnetism in $la_4ba_2cu_2o_{10}$: An *Ab Initio* wannier function analysis," *Phys. Rev. Lett.*, vol. 89, p. 167204, (2002).

[146] K. Schwarz, P. Blaha, and G. Madsen, "Electronic structure calculations of solids using the {WIEN2k} package for material sciences," *Computer Physics Communications*, vol. 147, no. 1-2, pp. 71 – 76, 2002. Proceedings of the Europhysics Conference on Computational Physics, Computational Modeling and Simulation of Complex Systems.

[147] P. W. Anderson, Phys. Rev. **109**, 1492 (1958).

[148] A. MacKinnon, Rep. Prog. Phys. **56**, 1469 (1993).

[149] A. MacKinnon and B. Kramer, Z. Phys. B **53**, 1 (1983).

[150] B. Kramer, A. MacKinnon, T. Ohtsuki and K. Slevin. Int. J. Mod. Phys. B **24**, 1841 (2010).

[151] E. Anderson, Z. Bai, C. Bischof, S. Blackford, J. Demmel, J. Dongarra, J. Du Croz, A. Greenbaum, S. Hammarling, A. McKenney and D. Sorensen, *LAPACK Users' Guide*. Society for Industrial and Applied Mathematics (1999).

[152] P. M. A. Thomas and G. A. Helv, Phys Acta. **56**, 27 (1983).

[153] N. F. Mott and E. A. Davis, *Electronic Processes in Non-Crystalline Materials* 2nd edn. Oxford. (1979).

[154] A. Altland and M. R. Zirnbauer, Phys. Rev. B **55**, 1142 (1997).

[155] A. P. Schnyder, S. Ryu, A. Furusaki, and A. W. W. Ludwig, Phys. Rev. B **78**, 195125 (2008).

[156] E. P. Wigner, Phys. Rev. **98**, 145 (1955).

[157] T. Nakayama and K. Yakubo, *Fractal Concepts in Condensed Matter Physics* Springer-Verlag Berlin Heidelberg (2003).

[158] C. Castellani and L. Peliti, J. Phys. A **19**, L429 (1986).

[159] F. Evers and A. D. Mirlin, Rev. Mod. Phys. **80**, 1355 (2008).

[160] N. N. Bogoliubov, Sov. Phys. JETP **7**, 41 (1958).

[161] C. W. J. Beenakker, Rev. Mod. Phys. **87** 1037 (2015).

[162] S. Vishveshwara, T. Senthil and M. P. A. Fisher, Phys. Rev. B **61** 6966 (2000).

[163] S. Vishveshwara and M. P. A. Fisher, Phys. Rev. B **64**, 174511 (2001).

[164] B. B. Mandelbrot, J. Fluid Mech. **62**, 331 (1974).

[165] T. C. Halsey, M. H. Jensen, L. P. Kadanoff, I. Procaccia, and B. I. Shraiman, Phys. Rev. A **33**, 1141 (1986).

[166] F. Wegner, Z. Phys. B **36**, 209 (1980).

[167] A. Rodriguez, L. J. Vasquez, K. Slevin, and R. A. Römer, Phys. Rev. B **84**, 134209 (2011).

[168] A. Rodriguez, L. J. Vasquez, K. Slevin, and R. A. Römer, Phys. Rev. Lett. **105**, 046403 (2010).

[169] L. Ujfalusi and I. Varga, Phys. Rev. B **91**, 184206 (2015).

[170] Y. Harashima and K. Slevin, Phys. Rev. B **89**, 205108 (2014).

[171] J. Mayoh and A. M. Garcia-Garcia, Phys. Rev. B **92**, 174526 (2015).

[172] I. S. Burmistrov, I. V. Gornyi, and A. D. Mirlin, Phys. Rev. Lett. **108**, 017002 (2012).

[173] M. Sakaida, K. Noda, and N. Kawakami, J. Phys. Soc. Jpn. **82**, 074715 (2013).

[174] Y. L. Loh and N. Trivedi, "Theoretical Studies of Superconductor-Insulator Transitions" Chapter 17, pp. 492-548 in *Conductor-Insulator Quantum Phase Transitions*. Oxford University Press (2012).

[175] A. Ghosal, M. Randeria and N. Trivedi, Phys Rev B **65**, 014501 (2001).

[176] M. Bollhöfer and Y. Notay, Comput. Phys. Commun. **177**, 951 (2007).

[177] M. Bollhöfer and Y. Notay, JADAMILU code and documentation. Available online at http://homepages.ulb.ac.be/ jadamilu/.

[178] E. Jones, E. Oliphant, P. Peterson, et al. SciPy: Open Source Scientific Tools for Python, 2001-, http://www.scipy.org/

[179] J. J. Moré, D. C. Sorensen, K. E. Hillstrom, and B. S. Garbow, The MINPACK Project, in Sources and Development of Mathematical Software, W. J. Cowell, ed., Prentice-Hall,pages 88-111 (1984).

[180] A.D. Mirlin, Y.V. Fyodorov, A. Mildenberger, and F. Evers, Phys Rev. Lett. **97**, 046803 (2006).

[181] I. A. Gruzberg, A. W. W. Ludwig, A. D. Mirlin, and M. R. Zirnbauer, Phys. Rev. Lett. **107**, 086403 (2011).

[182] N. A. Kamar and N. S. Vidhyadhiraja, J. Phys. C **26**, 095701 (2014).

[183] A. Ghosal, M. Randeria, and N. Trivedi, Phys. Rev. B **65**, 014501 (2001).

[184] M. Jiang, R. Nanguneri, N. Trivedi, G. G. Batrouni, and R. T. Scalettar, New J. Phys. **15**, 023023 (2013).

[185] G. Seibold, L. Benfatto, C. Castellani, and J. Lorenzana, Phys. Rev. Lett. **108**, 207004 (2012).

[186] B. Sacépé, T. Dubouchet, C. Chapelier, M. Sanquer, M. Ovadia, D. Shahar, M. Feigel'man, and L. Ioffe, Nat Phys **7**, 239 (2011).

[187] K. Bouadim, Y. L. Loh, M. Randeria, and N. Trivedi, Nat Phys **7**, 884 (2011).

[188] K. Aryanpour, T. Paiva, W. E. Pickett, and R. T. Scalettar, Phys. Rev. B **76**, 184521 (2007).

[189] M. V. Feigel'man, L. B. Ioffe, V. E. Kravtsov, and E. A. Yuzbashyan, Phys. Rev. Lett. **98**, 027001 (2007).

[190] Z.-J. Qin and S.-J. Xiong, Eur. Phys. J. B **46**, 325 (2005).

[191] Tom Lancaster and Stephen Blundell. *Quantum Field Theory for the Gifted Amateur*. Oxford University Press. (2014)

[192] B. Abeles, Roger W. Cohen, and G. W. Cullen, Phys Rev Lett. **17**, 632 (1966).

[193] P.W. Adams, H. Nam, C.K. Shih, and G.Catelani. Phys. Rev. B. **95**, 094520 (2017).

[194] Y. Liu, D. B. Haviland, B. Nease and A. M. Goldman, Phys. Rev. B **47**, 5931 (1993).

Appendix A: Permissions

American Physical Society (APS) Permission

The following agreement outlines the rights provided by APS to authors.

BG13571
Manuscript Number

AMERICAN PHYSICAL SOCIETY

Multifractal study of quasiparticle localization in disordered superconductors
Article Title

C. W. Moore, Ka-Ming Tam, Yi Zhang, et al.
Names of All Authors

TRANSFER OF COPYRIGHT AGREEMENT

Copyright to the above-listed unpublished and original article submitted by the above author(s), the abstract forming part thereof, and any subsequent errata (collectively, the "Article") is hereby transferred to the American Physical Society (APS) for the full term thereof throughout the world, subject to the Author Rights (as hereinafter defined) and to acceptance of the Article for publication in a journal of APS. This transfer of copyright includes all material to be published as part of the Article (in any medium), including but not limited to tables, figures, graphs, movies, other multimedia files, and all supplemental materials. APS shall have the right to register copyright to the Article in its name as claimant, whether separately or as part of the journal issue or other medium in which the Article is included.

The author(s), and in the case of a Work Made For Hire, as defined in the U.S. Copyright Act, 17 U.S.C. §101, the employer named below, shall have the following rights (the "Author Rights"):

(1) All proprietary rights other than copyright, such as patent rights.

(2) The nonexclusive right, after publication by APS, to give permission to third parties to republish print versions of the Article or a translation thereof, or excerpts therefrom, without obtaining permission from APS, provided the APS-prepared version is not used for this purpose, the Article is not republished in another journal, and the third party does not charge a fee. If the APS version is used, or the third party republishes in a publication or product charging a fee for use, permission from APS must be obtained.

(3) The right to use all or part of the Article, including the APS-prepared version without revision or modification, on the author(s)' web home page or employer's website and to make copies of all or part of the Article, including the APS-prepared version without revision or modification, for the author(s)' and/or the employer's use for educational or research purposes.

(4) The right to post and update the Article on free-access e-print servers as long as files prepared and/or formatted by APS or its vendors are not used for that purpose. Any such posting made or updated after acceptance of the Article for publication shall include a link to the online abstract in the APS journal or to the entry page of the journal. If the author wishes the APS-prepared version to be used for an online posting other than on the author(s)' or employer's website, APS permission is required; if permission is granted, APS will provide the Article as it was published in the journal, and use will be subject to APS terms and conditions.

(5) The right to make, and hold copyright in, works derived from the Article, as long as all of the following conditions are met: (a) at least one author of the derived work is an author of the Article; (b) the derived work includes at least ten (10) percent of new material not covered by APS's copyright in the Article; and (c) the derived work includes no more than fifty (50) percent of the text (including equations) of the Article. If these conditions are met, copyright in the derived work rests with the authors of that work, and APS (and its successors and assigns) will make no claim on that copyright. If these conditions are not met, explicit APS permission must be obtained. Nothing in this Section shall prevent APS (and its successors and assigns) from exercising its rights in the Article.

(6) If the Article was prepared under a U.S. Government contract, the government shall have the rights under the copyright to the extent required by the contract.

All copies of part or all of the Article made under any of the Author Rights shall include the appropriate bibliographic citation and notice of the APS copyright.

By signing this Agreement, the author(s), and in the case of a Work Made For Hire, the employer, jointly and severally represent and warrant that the Article is original with the author(s) and does not infringe any copyright or violate any other right of any third parties, and that the Article has not been published elsewhere, and is not being considered for publication elsewhere in any form, except as provided herein. If each author's signature does not appear below, the signing author(s) represent that they sign this Agreement as authorized agents for and on behalf of all authors who have the legal right to transfer copyright and that this Agreement and authorization is made on behalf of the same. The signing author(s) (and, in the case of a Work Made For Hire, the signing employer) also represent and warrant that they have the full power to enter into this Agreement and to make the grants contained herein.

C. Moore — 21Jul2017 12:16:31
ELECTRONICALLY SIGNED — Date

Vita

Conrad Moore was born in Norwalk Connecticut in 1987. He attended Winnacunnet High School in Hampton NH which is when he became interested in physics. He enrolled at Bucknell University in 2006 and while there participated in two National Science Foundation funded Research Experience for Undergraduates (REU) programs. First was at Ohio Wesleyan University under Dr. Harmond studying stellar surface imaging from light curve data. The second at the College of Wooster under Dr. Lindner numerically studying exotic space-time metrics. He graduated from Bucknell University with a Bachelor of Science with honors for a thesis entitled *Closed Time-like Curves and Inertial Frame Dragging: How to Time Travel via Space Time Rotation* in 2010. He then entered Louisiana State University and studied under Mark Jarrell for the duration of the work enclosed in this doctoral thesis.